A newly developed chamber setup for investigations of the spatial distribution of pharmaceutical dusts in containment

Dissertation

with the aim of achieving a doctoral degree

at the Faculty of Mathematics, Informatics and Natural Sciences

Department of Chemistry

University of Hamburg

submitted by

Hendrik Küllmar

Hamburg 2026

Reviewer of the thesis:	**Professor Dr. Dr. h.c. Claudia S. Leopold**
	Professor Dr. Hans-Ulrich Moritz
Thesis defence committee:	**Professor Dr. Dr. h.c. Claudia S. Leopold**
	Professor Dr. Peter Burger
	Priv. Doz. Dr. Christoph Wutz
Date of thesis defence:	**04.09.2026**
Date of print approval:	**04.09.2026**

The experimental studies and the preparation of this thesis were carried out between December 2019 and May 2026 in the Department of Chemistry at the University of Hamburg, in the division of Pharmaceutical Technology, on the initiative and under the supervision of Professor Dr. Dr. h.c. Claudia S. Leopold.

Conference contributions and publications

The following contributions related to this work have been presented at conferences and published in journals.

Conference contributions - Poster presentations

Küllmar, H., Schöler, M., Leopold, C. S.
Determination of the evacuation time of a newly developed chamber setup for the investigation of the spatial dust distribution of pharmaceutical powders
Meeting of the American Association of Pharmaceutical Scientists (PharmSci360), 2022, Boston (MA), USA

Küllmar, H., Schöler, M., Leopold, C. S.
Pneumatic aerosolization of the surrogate acetaminophen in a newly developed chamber setup for containment investigations with special focus on spatial dust distribution
Meeting of the American Association of Pharmaceutical Scientists (PharmSci360), 2023, Orlando (FL), USA

Küllmar, H., Schöler, M., Leopold, C. S.
Influence of the particle size distribution on powder dustiness in a newly developed chamber setup for the investigation of spatial dust distribution
14th PBP World Meeting, 2024, Vienna, Austria

Küllmar, H., Schöler, M., Leopold, C. S.
Real time spatial dust distribution of pharmaceutical powders with low-cost particulate matter sensors for containment detection in continuous manufacturing
5th APV Continuous Manufacturing Conference, 2024, Mölndal, Sweden

Conference contributions - Oral presentations

Küllmar, H., Schöler, M., Leopold, C. S.
Rapid-fire talk: ‘Real time spatial dust distribution of pharmaceutical powders with low-cost particulate matter sensors for containment detection in continuous manufacturing’
5th APV Continuous Manufacturing Conference, 2024, Mölndal, Sweden

List of publications

Title	Journal	Authors	Contribution to the work	Percentage
Investigations on the spatial dust distribution for emission site localization in containment	AAPS PharmSciTech (doi.org/10.1208/s12249-025-03236-y)	Küllmar, H.	Project plan, experiments, data analysis, publication	85 %
		Schöler, M.	Co-supervisor	2.5 %
		Brügmann, J.	Technical support	2.5 %
		Leopold, C.S.	Supervisor	10 %
Optimization of a newly developed chamber setup for spatial dust measurements in the context of containment	Pharmaceutics (doi.org/10.3390/pharmaceutics17050565)	Küllmar, H.	Project plan, experiments, data analysis, publication	87.5 %
		Schöler, M.	Co-supervisor	2.5 %
		Leopold, C.S.	Supervisor	10 %
Low-cost particulate matter sensors for real-time spatiotemporal detection of pharmaceutical dust in containment	European Journal of Pharmaceutics and Biopharmaceutics (doi.org/10.1016/j.ejpb.2026.115069)	Küllmar, H.	Project plan, experiments, data analysis, publication	85 %
		Schöler, M.	Co-supervisor	2.5 %
		Braunschweig, K.U.	Technical support	2.5 %
		Leopold, C.S.	Supervisor	10 %

Table of contents

Conference contributions and publications **I**

List of publications **III**

List of abbreviations **VII**

Zusammenfassung **X**

Abstract **XII**

1. Introduction **1**

1.1 Highly potent active pharmaceutical ingredients (HPAPIs) **1**

1.1.1 Definition of HPAPIs 1

1.1.2 Increasing relevance of HPAPIs 1

1.1.3 Risks posed by HPAPIs 2

1.1.4 Control of occupational exposure to HPAPIs 3

1.2 Containment **6**

1.2.1 General aspects 6

1.2.2 Primary and secondary containment 6

1.2.3 Legal and regulatory framework for containment 7

1.2.4 Hierarchy of controls and implementation of containment technologies 8

1.2.5 Validation of containment performance 10

1.3 Surrogate substances in pharmaceutical containment **10**

1.3.1 Reasons for the use of surrogate substances 10

1.3.2 Criteria for selecting a surrogate substance 11

1.3.3 Commonly used surrogate substances 11

1.4 Dust and dustiness **14**

1.4.1 Definition of dust and deposition in the human body 14

1.4.2 Definition of dustiness 16

1.4.3 Physicochemical powder properties affecting dustiness 17

1.5 Dustiness determination **20**

1.5.1 Mechanisms for atomization 20

1.5.2 Sampling of airborne dust 21

1.5.3 Laboratory dustiness testers 23

1.5.3.1 UNC dustiness tester (Venturi device) 24

1.5.3.2 Heubach dustmeter (rotating drum tester) 25

1.5.3.3 Continuous drop test apparatus 26

1.5.3.4 MRI dustiness tester 28

1.5.3.5 Palas dustview 29

1.5.3.6 Low-mass dustiness tester (LMDT) 30

1.5.3.7 Two-chamber setup (TCS) 31

1.5.4 Comparability of the dustiness testers for exposure prediction 32

1.6 Novel approaches for airborne dust detection **33**

1.6.1 Aerodynamic particle sizing 33

1.6.2 Optical particle counter (OPC) 34

1.6.3 Substance-specific real-time monitoring of airborne dust 36

1.7 Computational Fluid Dynamics (CFD) **36**

1.7.1 CFD and its application in pharmaceutical contexts 36

1.7.2 CFD coupled with discrete element modeling (DEM) 37

2. Aim of the work **38**

3. Cumulative part of the dissertation **40**

3.1 Investigations on the spatial dust distribution for emission site localization in containment **40**

3.2 Optimization of a newly developed chamber setup for spatial dust measurements in the context of containment **59**

3.3 Low-cost particulate matter sensors for real-time spatiotemporal detection of pharmaceutical dust in containment **77**

Discussion **90**

References **96**

Appendix **121**

Hazardous materials **121**

List of figures **122**

List of tables **123**

Curriculum vitae **124**

Acknowledgements **125**

Declaration on oath / Eidesstattliche Versicherung **127**

List of abbreviations

ACAM	Acetaminophen
ACGIH	American Conference of Governmental Industrial Hygienists
ADE	Acceptable daily exposure
APS	Aerodynamic particle sizer
AI	Artificial Intelligence
AMWHV	Arzneimittel- und Wirkstoffherstellungsverordnung
API	Active pharmaceutical ingredient
BMD_{10}	Benchmark dose
BW	Body weight
CEN	Comité Européen de Normalisation
CFC	Closed-face cassettes
CFD	Computational fluid dynamics
CIP	Clean in place
CPT	Containment performance target
DIS	Disposable inhalable sampler
DL	Detection limit
DoE	Design of experiments
EN ISO	European Norm for International Organization for Standardization
Eq.	Equation
EU	European Union
FAT	Factory acceptance test
GMP	Good Manufacturing Practice
HEPA	High efficiency particulate air filter

HHC	Health hazard categories
HMI	Human machine interface
HPLC	High-performance liquid chromatography
HPAPI	Highly potent active pharmaceutical ingredient
ICH	International Council for Harmonisation of Technical Requirements for Registration of Pharmaceuticals for Human Use
IGF	Institut für Gefahrstoff-Forschung
ILO	International Labour Organisation
IOM	Institute of Occupational Medicine
ISO	International Organization for Standardization
ISPE	International Society for Pharmaceutical Engineering
LAC	Spray-dried agglomerates of α-lactose monohydrate crystals bound by amorphous lactose
LMDT	Low-mass dustiness tester
MF	Modifying factor
NOAEL	No observable adverse effect level
NOEL	No observed effect level
OEB	Occupational exposure band
OEL	Occupational exposure limit
ORB	Overall respiratory burden
OSHA	Occupational Safety and Health Administration
PDI	Polydispersity index
PK	Pharmacokinetic adjustment factor
PLC	Programmable logic controller
PM sensors	Low-cost particulate matter sensors

PoD	Point of departure
PPE	Personal protective equipment
QL	Quantification limit
RP	Reversed-phase
RPM	Revolutions per minute
SAT	Site acceptance test
SD	Standard deviation
SEM	Scanning electron microscopy
SMEPAC	Standardized Methodology for the Evaluation of Pharma Airborne Particle Emissions from Containment Systems
TCS	Two-chamber setup
TGA	Thermogravimetric analysis
UF	Uncertainty factor
UNC	University of North Carolina
V	Volume
WHO	World Health Organization

Zusammenfassung

Die in den letzten Jahren neu entwickelten Arzneistoffe umfassen einen hohen Anteil an hochpotenten Wirkstoffen. Daher gewinnt deren sichere Handhabung immer mehr an Bedeutung zum Schutz des Personals in Produktion und Forschung sowie der Patienten. Die größte Gefahr geht hierbei von luftgetragenem Staub aus, welcher bei der Handhabung des Arzneistoffes entsteht. In der vorliegenden Arbeit wurde in drei Studien mittels eines neu entwickelten Messsystems die Staubentstehung sowie die anschließende räumliche Ausbreitung des luftgetragenen, wirkstoffhaltigen Staubes untersucht. In der Emissionskammer des Messsystems wird eine Pulverprobe zerstäubt, die dann über eine definierte Öffnung in eine Detektionskammer übertritt, in der anhand von neun filterbasierten Messpunkten die räumliche Ausbreitung der Staubemission detektiert werden kann.

Die erste Studie befasste sich mit dem Konzeptnachweis des Messsystems. Versuche mit der Surrogatsubstanz Paracetamol zeigten, dass reproduzierbare Messungen der Staubemission kleinster Mengen des Arzneistoffes als auch seiner räumlichen Ausbreitung mit dem Messsystem möglich sind. Es konnte ein linearer Zusammenhang zwischen Probenmasse und detektiertem Gesamtstaub gezeigt werden. Interessanterweise verhielt sich die räumliche Staubausbreitung nicht wie erwartet, also mit der höchsten Konzentration in der Nähe des Emissionsortes, sondern umgekehrt. Daher wurde dieses Ergebnis mittels Computational Fluid Dynamics-Simulationen überprüft, was ergab, dass die Ausbreitung des Aerosols der Luftströmung, welche im Messsystem entsteht, entspricht.

Basierend auf diesen Ergebnissen wurde in einer zweiten Studie der Einfluss der Zerstäubungsparameter auf die gemessene Staubemission und die räumliche Staubausbreitung genauer untersucht. Mittels statistischer Versuchsplanung konnte der lineare Zusammenhang zwischen Probenmasse und detektierter Staubemission bestätigt und eine Interaktion zwischen dem zur Zerstäubung genutzten Druckluft-Volumenstrom und

der Zerstäubungsdauer sowohl bezüglich der detektierten Staubemission als auch der räumlichen Staubausbreitung festgestellt werden. Darüber hinaus wurde der Einfluss der Partikelgrößenverteilung sowie der Partikelform der Pulverprobe auf die gemessenen Staubemissionen deutlich. Anhand dieser Ergebnisse sowie einer Optimierung der Messprozedur, konnte die detektierte Staubemission bei gleichbleibender Probenmasse mehr als verzehnfacht und der Einfluss der Zerstäubungsparameter auf die räumliche Ausbreitung charakterisiert werden.

In einer dritten Studie wurde das entwickelte Messsystem mit laserbasierten optischen Sensoren ausgestattet, welche den Feinanteil des Staubes (Partikel < 2,5 µm) detektieren können. Dies ermöglichte die zeitlich aufgelöste und sofortige Detektion der räumlichen Ausbreitung des Staubes. Die Ergebnisse der Studie bestätigten nicht nur die in den ersten beiden Studien beobachtete räumliche Ausbreitung der Staubemission, sondern zeigten darüber hinaus, dass die räumliche Staubausbreitung innerhalb der ersten Minuten nach Zerstäubung stattfindet und es anschließend zu einem Konzentrationsausgleich im Messsystem kommt. Mit den optischen Sensoren war es möglich die Staubemission einer typischen Tablettiermischung aus feinpartikulärem Paracetamol und grobkörniger Lactose zu untersuchen. Diese Mischung wies eine reduzierte Staubemission im Vergleich zu reinem Paracetamol auf.

Zusammenfassend konnte in den drei Studien gezeigt werden, dass nicht nur die Untersuchung der Staubemission, sondern auch die der räumlichen Ausbreitung des Staubes mit dem vorgestellten Messsystem möglich ist. Die vorliegende Arbeit liefert somit wichtige Erkenntnisse zur Detektion von Kontaminationsquellen einer Produktionsanlage, welche durch stationäre Messungen lokalisiert werden könnten, sowie über eine mögliche Verringerung der Staubexposition durch gezielte Luftführung in Produktionsräumen zum Schutz von Personal, Produkten und somit letztendlich auch von Patienten.

Abstract

In recent years, the percentage of highly potent active pharmaceutical ingredients among the newly developed drugs has increased significantly. Thus, safe handling is becoming increasingly important to protect employees as well as patients. The major hazard is airborne dust generated during handling of these compounds. In the present work, the generation of dust and the subsequent spatial distribution of airborne dust containing active pharmaceutical ingredients were investigated in three studies using a newly developed chamber setup. With this setup, a powder sample is atomized within an emission chamber and then passes through a defined orifice into a detection chamber, in which the spatial distribution of the dust emission may be detected using nine filter-based measurement spots.

In a first study, the proof of concept of the chamber setup was focused on. Experiments with the surrogate substance acetaminophen showed that reproducible measurements of both dust emission of very small quantities of the active pharmaceutical ingredient as well as its spatial distribution are possible with the chamber setup. A linear relationship between the sample mass and the total dust detected was shown. Interestingly, the spatial distribution was not as expected, with the highest concentration close to the emission site, but the opposite. This finding was verified by computational fluid dynamics simulations and it was demonstrated that the distribution of the aerosol corresponds to the airflow generated in the chamber setup.

Based on these results, the influence of the atomization parameters on the measured dust emission and the spatial dust distribution was investigated in detail in a second study. With a statistical experimental design, the linear relationship between sample mass and detected dust emission was confirmed and an interaction between the compressed air volume flow used for atomization and the atomization duration was found with regard to

both the detected dust emission and the spatial dust distribution. In addition, there was an influence of the particle size distribution and the particle shape of the sample on the measured dust emissions. Based on these results and an additional optimization of the measurement procedure, the detected dust emission could be increased more than tenfold at a constant sample mass and the influence of the atomization parameters on the spatial dust distribution was successfully characterized.

In a third study, the newly developed chamber setup was equipped with laser-based optical sensors, which allow the detection of the fine fraction of the dust (particles < 2.5 µm). With these sensors, the immediate spatiotemporal detection of the dust distribution was possible. The results of the study not only confirmed the spatial dust distributions already observed in the first two studies but also showed that the spatial distribution occurs within the first few minutes after atomization and that there is a subsequent equilibration of the dust concentration in the measuring system. Moreover, the optical sensors allowed to investigate the dust emission of a binary powder blend, used for direct compression in tableting, consisting of fine particulate acetaminophen and coarse lactose. This powder blend showed a decreased dust emission compared to plain acetaminophen.

In summary, the three studies demonstrated that with the novel chamber setup it is not only possible to investigate dust emissions, but also the spatial distribution of dust. This work thus provides important information on how to localize sources of contamination in a production environment using stationary measurements and how to possibly reduce dust exposure through directed airflow in production facilities to protect personnel and ultimately also patients.

1. Introduction

1.1 Highly potent active pharmaceutical ingredients (HPAPIs)

1.1.1 Definition of HPAPIs

HPAPIs are active pharmaceutical ingredients that meet at least one of the following criteria [1–4]:

- A pharmacologically active substance or intermediate that exhibits biological activity in humans at a concentration of 150 µg/kg body weight or less.
- An active pharmaceutical ingredient with a maximum workplace concentration of 10 µg/m^3.
- A pharmacologically active substance or intermediate with a high selectivity (e.g. binding to receptors or inhibition of enzymes) or a substance that can trigger cancer or mutations.
- A new compound whose effects and toxicity are still unknown.

A broader definition comprises compounds with a therapeutic dose of 1 mg or less [2].

1.1.2 Increasing relevance of HPAPIs

In recent decades, there has been great progress in the field of pharmaceutical drug development. An increasing number of innovative and often highly potent active pharmaceutical ingredients are being developed with combinatorial chemistry and high-throughput screening [2,4–6]. In addition, this developmental progress was further accelerated by Artificial Intelligence (AI). For example, the application of AI enables scientists to streamline the scientific discovery of drug–target interactions [7–9]. This development is of great benefit for patients worldwide as it enables therapies of diseases such as cancer, autoimmune diseases, and hormone imbalances [10–12]. In the field of tumor therapy, approximately 60 % of approved oncological treatments are based on HPAPIs [10].

1.1.3 Risks posed by HPAPIs

Although beneficial for patients, HPAPIs often pose an increased risk with regard to the environment, product quality assurance/cross-contamination, and workers' health because of their high pharmacological and toxicological potential [13–16].

For environmental protection in the pharmaceutical industry, two aspects have to be taken into consideration.

The first aspect is the management of HPAPI-containing wastewater, which results from cleaning of production equipment and facilities [17]. These HPAPIs in wastewater represent pharmaceutical pollutants of an emerging class of recalcitrant toxicants threatening drinking water and therefore must be eliminated from wastewater [18]. To remove these pollutants, several purification methods such as adsorption, biological treatments with bacteria or microalgae, membrane bioreactors, microbial electro-chemical technologies, and advanced oxidation processes were implemented [18–20].

The second aspect is the elaborate filtration of exhaust air to protect the environment. Therefore, all air released into the environment from potentially hazardous areas during normal operation and in the event of disruptions must be appropriately filtered [17]. For filtering, different methods are available, such as high efficiency particulate air filters (HEPA), cyclones, and electrostatic separators [17,21,22].

With regard to product quality and thus patient safety, cross-contamination during manufacturing has to be prevented [17,23]. Therefore, the spread of hazardous substances on the production equipment and in the production environment must be minimized [17]. Also, to protect the personnel, exposure to HPAPIs must not exceed a tolerable level. To ensure that the exposure does not exceed this level, so-called occupational exposure limits (OELs) are implemented [6,14,15,24–29].

1.1.4 Control of occupational exposure to HPAPIs

The knowledge of a relationship between health and occupation dates back to the 17th century. In his book *De Morbis Artificum Diatriba*, Bernardino Ramazzini not only describes the adverse effects of inhaled mineral dusts on the health of miners and stonecutters but also suggests preventive measures such as limiting the exposure to hazards to prevent injuries [30]. In modern days, this exposure control is still a sound concept, defined as the acceptable daily exposure (ADE), and is controlled by the implementation of OELs in the pharmaceutical industry [4,17,27,28,31–34]. The ADE is described as follows (modified from [35]):

$$ADE = \frac{NOAEL \bullet BW}{UF \bullet PK} \qquad \text{(Eq. 1)}$$

ADE: acceptable daily exposure (mg/day), NOAEL: no observed adverse effect level (mg/kg/day), BW: body weight (kg), UF: uncertainty factor accounting for inter-individual variability and interspecies extrapolation (usually a value of 10 is chosen), PK: pharmacokinetic adjustment factor to account for the difference in bioavailability between inhaled exposure and intended administration from which the NOAEL is derived [4,35,36].

An OEL is based on the ADE and is defined as the maximum airborne dust concentration, expressed as the time-weighted average for a conventional 8 h workday and a 40 h work week, of a substance to which workers may be repeatedly exposed for a working lifetime without adverse effects [2,4]. There are different methods to specify OELs. One method is the therapeutic dose/safety factor approach. In this approach, the lowest recommended therapeutic drug dose is identified and divided by a safety factor. Usually, a safety factor of 100 is applied for adjusting a therapeutic effective dose to a therapeutically noneffective dose to take into account the individual variability in response [27]. Unfortunately, this approach has several drawbacks. The first is a

possible difference between the route of administration of an active pharmaceutical ingredient (API) for disease treatment and the occupational setting. For example, the bioavailability of an API may be much lower if administered orally than via the respiratory tract [23,27]. In addition, the exposure pathway in occupational settings is not always known [16]. Another drawback represent drugs used for life-threatening diseases, where considerable toxicities may be accepted, whereas an exposure of employees to these drugs would not [27].

Therefore, another method to specify OELs has been introduced, which is based on the determination of acceptable daily exposure values and occupational exposure limits of HPAPIs, taking toxicokinetic and toxicodynamic data into account [33,37,38]. The OEL is described as follows (modified from [36]):

$$OEL = \frac{NOAEL \bullet BW}{UF \bullet V \bullet PK} \quad \text{(Eq. 2)}$$

OEL: occupational exposure limit (mg/m^3), V: volume of air (m^3/day) inhaled by a worker in 8 h (typically 10 m^3/day). For the other abbreviations, please refer to Equation 1. The NOAEL in Equations 1 and 2 may be replaced by the point of departure (PoD) comprising other effect levels such as the no observed effect level (NOEL) or the benchmark dose (BMD_{10}), which may represent critical effect levels [31,39].

The calculated OELs may result in extremely low acceptable airborne dust concentrations of less than 1 µg/m^3 [4,17,39]. It must be noted that the average level of OELs may differ substantially between institutions. For example, exposure limits established by the US Occupational Safety and Health Administration (OSHA) are almost 40 % higher than those specified in Poland [34]. Whether these differences are scientific or policy-related remains to be questioned [34].

If there is no sufficient data available to determine a precise OEL of a substance, it is categorized into classes or bands used in different systems, for example the health hazard categories (HHC) or the occupational exposure bands (OEB) [17,40]. This concept of hazard-based categories to inform employers and workers of the need for risk management and exposure control was developed in the pharmaceutical industry and has been utilized for decades [3,40]. The categorization systems as well as the assignment of substances to specific HHCs or OEBs are not harmonized and therefore may differ between organisations and companies [11,17,41]. Usually, such a system comprises four to six categories, whereby substances of very low pharmacologic and toxic effects are assigned to category one and those with very high effects to the highest category number [17,25,42]. In Table 1, the example of an occupational exposure band classification system is shown.

Table 1: Example of an OEB classification system (modified from [4,17]).

Category	**OEL range (µg/m³)**	**Effect**
OEB 1	> 1,000	Very low pharmacologic and/or toxic effect
OEB 2	100-1,000	Low pharmacologic and/or toxic effect
OEB 3	10-100	Medium pharmacologic and/or toxic effect
OEB 4	1-10	High pharmacologic and/or toxic effect
OEB 5	< 1	Very high pharmacologic and/or toxic effect

An overview of a classification system, extended by a sixth hazard category and presenting the relationship between ADE, OEL, and OEB, is shown in Figure 1.

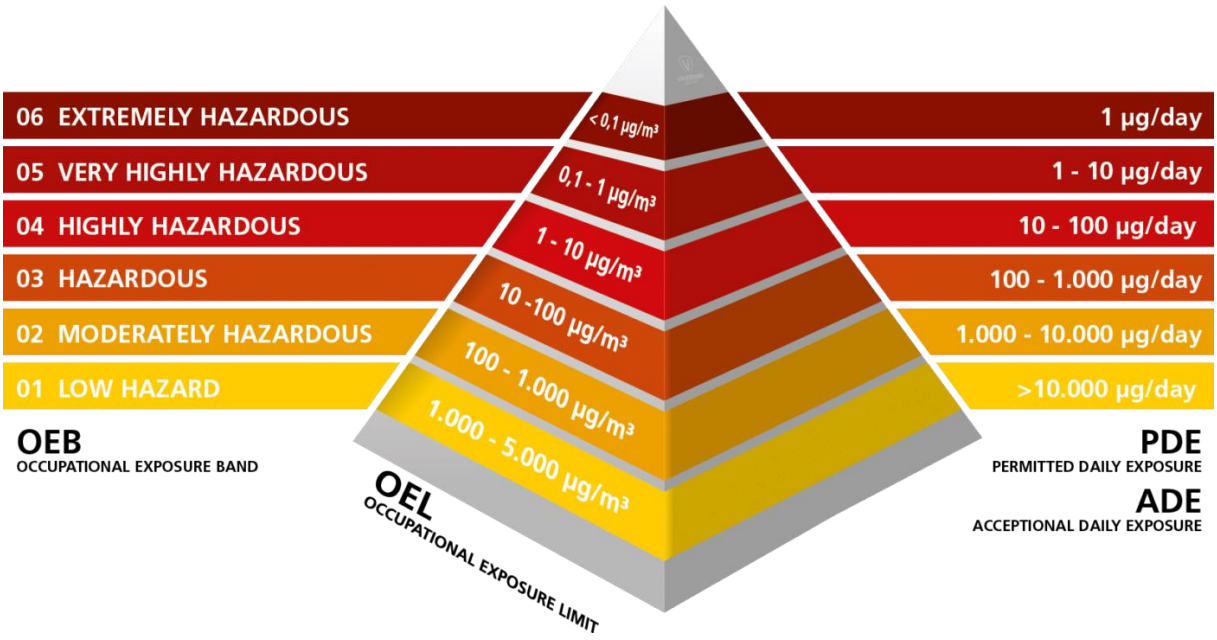


Figure 1: Relationship between ADE, OEL, and OEB [43].

1.2 Containment

1.2.1 General aspects

As mentioned in Chapter 1.1, HPAPIs pose a risk to the environment, the product quality, and workers' health [13–17]. Therefore, the so-called containment technology is implemented in the pharmaceutical industry. The term 'containment' refers to all measures taken, i.e. methods, procedures, and technologies, to prevent the release of a hazardous substance or the contamination of pharmaceuticals during manufacturing and handling [17]. As completely closed production units are impossible to realize, an effective containment strategy is essential and should include fail-safes in case of a manufacturing incident [11,17,44].

1.2.2 Primary and secondary containment

Overall, containment can be divided into primary and secondary containment. Primary containment refers to all measures that reduce the spread of a substance from the actual production equipment [17]. Among others, these measures include housings for tablet presses, isolators, split butterfly valves, and local exhaust systems

[6,14,17,25,42,45]. Secondary containment refers to all measures that reduce a further spread of substances which were not retained by the primary containment. Examples of secondary containment are cleanrooms, airlock systems, pressure differentials between production and surrounding rooms, such as corridors as well as high performance filter systems [17,45–47].

1.2.3 Legal and regulatory framework for containment

A regulatory framework with basic requirements for health protection at the workplace is given by the European Union (EU) in the Directive 89/391/EEC [48]. In this directive, it is specified that the employer is obliged to protect the employees from health and safety risks. Therefore, appropriate risk assessments must be carried out [17,48]. The employees must primarily be protected by 'collective protective measures', i.e. technical measures, supported by organizational interventions. Personal protective equipment (PPE) may only be used as primary protection against any hazard if no sufficient technical measures exist [17]. Furthermore, the primary and secondary containment measures have to be aligned with each other while prioritizing the optimization of the primary containment [17]. Many countries outside of the EU have similar laws in place. For example, the US equivalent of the EU Directive 89/391/EEC is the Occupational Safety and Health Act of 1970 (OSH Act) [49]. The International Labour Organisation (ILO) has taken up these national directives and combined them in their guidelines, which in turn have been ratified by numerous countries [17,50]. A detailed description of occupational exposure control based on ADEs, OELs, and OEBs, recommended by these guidelines, was presented in Chapter 1.1.4.

In their Good Manufacturing Practice (GMP) guidelines, the International Council for Harmonisation of Technical Requirements for Registration of Pharmaceuticals for Human Use (ICH) mentions the requirement of product protection against cross-contamination [51]. Again, other countries, such as the USA, have their own equivalent

guidelines [52]. This cross-contamination protection is especially of interest in multi-product pharmaceutical manufacturing facilities [53–55]. The guidelines emphasize the necessity of separated production areas or production times with adequate cleaning procedures in between manufacturing processes [51,53]. A considerable reduction of the required cleaning procedures may be achieved by the use of disposable single-use production equipment, despite raising environmental concerns [56–59]. In addition to these international guidelines, the German 'Arzneimittel- und Wirkstoff-herstellungsverordnung' (AMWHV) specifies in § 5 the necessity of suitable production rooms to avoid any adverse effects with regard to product quality [60]. The International Society for Pharmaceutical Engineering (ISPE) states: 'This protective goal is all the easier to achieve, the less substance escapes from the equipment, i.e. the more effective the containment is' [17].

1.2.4 Hierarchy of controls and implementation of containment technologies

Occupational hygienists use a hierarchy of controls to rank occupational hygiene control strategies according to the order in which they should be considered [61,62]. The first control strategy taken should be the elimination or reduction of the source of hazardous material. In the contained manufacture of pharmaceuticals, this measure is impossible, as HPAPIs cannot be exchanged by less hazardous substances. The second control strategy is defined as the elimination or reduction of hazardous substances in production environments by means of engineering controls and administration procedures. Thus, if a contaminant must be processed, its release has to be prevented, for instance by means of containment technology. The last control strategy is the exposure reduction at the employees' site, preventing them from harm with personal protective equipment [17,61,62].

The implementation of containment technologies starts with the conceptualization of production buildings, no matter whether new or existing buildings are chosen for the

contained manufacture of pharmaceuticals [17,61,63]. It has to be taken into consideration, that certain pharmaceuticals, such as live vaccines, radiopharmaceuticals or highly potent allergens must be produced in dedicated facilities as their production in multi-purpose facilities is prohibited by EU GMP guidelines [17,64,65]. In general, building concepts must take the flows of personnel and material into consideration and planning of all containment measures should always follow an inside-out approach. For example, the layout of a clean room should be based on the dimensions of the production equipment [17,66]. A description of primary and secondary containment equipment and measures may be found in Chapter 1.2.2. The selection of equipment and measures is based on risk assessment, taking multiple factors, such as health risks for people and the environment, quality risks for the product, and process risks into consideration [17,53]. Production equipment should be tested by the supplier in a factory acceptance test (FAT) to ensure that all critical functions are working correctly before delivering the equipment to the production site. In addition, after the installation of the equipment with its containment measures at the production site, a site acceptance test (SAT) should be carried out. Following a successful SAT, the operation of the production line may be started with a surrogate substance of similar characteristics to the intended product [17,67]. During this initial operation, it is recommended to carry out containment measurements in short time intervals to validate that the required threshold value of airborne dust, i.e. the containment performance target (CPT), is not exceeded [17,68]. These measurements may be performed following the Standardized Methodology for the Evaluation of Pharma Airborne Particle Emissions from Containment Systems (SMEPAC) [17,29]. Subsequently, the production of pharmaceutical dosage forms containing HPAPIs may begin [17].

1.2.5 Validation of containment performance

In the SMEPAC, the ISPE describes how containment capabilities of production equipment may be assessed with regard to the CPT [29]. Therefore, the airborne particle concentration during the production process is determined at critical spots, for example at the product in- and outlets of a tablet press or the human-machine interface (HMI) [29]. The location of these measurement spots is based on the assessment of a potential contamination risk. For detection of airborne particles, filter-based IOM samplers (Institute of Occupational Medicine), DIS (disposable inhalable samplers) as well as CFC (closed-face cassettes) with subsequent gravimetric analysis or wet chemical analysis, such as UV/VIS-spectrophotometry or high-performance liquid chromatography (HPLC) for substance-specific quantification may be used [29,69–72]. Another possibility of airborne dust detection for the validation of containment equipment is real-time monitoring with light-scattering photometers or optical particle counters (OPC) [29,73–75]. Substance-specific real-time monitoring with optical methods is currently under development [29].

1.3 Surrogate substances in pharmaceutical containment

A surrogate substance in pharmaceutical containment may be defined as an alternative substance to a hazardous pharmaceutical compound or product. A surrogate should be used, if the compound to be processed cannot be used for the validation of containment equipment, for example because of its hazardous nature or its high costs [24].

1.3.1 Reasons for the use of surrogate substances

The use of surrogate substances offers several advantages, allowing for a safer and more cost-effective performance testing of containment systems [24,29,76]. In addition, with surrogate substances, an early identification and removal of containment

deficiencies is possible. Furthermore, the ISPE recommends surrogate substances for pharmaceutical dustiness investigations at laboratory scale [17,24,29,77].

1.3.2 Criteria for selecting a surrogate substance

The choice of a pharmaceutical surrogate substance should be based on multiple criteria, including safety considerations, transferability of results to the intended API, and analytical limitations. For selection of an appropriate surrogate substance, the criteria shown in Table 2 should be taken into consideration [24,29,76].

Table 2: Selection criteria for pharmaceutical surrogate substances.

Powder properties	**Analytics**	**Safety**	**Other aspects**
Dustiness	Detection and Quantification Limit (DL and QL)	Pharmacological effects (no risk for personnel, no cross-contamination)	Possible contamination of facility prior to testing (e.g. lactose or sucrose)
Particle size distribution and particle shape	Complexity and cost for analysis	Ease of disposal (environmental aspect)	Cost and availability of the surrogate
Powder flow	Solubility in water and other solvents	Dust explosion risk	GMP acceptability

1.3.3 Commonly used surrogate substances

An overview of commonly used surrogates recommended by the ISPE, their properties and typical applications is shown in Table 3. The surrogate Riboflavin was excluded, as it is used as an aqueous solution mainly for the evaluation of an equipment-specific cleaning system, e.g. clean in place (CIP) systems, but not recommended for airborne dust investigations or surface contamination assessments [29].

Table 3: Overview of commonly used pharmaceutical surrogate substances, their properties, and typical applications (modified from [29]).

Surrogate substance	Advantages	Disadvantages	Typical Application
Acetaminophen	Low toxicity	Relatively poor water solubility	Commonly used surrogate
	Inexpensive	Material is an API (potential GMP cleaning issues)	Largely replaced by lactose due to GMP concerns
	Reasonably dusty		Easier to analyze than lactose
	Multiple analytical methods available (QL: 0.05 - 1 ng/sample)		Commonly used for packaging applications in tablet form
Lactose	Multiple analytical methods available (QL: 0.05 - 5 ng/sample)	Tendency for agglomeration (especially if micronized)	Widely used surrogate down to concentrations of ~ 0.1 µg/m³
	Highly water soluble	Common excipient (may be present as environmental background)	Not as effective as extremely dusty materials
	Widely available	Multiple types may influence test results	Sieved grades should be used
	Inexpensive	Difficult analysis	
	Non-API material		
	Low toxicity		
Mannitol	Multiple analytical methods available (QL: 0.5 - 5 ng/sample)	Common excipient (may be present as environmental background)	Less widely used than lactose and hardly available in suitable grades
	Other advantages identical to lactose	Difficult analysis	Useful if a considerable lactose background is expected

Surrogate substance	Advantages	Disadvantages	Typical Application
Naproxen sodium	Highly water soluble at pH > 6	Relatively expensive	Commonly used surrogate
	Low toxicity	Material is an API (potential GMP cleaning issues)	High dustiness presents a challenge
	Simple analytical method (low QL: 0.005 ng/filter)	Aggregates if micronized	Very useful for testing of systems for handling highly hazardous or dusty materials
	Extremely dusty		
Sucrose	Widely available	Tendency for aggregation (especially if micronized)	Less widely used than lactose and hardly available in suitable grades
	Highly water soluble	Common excipient (may be present as environmental background)	Useful if considerable lactose or mannitol background is expected
	Low toxicity	Difficult analysis	
	Inexpensive	QL: 10 - 100 ng/filter	
	Non-API material		

As an example, acetaminophen (ACAM) is an industry-accepted safe surrogate substance because of its low LD_{50} with 338 mg/kg (mouse, oral) or 1944 mg/kg (rat, oral). In human adults, ACAM is used for safe and effective analgesic and antipyretic treatment in doses of up to 4 g/day [78,79]. In addition, the spectrophotometrical quantification limit of ACAM is low [24,68,80,81]. Potential disadvantages of ACAM include its high tendency for electrostatic interactions with processing vessels or laboratory devices and its poor water solubility, resulting in a need of cosolvents for analysis [82–85].

1.4 Dust and dustiness

1.4.1 Definition of dust and deposition in the human body

In 1975, the Inhaled Particles Symposium pointed out the inconsistency of national practices for dust monitoring [86]. At this symposium, the necessity for application of scientific principles to dust exposure was discussed and resulted in the concept of ‘inhalable dust’ required for occupational dust monitoring [86]. In the following years, a multitude of studies were carried out to determine the size range of airborne particles inhalable by humans, the concentration changes of airborne dust in the personal space close to workers, and adequate sampling methods for occupational monitoring [69,70,87–94].

By combining the results of these studies in the mid-1990s, the International Organization for Standardization (ISO), the American Conference of Governmental Industrial Hygienists (ACGIH), and the Comité Européen de Normalisation (CEN) agreed on common definitions for size-selective aerosol sampling conventions for three health-related aerosol fractions, namely the inhalable fraction with the thoracic and the respirable subfractions (the latter being deposited in the alveolar/gas-exchange region) [29,95–98]. These fractions can further be subdivided by their deposition area in the human respiratory tract, as shown in Figure 2.

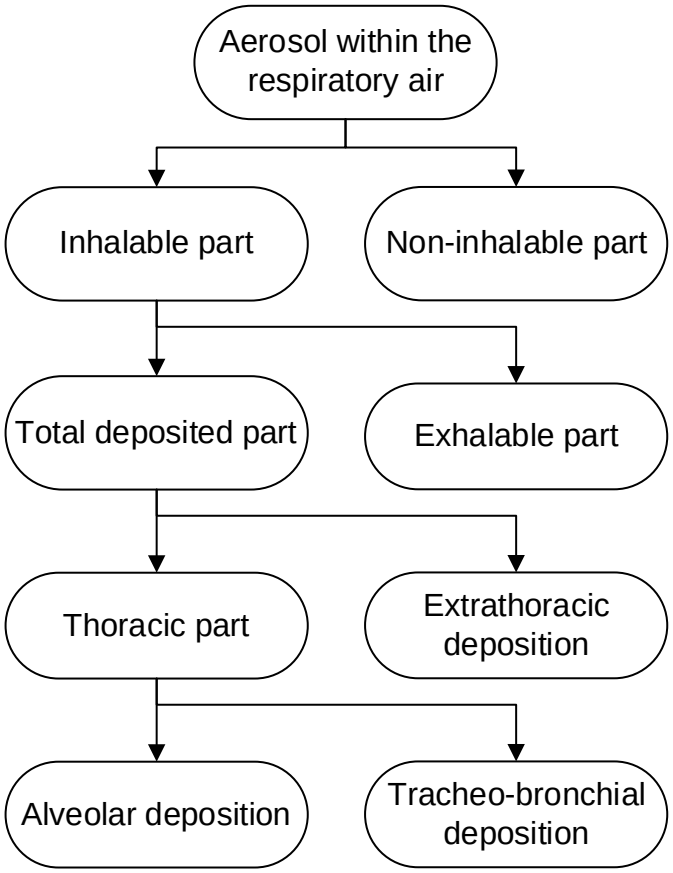


Figure 2: Classification of airborne aerosols according to occupational health criteria, modified from [99,100].

The World Health Organization (WHO) defines the upper particle size limit for inhalable dust particles at an aerodynamic diameter of 100 µm, whereas the ISO defines it at 75 µm [101–103]. The largest inhalable particles with an aerodynamic diameter of less than 100 µm are deposited between the point of entry (mouth or nares) and the larynx. Particles with a maximum diameter of 10 µm may be deposited in the thoracic region, where only 1 % of them reach the alveolar region. The maximum deposition in the alveolar region takes place with particles of an aerodynamic diameter of approximately 1 to 2 µm. Particles < 0.5 µm are usually exhaled and thus not deposited in the lungs [98,101,104–107]. These size limits may vary in the literature as they are dependent on the breathing passage, e.g. nasal versus mouth breathing [108].

The ISO, ACGIH, and CEN conventions for airborne dust sampling for occupational monitoring are based on the above-mentioned size limits of the particle fractions and are defined as follows [29,95–97]:

- Inhalable fraction: airborne particles that enter the body through the lips and/or nares during breathing. The 50 % cutoff for sampler collection efficiency is at 100 µm.
- Thoracic fraction: particles that penetrate the respiratory tract below the larynx and enter the trachea, bronchi, and even the alveolar region of the lungs. The 50 % cutoff for sampler collection efficiency is at 10 µm.
- Respirable fraction: particles that penetrate the bronchioles and enter the alveolar region of the lungs. The 50 % cutoff for sampler collection efficiency is 1 µm.

Where the 50 % cutoff for sampler collection efficiency indicates that only 50 % of particles at that diameter will be collected by the sampler.

The occupational exposure of a worker to an HPAPI, limited by established OELs, comprises the entire inhalable fraction, as every inhaled particle has the potential of being absorbed by the human body and may cause adverse effects [29]. The subdivision into thoracic and respirable dust fractions is especially of interest for occupational exposure to particulate matter with no pharmacologic and/or toxicologic potential but still causing adverse health effects, e.g. nanoparticles or asbestos fibers [104,106,109–111].

1.4.2 Definition of dustiness

Dustiness may be defined as the propensity of a material to generate airborne dust during its handling, such as mixing, milling or transferring and/or the tendency of a powder to form an aerosol after it receives a given energy input [45,76,101,112–114]. Dustiness may be measured as a collected amount of dust under defined conditions

and may be determined with dustiness testing devices [76,81,120–125,99,100,112,115–119]. To compensate for varying defined conditions, dustiness indices have been introduced [115,123,126]. These indices usually relate the collected dust, i.e. the suspended particulate matter to the total amount of atomized sample mass [115,123]. The energy input for atomization must overcome interparticle binding forces, such as van der Waals, capillary, and electrostatic forces to generate dust, thus releasing loosely bound primary particles and aggregates from the bulk powder without decreasing the size of the primary particles [112,114,127,128]. A model of the dust generation and quantification processes is shown in Figure 3.

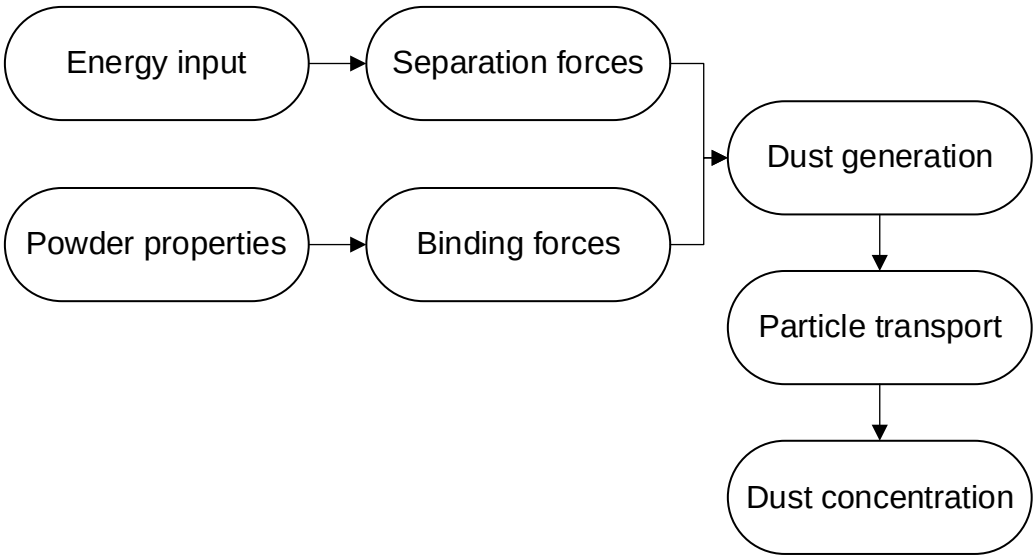


Figure 3: Model of the dust generation and quantification processes, modified from [127].

1.4.3 Physicochemical powder properties affecting dustiness

Dustiness is not an intrinsic physical or chemical property of a substance [114,127]. It is dependent on various physicochemical powder properties, which include true and bulk densities, residual moisture content, sample mass, particle morphology, as well as particle size and distribution, as all of these properties influence particle interactions [77,99,130–136,100,112–114,122,123,127,129].

The bulk density of a powder has significant influence on dustiness, as it represents the powder's packing state and is dependent on the interparticle distance [114]. If this distance is reduced, i.e. the bulk density is increased, the interparticle secondary valence forces also increase, leading to a reduction of powder dustiness [114,128,137]. This is especially of interest in dustiness tests in which the powder is dropped onto a surface for atomization [129]. The bulk density may be affected by handling of the powder prior to measurements and thereby directly influences dustiness [76]. The true density also affects dustiness, in particular how long particles stay airborne, as particles of high true density sediment faster in accordance with Stokes' law of sedimentation [138].

The residual moisture content of a powder affects two of the most influential interparticle binding forces. On the one hand, residual moisture decreases the tendency of a powder to be electrostatically charged [139–141]. The resulting decrease leads to less interactions between the powder particles and those between powder particles and measuring device surfaces, thus increasing dustiness [84,114]. On the other hand, a high residual moisture content affects the capillary forces of attraction within the powder, such as water sorption and the formation of capillary bridges, thereby significantly decreasing its dustiness [112,114,127,142–145]. The residual moisture content is directly related to the hygroscopicity of the powders and the relative humidity of the surrounding air. An increase in relative humidity and thus an increase in the residual moisture content results in a substantial decrease of powder dustiness [114,119,134,146,147].

The sample mass correlates with the measured dustiness, usually in a linear manner [77,81,116,125]. In some studies, the measured dustiness reaches a maximum, sometimes even followed by a decrease of dustiness despite a further increase of the

sample mass [81,85,118,129]. This observation is assumed to be caused by the atomization device geometry limiting the atomization process and/or a powder densification decreasing its dustiness [81,85,114,118,129].

The particle morphology, i.e. particle shape, surface structure, and resulting specific surface area, affects the powder flow and mixing behavior. These powder characteristics are caused by adsorption phenomena such as interparticle adherence as well as attraction to or repulsion from surfaces, which ultimately influence powder dustiness [100,122,129,130,132,148–151]. For example, fibrous elongated particles show a lower dustiness in comparison to granular particles [122].

The particle size and size distribution are also of major influence on dustiness [80,122,127,132,152,153]. The particle size directly affects binding and separation forces. In accordance with the Lifshitz theory of van der Waals forces and the mathematical description of rotationally symmetric liquid bridges by Schubert, binding forces based on van der Waals attraction and capillary forces are proportional to the particle diameter d. The separation forces, such as aggregate impaction, increase with d^3 according to the kinetic energy formula [127,154,155]. Nevertheless, because of several overlaying effects of the particle size, i.e. sedimentation of particles > 10 µm preventing their transport from the atomization site to the measuring site, the measured dustiness of a powder tends to increase with decreasing particle size [80,85,127,148,153]. In addition, the particle size distribution affects powder flow and powder dustiness, as the polydispersity index (PDI) is negatively correlated with dustiness [114,136,142].

Another important factor that has to be kept in mind when investigating dustiness, but which is not directly related to the powder, is the type and amount of energy introduced into the powder sample for atomization [123,127]. An increase in drag force or shear energy used for atomization results in higher fractions of atomized powder because of

a more effective powder disaggregation [114]. It must be ensured that the energy input is sufficient for atomization of the powder sample by disaggregation and separation of particles, but not too high to prevent grinding, cutting, or crushing of primary particles [112].

1.5 Dustiness determination

As described in Chapters 1.4.2 and 1.4.3, the dustiness of a substance may be determined with testing devices by application of a specified type and amount of energy to a predefined amount of test material. The resulting atomization of the material leads to a release of particles into the air and may be collected for quantification [112,114,127]. In an early study on this topic, Heitbrink et al. were able to find a significant correlation between worker dust exposure from a bag packing operation and the measured dust with two dustiness testers, in particular the Heubach dustmeter and the Midwest Research Institute (MRI) dustiness tester [156]. In the following decades, further dustiness testers were developed to predict the potential of different materials to cause dust exposures of workers in occupational settings [100,114,142,156–158].

1.5.1 Mechanisms for atomization

There are three basic underlying mechanisms for atomization of powder samples in dust testing devices [113,159]:

- Gravity dispersion: A powder sample is dispersed by dropping it into an enclosed space, such as a box shaped chamber, for example the Midwest Research Institute dustiness tester or the Palas dustview [115,160].
- Mechanical dispersion: The powder sample is placed in a drum with baffles and the powder is dispersed by rotation of the drum. The resulting aerosol is transported to the detection spot via an airflow directed through the longitudinal axis of the drum. An example is the Heubach dustmeter [115,127,161].

- Gas dispersion: Powder dispersion is achieved by directing a gas flow through the sample, for example in the University of North Carolina (UNC) dustiness tester or the Two-chamber setup (TCS) [76,81,126].

1.5.2 Sampling of airborne dust

As described in Chapter 1.4.1, certain particle fractions are of interest with regard to occupational exposure, especially the inhalable and respirable fractions [162,163]. For the collection of these fractions, different samplers have been designed and investigated for occupational dust monitoring. One of the first samplers was the overall respiratory burden (ORB) sampler with a spherical design. At the time of its development, no systematic studies of variables affecting particle entry efficiency existed. Thus, its design was largely based on trial and error [164]. Further inventions included portable rotating samplers to collect coarse particles and different blunt or close/open faced samplers as well as isokinetic probes for static or personal use [69,70,165–168]. Among other factors, these samplers were investigated and compared based on their particle size-specific sampling efficiency, sampling bias, precision, accuracy, and the effect of moving air on them [91,166,167,169–172]. So far, there is no ideal, universally accepted sampler for dust monitoring in occupational settings available. However, IOM samplers are currently the most scientifically well characterized personal dust samplers [29,36,173]. Other popular samplers include the DIS as well as CFC samplers [29,72]. An overview of the IOM sampler layout in its assembled (a) and disassembled state (b) is shown in Figure 4.

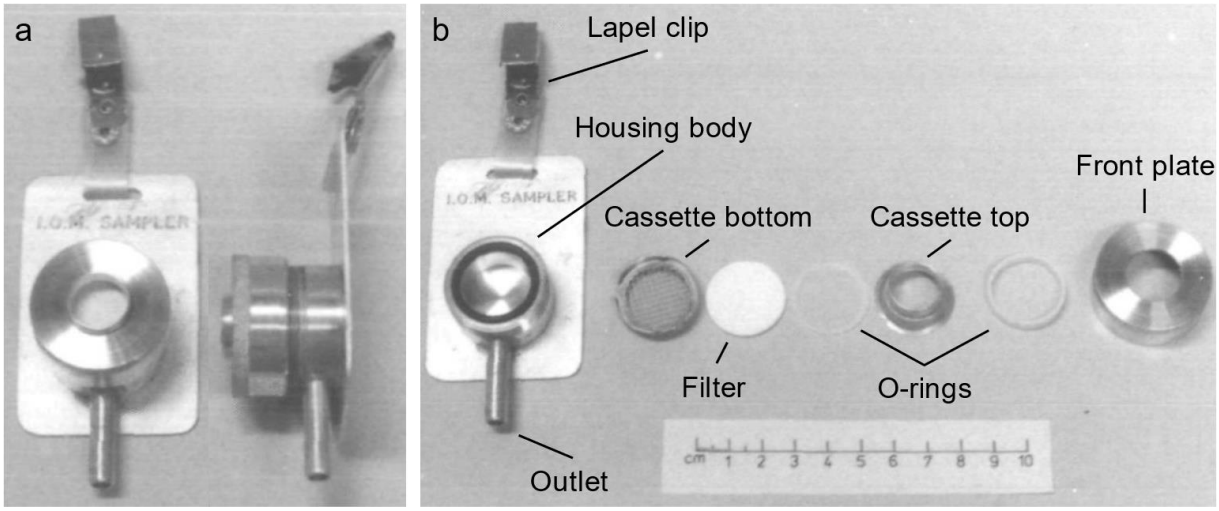


Figure 4: The original IOM sampler in its assembled (a) and disassembled (b) state, modified from [70].

The IOM sampler consists of a housing, into which a filter cassette with a 25 mm round filter is placed. The housing is closed with a front plate and O-rings ensure air tightness of the cassette. The filter cassette has a 15 mm circular orifice for entry of dust, with a protruding lip of 1.5 mm. For sampling, a vacuum pump connected to the outlet of the samplers generates an airflow with a volume flow rate of 2 L/min through the filter [70]. The sampler design has not changed since its first presentation in the literature in 1986 [29,70]. For occupational exposure measurements, the samplers are worn at the lapel of workers to be as close to their breathing region as possible [70]. In addition, they may be used for static sampling in the working environment [69]. The samplers collect particles of up to 90 µm corresponding to the inhalable fraction at wind speeds ranging from 1 to 3 m/s [69]. Dust detection with dustiness testing devices also follows the criteria for inhalable and respirable dust. Therefore, the above-mentioned samplers are also used for dust collection in dustiness testers.

1.5.3 Laboratory dustiness testers

A wide variety of devices for dustiness measurements of powders were presented in the last decades [99,100,174,118,120,123–125,127,157,158]. Most of these devices need a considerable amount of powder sample, up to hundreds of grams, and only a few of these systems are suitable for small sample quantities, for example powders of limited availability. These powders include APIs with high production costs and/or limited quantities [76,77,81,115,120,122,127,156,175].

As described in Chapter 1.5.1, there are three underlying mechanisms for atomization in dustiness investigations: gravity, mechanical and gas dispersion. These mechanisms involve and combine several factors affecting the atomization process, such as friction between particles and the atomization device, as well as particle interactions. An overview of forces involved in the atomization process of different dustiness testers is given in Table 4.

Table 4: Atomization forces for different dustiness testing devices, modified and extended from [123].

Atomization force	UNC dustiness tester	Heubach dustmeter	Continuous drop test apparatus	MRI dustiness tester	Palas dust-view	Two-chamber setup
Gravity	+	+	+	++	++	+
Friction (device)	0	++	0	0	+	0
Friction (air)	++	+	++	+	+	++
Particle interactions	0	++	0	0	0	0
Impaction	0	+	0	++	++	+
Dispersion	++	+	+	+	0	+

With 0 = no effect on the powder, + = effect on the powder, and ++ = high effect on the powder [123].

A brief introduction to the most commonly used devices and to those specifically developed for dustiness investigations of small powder quantities is given in the following subchapters.

1.5.3.1 UNC dustiness tester (Venturi device)

The UNC dustiness tester, in some references referred to as the Venturi device, is a chamber setup, specifically developed by the University of North Carolina for dustiness investigations of small pharmaceutical powder samples [76,152]. An illustration of its design and function is shown in Figure 5. With this tester, a powder sample of 5 ± 0.1 mg is turbulently dispersed through the nozzle of an injector into a 5.7 L sealed glass jar [76,126]. The device collects the resulting aerosol in a respirable mass cyclone with a 50 % cutoff at particles > 4 µm, followed by a filter cassette in which a Ø 37 mm filter is placed, collecting the respirable dust with an airflow of 4.2 L/min. A second filter cassette in the jar directly collects the total suspended dust with an airflow of 2 L/min. Dust is quantified gravimetrically by weighing the filters on which the dust had settled [76]. The Venturi device disperses powder samples at significantly higher Reynolds numbers than gravity-driven rotating drum or falling powder techniques and therefore has a unique ability in simulating high energy dust dispersion operations in the workplace [126,152].

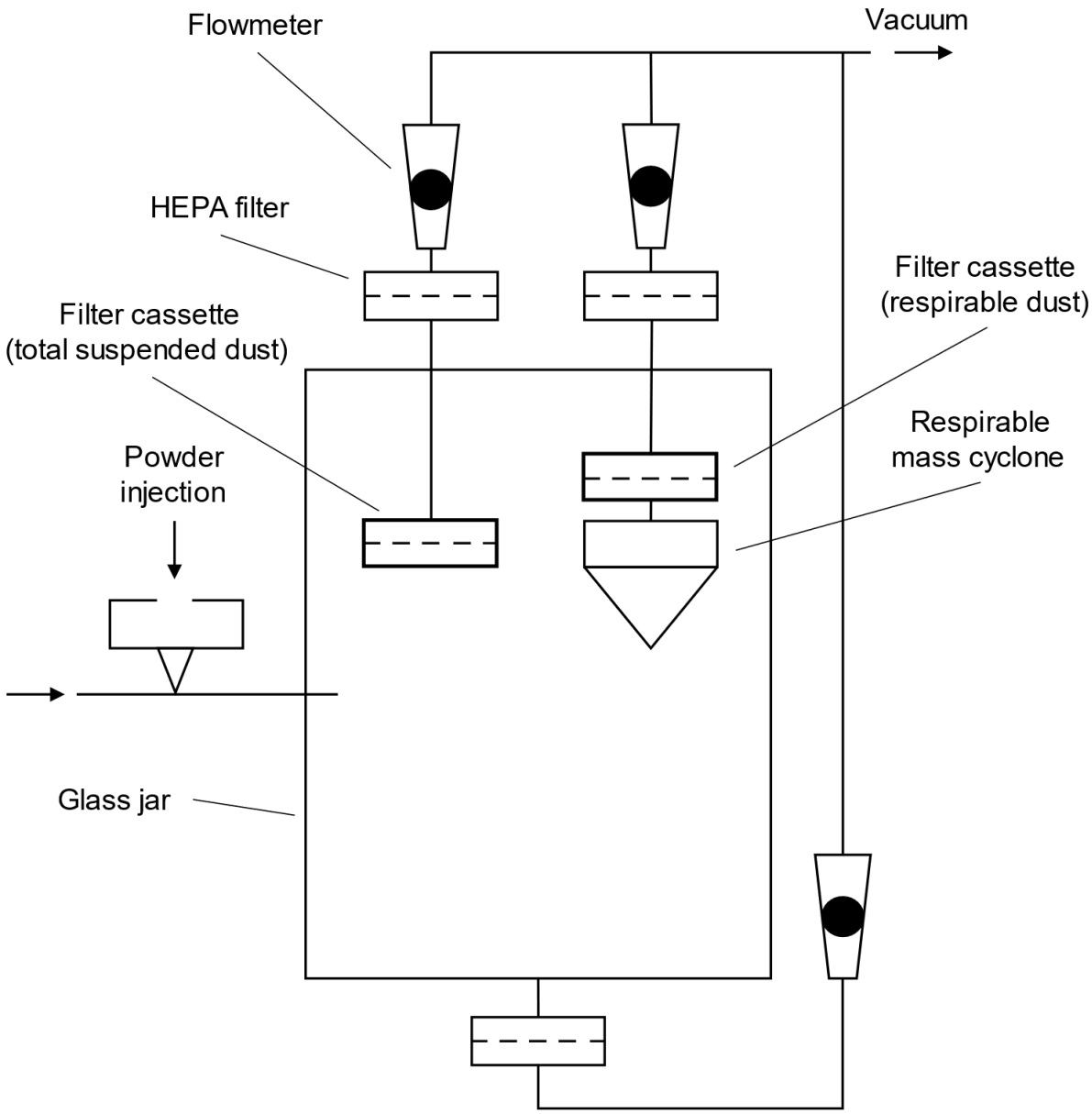


Figure 5: Schematic illustration of the UNC dustiness tester, modified from [76].

1.5.3.2 Heubach dustmeter (rotating drum tester)

The Heubach dustmeter is a rotating drum tester for powder samples of 1 up to 100 g, depending on the powder density [77,115,127,156]. A simplified scheme of the Heubach dustmeter is presented in Figure 6. For dustiness testing, the powder sample is placed in a dust-generating drum that rotates at 30 rpm [115,120,127]. Within this drum, three baffles are installed at an angle of 45° [113,127]. The baffles repeatedly lift the powder from the bottom to the top of the drum, from where the powder falls

down 14 cm [127]. An airflow of 2 up to 75 L/min is generated with a vacuum pump and the turbulent airflow is led horizontally through the dust-generating drum, carrying along airborne particles.

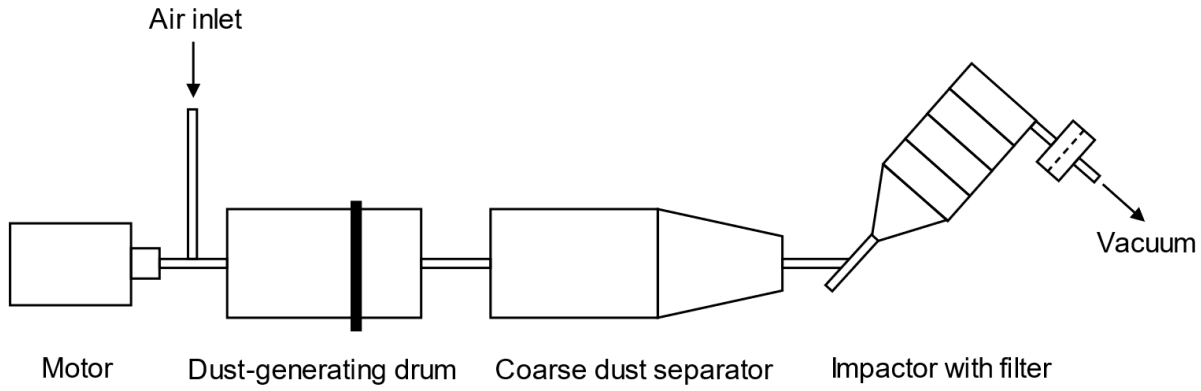


Figure 6: Simplified scheme of the Heubach dustmeter, modified from [115,127].

Coarse particles are separated in a dust separator and airborne particles are collected by an impactor and a Ø 37 mm glass fiber filter [115,120,127,174,176]. Measured dustiness is described by the Heubach dustiness index, which is calculated as follows:

$$\text{Dustiness index (\%)} = \frac{\text{Dust collected on the filter (g)}}{\text{Sample mass (g)}} \cdot 100\ \% \qquad \text{(Eq. 3)}$$

1.5.3.3 Continuous drop test apparatus

The continuous drop test apparatus developed by the 'Institut für Gefahrstoff-Forschung' (IGF) is described in the EN 15051 as reference test method B [120,175,177]. A schematic illustration of the apparatus is shown in Figure 7. For dustiness investigations, bulk material is transported via a metering device at mass flow rates between 6 and 10 g/min from the sample tank towards the drop pipe. Subsequently, the powder sample falls through the drop pipe into the airflow of the back flow pipe. This airflow is caused by a pump on top of the apparatus, and the air enters the device through holes in the collector tank. Simultaneously, sampling pumps generate an airflow of 2 L/min through Ø 37 mm glass fiber filters mounted within the

inhalable and respirable sampling heads to separate and collect the corresponding aerosol fractions [120,177].

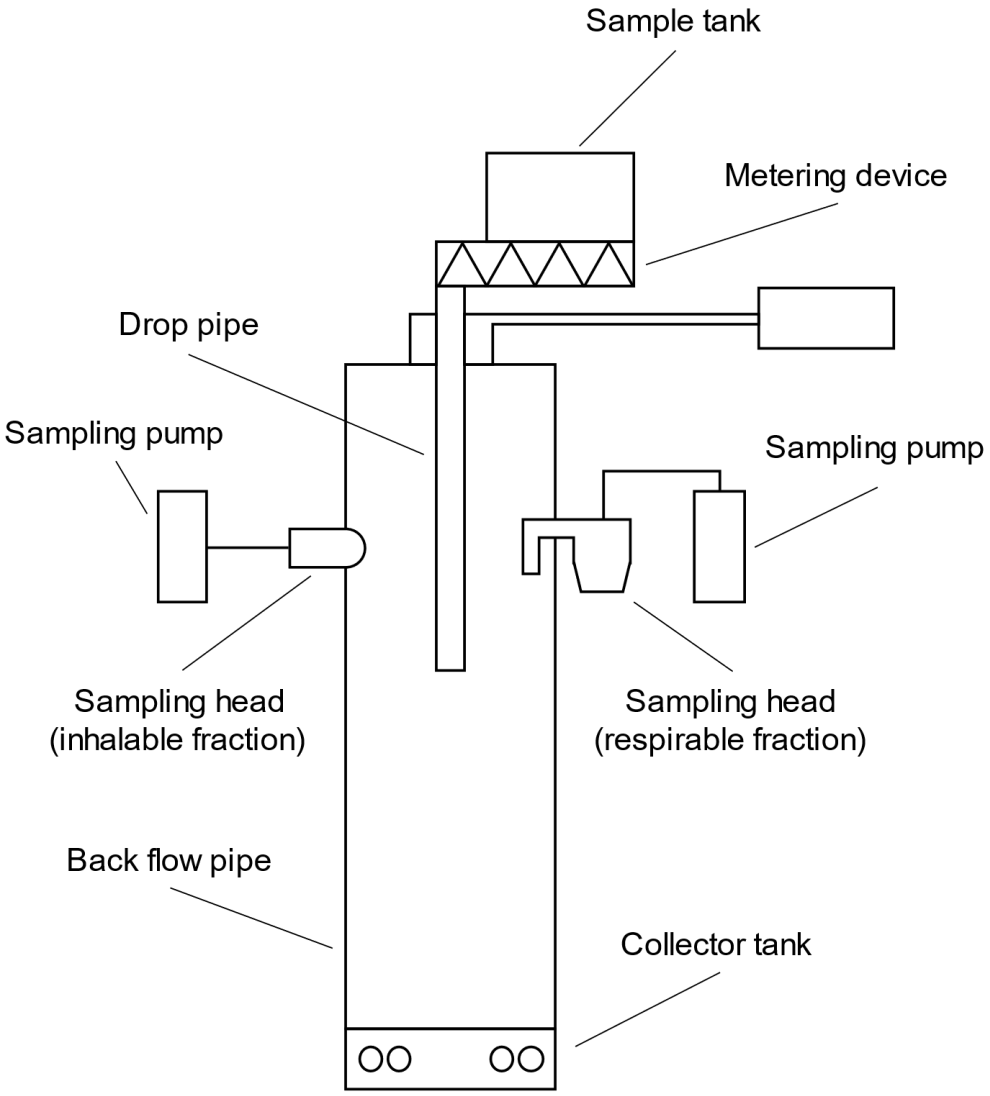


Figure 7: Schematic illustration of the continuous drop test apparatus, modified from [120,175].

Because of its relatively high feeding rates, the total sample amount may be as high as 180 g [120].

1.5.3.4 MRI dustiness tester

The MRI dustiness tester is a single-drop test apparatus and its design is shown in Figure 8. For measurements, a metal beaker with a volume of 270 mL is filled with a powder sample and the weight of the sample is noted. Subsequently, the beaker is rotated by 180° at a rotating speed of 5.5 rpm, whereby the powder sample is dropped out of the beaker and falls down for 25 cm [127,174].

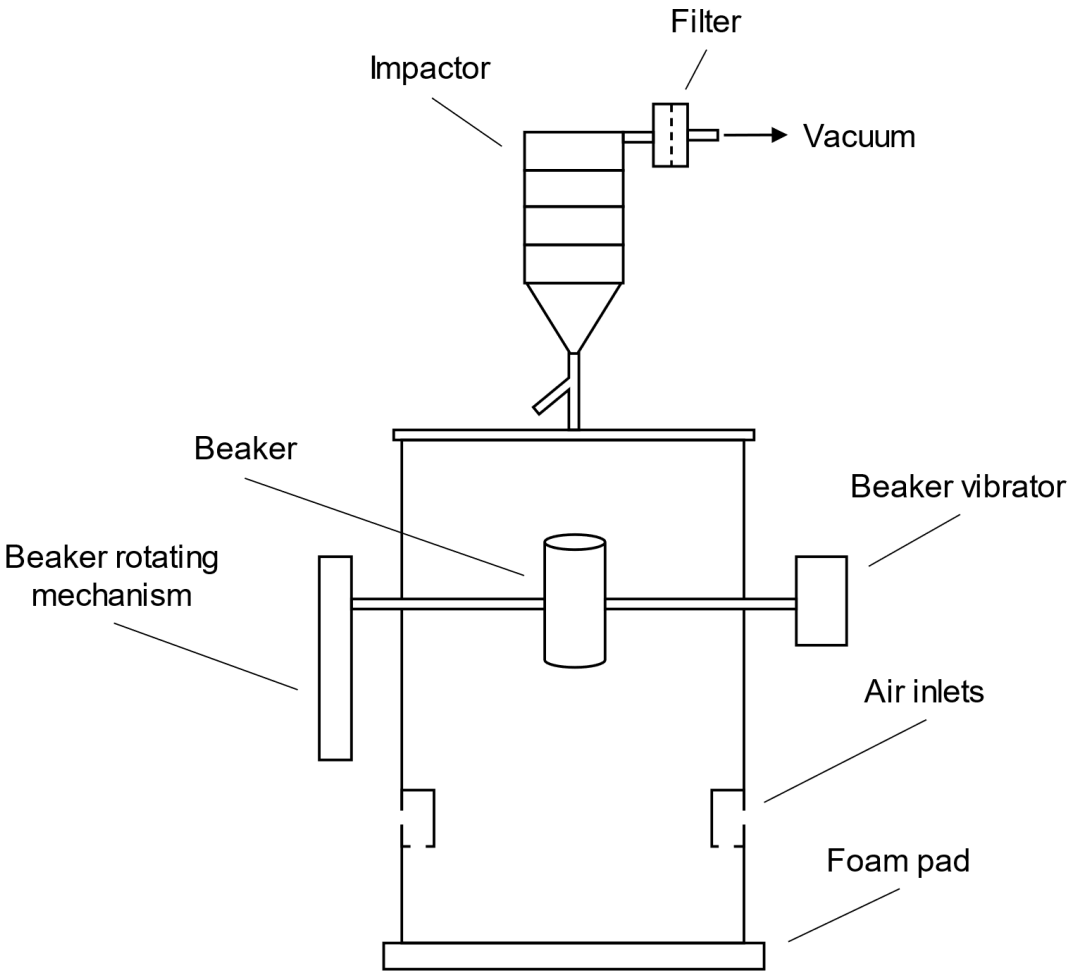


Figure 8: Schematic diagram of the MRI dustiness tester, modified from [127].

A vacuum pump draws an airflow with a rate of 10 L/min through a Ø 47 mm glass fiber filter, if necessary with a preconnected impactor positioned at the top of the chamber. Thereby, resulting airborne dust is collected for 10 min. The amount of airborne dust

is determined gravimetrically [127,156,174]. Dustiness is calculated similarly to the Heubach dustiness index (Eq. 3) [174].

1.5.3.5 Palas dustview

The Palas dustview is a commercially available dustiness tester, based on single drop atomization. A simplified illustration of the device is shown in Figure 9.

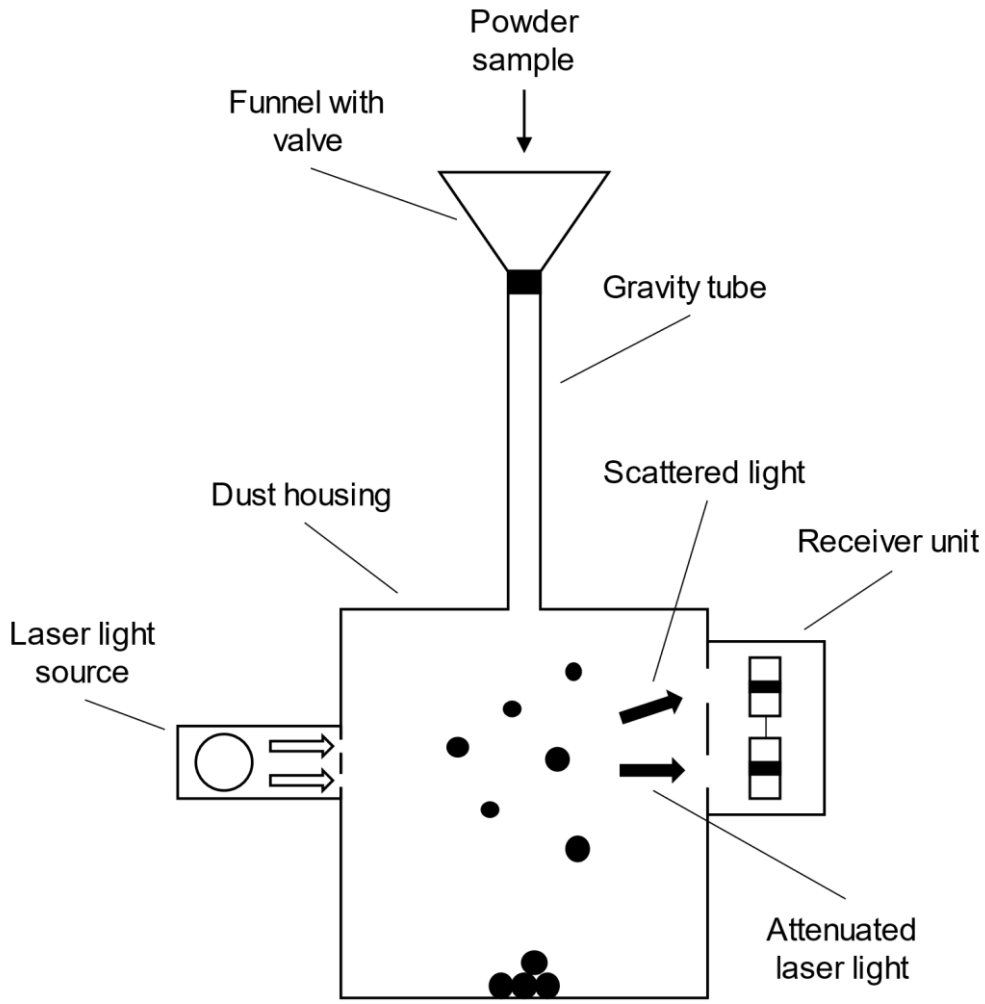


Figure 9: Simplified illustration of the Palas dustview, modified from [120,175].

For dustiness measurements, 30 g of a powder sample are transferred into a feed funnel. At the beginning of a measurement, the valve positioned underneath the funnel opens up automatically and the sample falls into the dust housing. Dustiness measurement is determined based on dust causing attenuation of the laser light. From the laser

light intensity detected 30 s after measurement start, as well as from the maximum intensity, the respirable and inhalable dust fractions are calculated [120,175].

1.5.3.6 Low-mass dustiness tester (LMDT)

In 2012, O'Shaughnessy et al. presented a low-mass dustiness tester (LMDT) based on the single drop method but capable of measurements of only milligram quantities of test powders [122]. A diagram of the LMDT is shown in Figure 10.

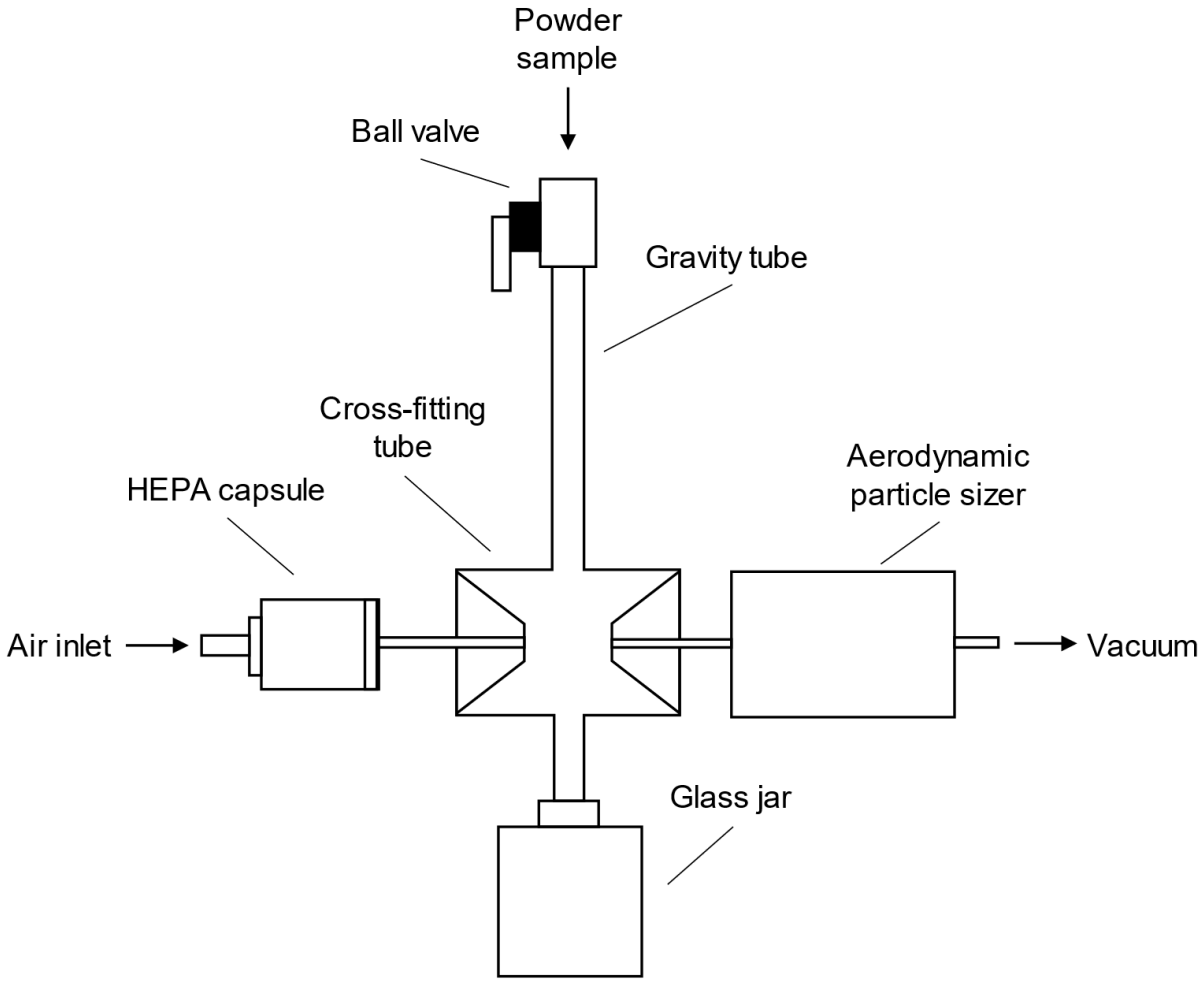


Figure 10: Diagram of the low-mass dustiness tester, modified from [122].

With the LMDT, sample quantities of 15 mg are sufficient to differentiate the respirable dustiness of various powder types. For dustiness measurements, the powder sample is transferred into a ball valve positioned at the top of the device. This ball valve is then opened, the powder falls down the gravity tube and enters a cross-flow section (cross-

fitting tube) in which small particles are captured by the sample airflow of 5 L/min and directed to the aerodynamic particle sizer (APS). The APS is an aerodynamic particle size spectrometer and determines the aerodynamic size of particles from 0.5 – 20 µm based on their time of flight [178]. Larger particles fall down through the cross-fitting tube and directly into a collecting jar. The respirable dustiness mass fraction of particles < 20 µm, detected with the APS, is calculated by multivariable regression analysis [122].

1.5.3.7 Two-chamber setup (TCS)

In recent years, a TCS was presented designed for investigations of the dustiness of pharmaceutical powders, for example APIs and binary mixtures of APIs with excipients in dependence on an oppositely directed airflow [80,81,148,179]. A simplified illustration of this setup is presented in Figure 11.

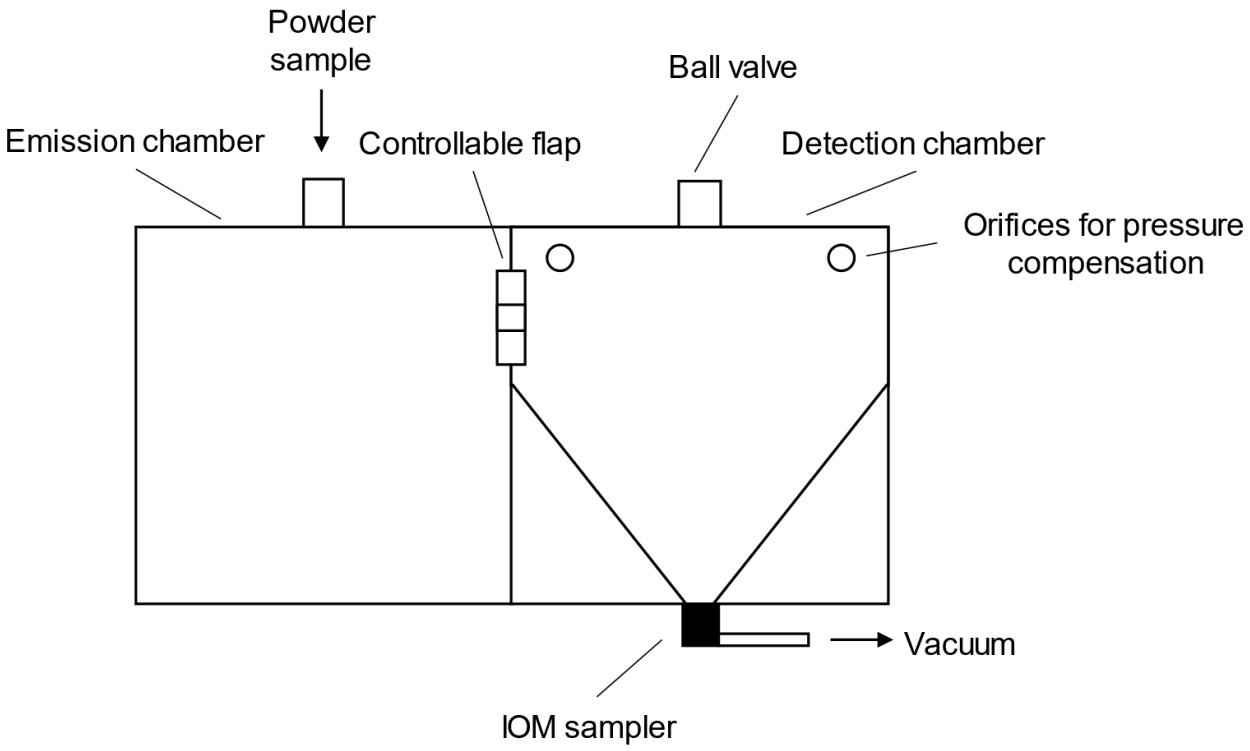


Figure 11: Simplified illustration of the Two-chamber setup, modified from [81].

The setup consists of two chambers, the emission and the detection chamber. Both chambers are connected by an orifice that may be opened and closed with a controllable flap. For measurements with the TCS, a powder sample between 50 and 400 mg is transferred into a double-acting ball valve and pneumatically atomized with compressed air [81]. After atomization, the controllable flap is opened and depending on the pressure difference between both chambers, which is achieved by compressed air led through the corresponding ball valve on top of the detection chamber, the distribution of dust under diffusive and/or convective conditions may be investigated. For dust collection, an airflow of 5 L/min is directed through a glass fiber filter within the IOM sampler, which is positioned beneath the detection chamber. The subsequent quantification of the collected dust is performed by HPLC analysis [80,81,148].

1.5.4 Comparability of the dustiness testers for exposure prediction

In a study by Carlson et al., the authors state that the results of laboratory dustiness measurements of the same substance strongly vary depending on the applied test method. If at all, the results may be compared qualitatively, but not quantitatively. The authors further postulate that no laboratory dustiness tester provides accurate predictions about workplace exposure [115]. These results are underlined by a comparison of dustiness data determined with three dustiness testers (continuous drop test apparatus, Heubach dustmeter, and Palas dustview), which did not confirm equivalence between the testers [120]. Furthermore, the correlation of laboratory dustiness data with dust emissions released by mechanical powder stressing during production processes is impossible in most cases [99]. To address these problems, dustiness measurements should always be referred to a reference powder. Thereby, it should be possible to make ‘informed judgements’ about the dustiness of a powder determined with different testing devices [76]. Moreover, the sampling of emitted dust has to focus on the health-related aerosol fractions, and the mechanism of atomization

must reflect the dust generation by handling of powdery materials at the workplace [112]. Even though the transferability of dustiness measurements to occupational settings is subject to discussion, with fixed location sampling it should be possible to identify areas within the workplace where dust is emitted. [68].

1.6 Novel approaches for airborne dust detection

As the filter-based sampling methods described in Chapter 1.5.2 have major limitations, novel approaches for airborne dust detection have been developed, which are based on optical methods. In contrast to sampling methods with subsequent gravimetrical or wet chemical analysis, optical detection allows time-resolved investigations of dust concentrations in real-time [180–183]. Furthermore, most of these methods allow the detection of size-specific particle concentrations, for example the monitoring of the inhalable fraction or of fine particulate matter of airborne dusts [181,184]. In the following subchapters, two of today's most commonly used methods for the determination of airborne dust concentrations are presented.

1.6.1 Aerodynamic particle sizing

The aerodynamic particle sizer, as part of the LMDT (please refer to Chapter 1.5.3.6), is based on time of flight measurements [122,185]. A schematic diagram of the particle sizer is displayed in Figure 12. Aerosol particles are accelerated through a nozzle in a sonic expansion flow until their velocity temporarily falls behind that of the surrounding air molecules (ultra-Stokesian flow) [183,186,187].

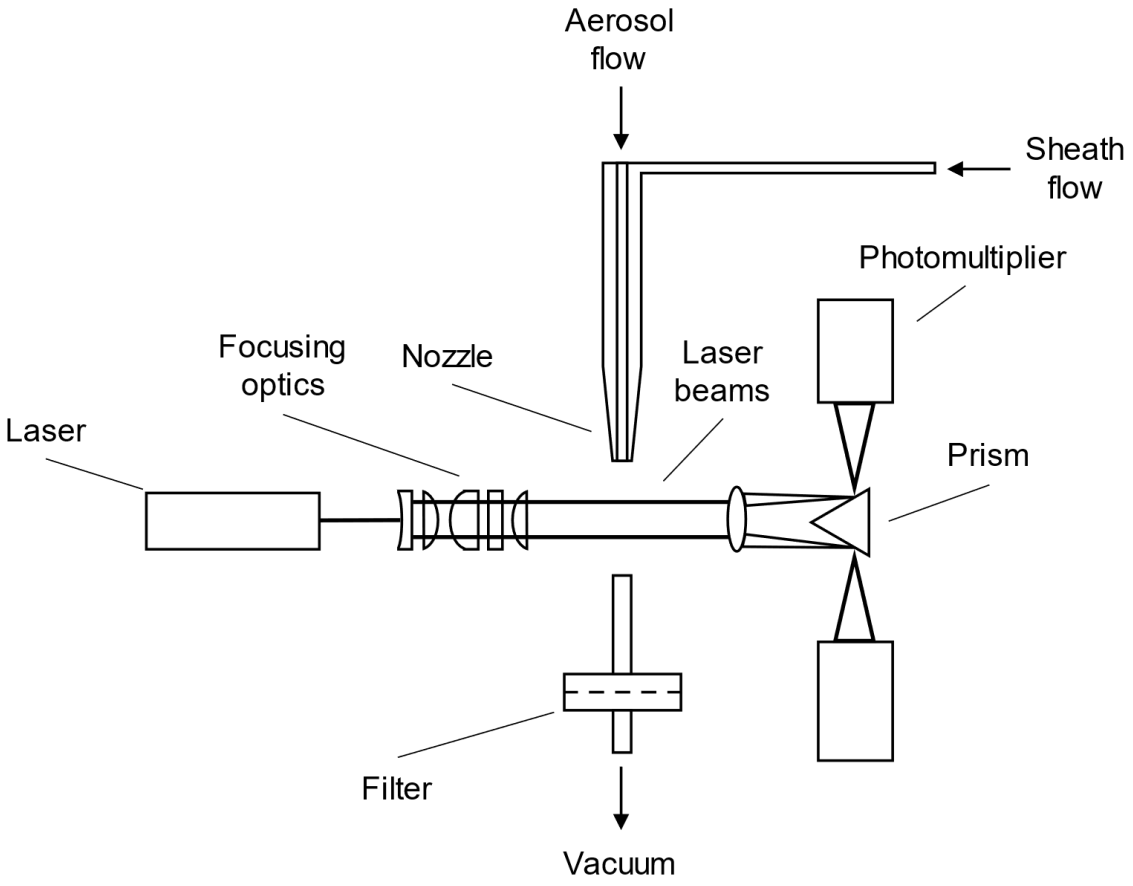


Figure 12: Schematic diagram of a time-of-flight aerodynamic particle sizer, modified from [185,186].

The aerosol particles then pass through two parallel light beams of fixed distance. Thereby, the time-of-flight of the particles needed for passing from the first to the second light beam is measured. The time-of-flight is dependent on the aerodynamic particle size [183,188]. With this method, particles within a range of 0.2 and 700 µm in aerodynamic diameter may be detected and the resulting individual particle signals are converted into a number-weighted size distribution [183,186].

1.6.2 Optical particle counter (OPC)

As mentioned in Chapter 1.4.1, not only inhalable particles of HPAPIs pose a health risk, but also fine particulate matter in general. Because of their ability to reach even deep regions of the lungs, particles < 10 µm (PM_{10}) and < 2.5 µm ($PM_{2.5}$) pose a threat to human health [104,109,189,190]. As the monitoring of air pollution, especially of fine

particulate matter, is of high priority concern in environmental hygiene, affordable low-cost particulate matter sensors (PM sensors) have been developed in recent years [181,184,191,192]. The majority of these sensors are OPCs and their principle of detection is based on light extinction (large particles) and/or on the Mie scattering theory (small particles) [74,193–195]. A simplified diagram of an OPC based on light scattering is presented in Figure 13.

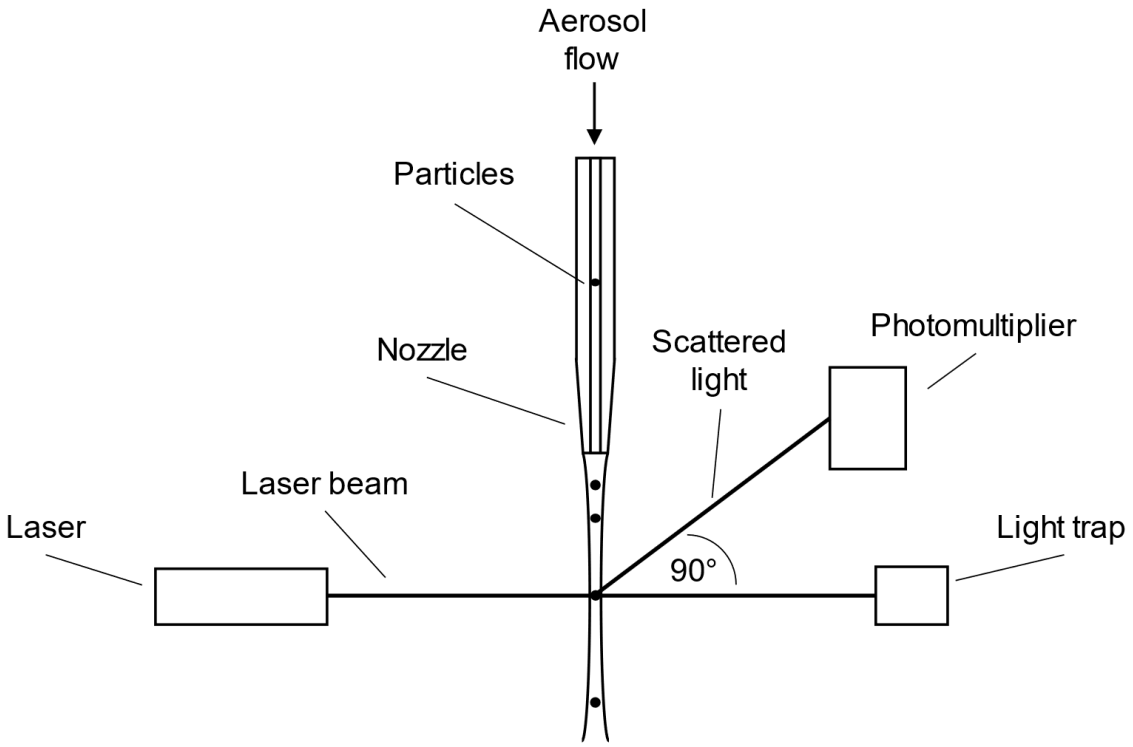


Figure 13: Simplified diagram of an OPC, modified from [194].

In the first step of a measurement, aerosol particles are drawn into a narrow inlet of the OPC by a fan. Subsequently, the particles pass through a laser curtain and the light scattered by the particles is detected at a perpendicular angle to limit the effects of stray light within the device. In accordance with the Mie theory, the pulse height of each of the measured signals correlates with the respective particle size [194,196]. Particles are counted and tabulated into size categories to determine their number concentration [194]. This number concentration may be subsequently converted into a

mass concentration as necessary for occupational exposure assessment [197–199]. In addition to their use in environmental hygiene, OPCs also play a role in other scenarios, for example in monitoring of dust containment at construction sites as well as personal dust exposure, and in pharmaceutical contexts such as aerosol characterization of single-dose inhalers [75,200,201].

1.6.3 Substance-specific real-time monitoring of airborne dust

As mentioned in Chapter 1.2.5, substance-specific real-time monitoring with optical methods is currently under development [29]. Such a monitoring would significantly improve the safety in the contained manufacture of pharmaceuticals. There are several potential detection methods being investigated for monitoring, including the electronic sum frequency scattering, ion mobility spectrometry, photoacoustic spectroscopy, and laser-induced breakdown spectroscopy [202–209]. Another promising approach for real-time aerosol monitoring has been presented in a study based on a polarized optical particle counter combined with deep learning of multi-angle synchronous polarization scattering indices [210,211].

1.7 Computational Fluid Dynamics (CFD)

1.7.1 CFD and its application in pharmaceutical contexts

CFD simulations are a versatile tool for analyzing complex air and fluid flow dynamics and are gaining importance in the pharmaceutical field [212]. The three-dimensional mathematical simulation of fluid motion is defined by the Navier-Stokes equation, which is based on the conservation of mass, momentum, and energy, whereby several physical properties of the fluid, such as pressure, density, and viscosity, have to be taken into consideration [212,213]. CFD simulations provide a numerical approximation to this equation and present the results in a graphical and easy to read format [213]. They have been used to characterize particle deposition in human lungs, to

simulate the dynamic flow and particle motion in dry powder inhalers as well as air movement in the UNC dustiness tester, Heubach dustmeter, and TCS [80,81,106,126,176,214].

1.7.2 CFD coupled with discrete element modeling (DEM)

A combined approach for aerosol simulation is CFD-DEM coupling. With this method, CFD is again used to simulate the airflow, but is combined with the simulation of individual aerosol particles via DEM [215–218]. This combination has been used to characterize particle-fluid, particle-particle as well as particle-device interactions in rotary drum dustiness testers, providing valuable insights on lift and drag forces caused by airflow and device geometry acting on individual particles [219]. Furthermore, the in vitro-in vivo correlation of aerosol particle deposition in the human respiratory tract has been predicted by the gas-aerosol flow behavior [220]. Additional studies in recent years include the investigation of the dispersion mechanism in dry powder inhalers, the characterization of fluidized beds, and even the simulation of non-spherical particles, emphasizing the increasing importance of CFD-DEM coupling in the pharmaceutical field [216–218].

2. Aim of the work

In recent years, an increasing number of innovative and highly potent APIs have been developed using high-throughput screening, combinatorial chemistry, and Artificial Intelligence. Although beneficial for the treatment of millions of patients worldwide, HPAPIs pose a major risk because of their high pharmacologic and toxicologic potential during handling. Dust emissions caused by handling HPAPIs must be minimized to prevent cross-contamination during the manufacture of pharmaceuticals, exposure of personnel, and contamination of the environment. Therefore, the so-called containment technology has been implemented in the manufacture of pharmaceuticals. However, in practice, dust emissions are still being detected in contained production environments and it has not yet been possible to draw conclusions from the determined exposure data with regard to the sources of contamination because of a lack of knowledge concerning aerosol transport mechanisms. So far, no device has been developed to investigate the spatial distribution of pharmaceutical airborne dusts. Therefore, the aim of this work was the development of a laboratory scale chamber setup to investigate not only dustiness but also the subsequent spatial distribution of airborne dust with small amounts of pharmaceutical powders. The newly developed chamber setup consists of an emission chamber in which a powder sample is atomized. This emission chamber is connected to a larger detection chamber equipped with nine measurement spots to determine the spatial distribution of dust. The detection chamber itself has a modular design and the emission chamber may be connected to the detection chamber at one of nine different positions. This setup allows an investigation of the spatial dust distribution in multiple spatial orientations. For the experiments, ACAM was used as a safe surrogate substance, as it is a suitable surrogate for small chemical compounds and shows low toxicity, a low quantification limit as well as high dustiness.

The aim of the first study of this work was to prove the functionality of the chamber setup with regard to the reproducible atomization of small powder quantities and the determination of the spatial distribution of airborne dust. Therefore, small amounts of ACAM were atomized in the setup and the spatial ACAM distribution was determined in an opposite and an orthogonal arrangement. In this first study, only one combination of atomization parameters was used, yet indicating a strong influence of the pneumatic atomization on the spatial dust distribution.

Because the pneumatic atomization of powder samples has not yet been characterized in the existing literature, the second study focused on the investigation of the atomization parameters in more detail by means of statistical design of experiments. Moreover, the measurement procedure was evaluated and subsequently optimized to increase the amount of detected airborne dust. Based on the results, the influence of particle size distribution and particle shape on dustiness and spatial distribution of dust was investigated.

The third study considered technological developments of recent years, and the chamber setup was therefore equipped with laser-based low-cost particulate matter sensors, originally developed for environmental hygiene scenarios. This modification of the chamber setup allowed the detection of the spatiotemporal distribution of airborne dust in real time. With this modified setup, it was not only possible to examine the plain surrogate ACAM but also the excipient lactose and a binary powder blend of both.

3. Cumulative part of the dissertation

3.1 Investigations on the spatial dust distribution for emission site localization in containment

This first study dealt with the development and proof of concept of a novel chamber setup designed for the investigation of the spatial distribution of pharmaceutical dusts. The setup consists of an emission chamber in which small powder quantities, in the case of this study the surrogate substance ACAM, were atomized by compressed air. The emission chamber is attached to a detection chamber at one of nine possible positions and the atomized sample may pass through a connecting orifice from the emission to the detection chamber via convective and diffusive mass transport. The detection chamber may be set up in an opposite or orthogonal arrangement and the airborne dust eventually settles on the filters located within the nine measurement spots.

The evacuation time required to gather the complete aerosol content of the detection chamber filled with the fume of sulfuric acid was determined to be 278 min. Based on this result, a subsequent investigation with varying sample amounts of ACAM revealed a linear relationship between sample mass and detected dust emission. The experiments with ACAM confirmed that with the presented chamber setup, a precise and reproducible atomization as well as detection of small amounts of powder samples may be realized.

The spatial dust distribution was expected to show the highest concentration of airborne dust close to the emission site, with decreasing concentrations at the more distant measurement spots. However, the results with the orthogonal arrangement of the detection chamber revealed the opposite. To explain these results, CFD simulations were carried out. The results of these simulations resembled exactly the pattern of the spatial dust distribution measurements, indicating a strong influence of the

airflow caused by the pressurized air for atomization on the spatial dust distribution. The combination of these results allowed an exact three-dimensional localization of the emission site within the chamber setup. In addition to the experiments with the chamber setup, the powder properties of ACAM were analyzed to identify factors that may influence dustiness or spatial dust distribution.

In Figure 14, a visual summary of the study is shown, pointing out the similarity of the spatial dust distributions detected in the chamber setup with both arrangements, and the simulated airflows of the computational fluid dynamics.

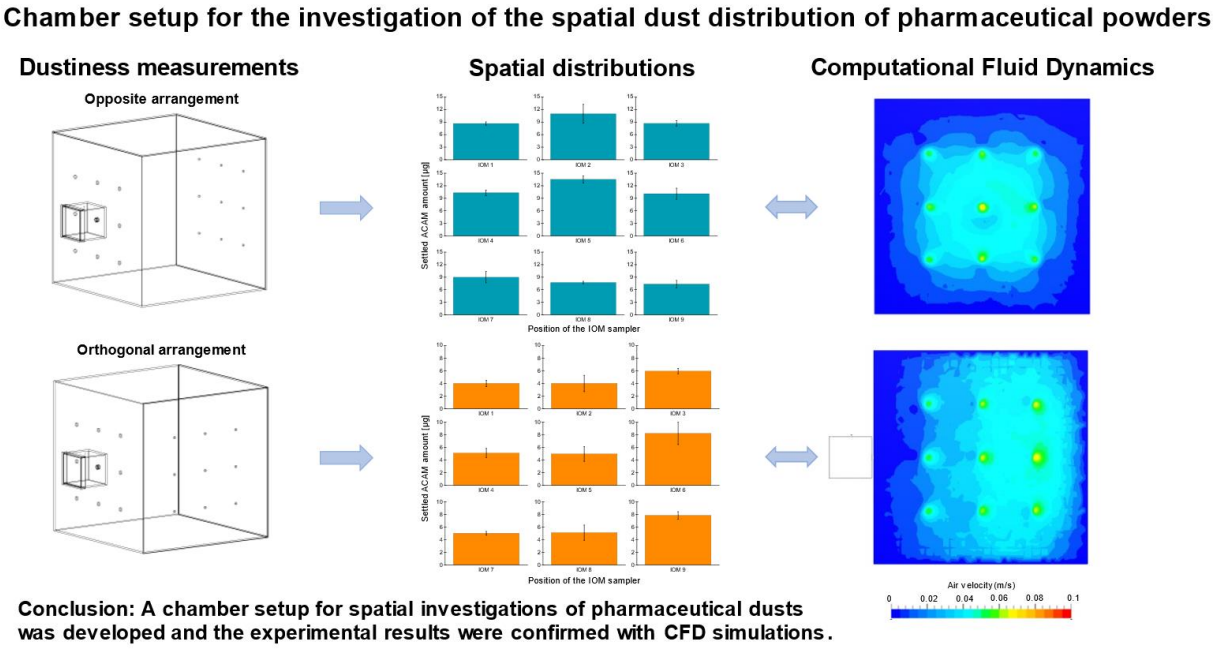


Figure 14: Visual summary of the study methodology and key results [221].

In summary, the first study was a successful proof of concept of the presented chamber setup. Because a strong influence of the pneumatic atomization on the detected dustiness and the spatial dust distribution became apparent, a subsequent study was performed to investigate the atomization process in detail.

AAPS PharmSciTech (2025) 26:239
https://doi.org/10.1208/s12249-025-03236-y

RESEARCH ARTICLE

Investigations on the Spatial Dust Distribution for Emission Site Localization in Containment

Hendrik Küllmar[1] · Martin Schöler[2] · Jonas Brügmann[2] · Claudia S. Leopold[1]

Received: 19 June 2025 / Accepted: 10 September 2025
© The Author(s) 2025

Abstract

Dustiness and the spatial distribution of dust are major problems when working with highly active pharmaceutical ingredients. Therefore, the aim of this study was to develop a chamber setup that allows a reproducible atomization of small powder quantities and the detection of not only dustiness but also the spatial distribution of airborne dust at extremely low concentrations, to prove that an emission site may be localized with stationary sampling even in a confined space. For this purpose, the time required for evacuation of the chamber setup was determined with fuming sulfuric acid. In subsequent atomization experiments, the safe surrogate acetaminophen was used. The spatial distribution of the surrogate was detected with nine IOM samplers (Institute of Occupational Medicine) and its quantification was carried out via HPLC. A linear tendency of the quantity of aerosol formed in dependence of the sample mass was demonstrated. In addition, significant differences between individual spots of detection and thus a spatial distribution in the detection chamber was observed. These results indicated a strong convective mass transport within the chamber setup. To verify these results, the airflow used for atomization was simulated using Computational Fluid Dynamics, confirming the convective mass transport and the spatial distribution of the airborne acetaminophen dust. In summary, it was shown that an emission site may be localized based on stationary exposure data even at concentrations as low as those mandatory in the contained manufacture of HPAPI-containing pharmaceuticals.

Keywords computational fluid dynamics · containment · dustiness chamber · IOM sampler · spatial particle distribution

Introduction

In the past decades, there has been great progress in the field of pharmaceutical drug development [1]. By high-throughput screening, combinatorial chemistry and computational techniques such as artificial intelligence, innovative and often highly potent active pharmaceutical ingredients (HPAPIs) have been developed [2–4]. Although beneficial for the patient, HPAPIs often pose an increased risk for the personnel in the pharmaceutical industry as well as a challenge during manufacturing. On the one hand, cross-contamination during manufacturing has to be avoided, and on the other hand, the exposure of personnel to the HPAPIs must not exceed a tolerable level. For this purpose, so called Occupational Exposure Limits (OELs) were defined, which specify the maximum acceptable airborne concentration of an API in production environments. Depending on the API these concentrations may be as low as 0.1 µg/m^3 [5–8]. Apart from this, environmental pollution is a global concern which is why the release of HPAPIs into the environment must be prevented [9]. In addition to these hazards, dust generated during manufacturing processes may pose a risk due to potential charge accumulation caused by tribocharging and local accumulation of dust in specific areas of the production environment, which may result in inadvertent contamination of materials and surfaces or even in dust explosions [10, 11]. With regard to dust explosions, key factors influencing the ease of ignition and burn rates include primary particle size distribution, cloud turbulence and the particle concentration distribution inside the dust cloud [12]. However, a basic condition for a dust cloud to be explosive, is that its concentration usually has to be several orders of magnitude higher than even typical dust concentrations in unpleasant dusty atmospheres in production environments,

✉ Claudia S. Leopold
claudia.leopold@uni-hamburg.de

[1] Division of Pharmaceutical Technology, University of Hamburg, Bundesstraße 45, 20146 Hamburg, Germany

[2] Fette Compacting GmbH, Grabauer Straße 24, 21493 Schwarzenbek, Germany

Published online: 09 October 2025

thus far exceeding any acceptable concentrations in the contained manufacture of pharmaceuticals [5–8, 11].

To effectively prevent the above-mentioned dust exposure risks, containment measures are implemented in the manufacture of pharmaceuticals. In tableting with rotary tablet presses, for example, these measures are realized by a housing around the tablet press itself and the application of reduced pressure inside that housing. In addition, high performance filter systems for the ambient air, special transfer valves for powder feed and isolators are implemented at the production site [13, 14]. Nevertheless, in practical applications, emissions of the active ingredient are still detected at stationary measuring points outside the containment housing due to the dust generated during the tableting process. The positioning of these measuring points is based on the assessment of the contamination risk at certain locations of the tablet press, such as the operator panel or the product outlet of the press. However, it has not yet been possible to draw conclusions from the stationary exposure data obtained by these measurements regarding the causal contamination sources, i.e. emission sites of the production machines [13, 15]. In addition to the pharmaceutical industry, the generation and spatial distribution of airborne dust poses a threat in various other industrial sectors, such as the mining, construction and woodworking industry [16–20]. Because of the large size of these production areas and the relatively high concentrations of generated airborne dust, these studies usually investigate the spatial distribution of dust with optical sensors or meteorological image analysis [16–20]. Unfortunately, these methods are neither substance-specific, as desired in containment investigations because only HPAPIs pose a threat to the health of employees, nor capable of detecting extremely low airborne dust concentrations due to their relatively high detection and quantification limits [21–23]. Optical sensors are thus only suitable to a limited extent for containment investigations, as substance-specific sensors are still under development [15].

Dustiness is defined as the propensity of a material to generate airborne dust during its handling. It can be tested by applying a specified type and amount of mechanical energy to a specified amount of test material for a specified time period in order to overcome adhesive binding forces within the test material, and thus to release particles into the air [24, 25]. It is a well-known fact that the dustiness of powders is dependent on various physicochemical powder properties such as moisture content, particle shape and density. In addition, there are statistical powder characteristics, for example the particle size distribution, which may have an influence on dustiness [24]. Beyond that, the type of energy input needed for atomization and the geometry of the measuring system itself have to be taken into account, because the energy input and the flight path from the atomization to the detection site may influence the measured dustiness [26].

As the handling of materials, for example milling, conveying, filling, and mixing leads to dust release and poses a problem in different industries, various chambers for dustiness measurements of powders have been described over the last decades [27–34]. Unfortunately, most of the above-mentioned systems require a relative high amount of powder sample, which presents a problem when working with active pharmaceutical ingredients (APIs) with high production costs and sometimes limited quantity. Considering the high number of publications focusing on dustiness only few describe systems suitable for small sample quantities and/or pharmaceutical powders [35–38].

Based on the above-mentioned remarks and the potential health risks associated with the handling of HPAPIs, safe surrogate substances are used for testing of containment equipment and pharmaceutical dustiness investigations. These substances include, among others, acetaminophen, naproxen sodium, lactose and insulin. The choice of the surrogate should be based on its physicochemical powder properties and limits of analytical quantification [6, 39].

For the analysis of complex dynamics of air and fluid flow, Computational Fluid Dynamics (CFD) simulations which are already established in the automotive and aerospace industries and gaining importance in the pharmaceutical field, are a versatile tool [40]. It has already been used to characterize the dynamic flow, particle motion and deposition in dry powder inhalers as well as in dustiness testing setups [41–43]. These simulations can be used for the investigation and visualization of atomization processes and the spatial distribution of the aerosols in a dustiness testing chamber setup [38, 42].

As mentioned above, only the dustiness of pharmaceutical powders but not the spatial distribution of dust, especially that of smallest amounts of atomized APIs resulting in very low concentrations, as necessary for investigations in the context of containment, has so far been investigated. Therefore, the objective of this study was to develop a novel chamber setup consisting of an emission and a detection chamber to investigate the spatial distribution of pharmaceutical dusts. One aim was to ensure that the chamber setup allows to gather the complete content of the detection chamber so that each atomized aerosol sample may be detected entirely with IOM samplers (Institute of Occupational Medicine). A further aim was to verify that the newly developed chamber setup is capable of reproducible and precise atomization of small amounts of pharmaceutical powders and that it allows the investigation of the spatial distribution of pharmaceutical dust inside the detection chamber to proof its ability of emission site localization based on stationary exposure data in laboratory scale containment investigations.

Materials and Methods

Chamber Setup

The experimental setup consists of two chambers, the emission and the detection chamber, as shown in Fig. 1. The inner dimensions of the emission chamber are 19.4 cm × 19.4 cm × 19.4 cm resulting in a volume of approximately 7.3 L. In the top plate of the emission chamber an orifice with an attachment point for a pneumatic double-acting ball valve is positioned. The detection chamber shows inner dimensions of 100 cm × 100 cm × 100 cm which results in a volume of 1 m^3. The chamber setup represents a modular system: The emission chamber can be connected to the detection chamber at one of nine possible positions through a protruding tube with an inner diameter of 2.54 cm fixed at the emission chamber. The eight unused attachment positions of the detection chamber are closed with specially designed seals. This allows the investigation of multiple emission site positions in one system.

The detection chamber can be set up in two different arrangements. Two of the panels of the detection chamber are interchangeable, so that the measurement spots may either be positioned on the opposite site of the emission chamber or in an orthogonal arrangement (Fig. 2).

For dust detection nine IOM samplers (I.O.M. Multi-Dust samplers, SKC, Blandford Forum, UK) are attached to the measurement spots and connected to independent flowmeters with a flow rate of 0.4–5 L/min (MR3000, Key Instruments, Croydon, USA). The flowmeters are connected to an air sampling pump (Flite 4, SKC, Blandford Forum, UK) as

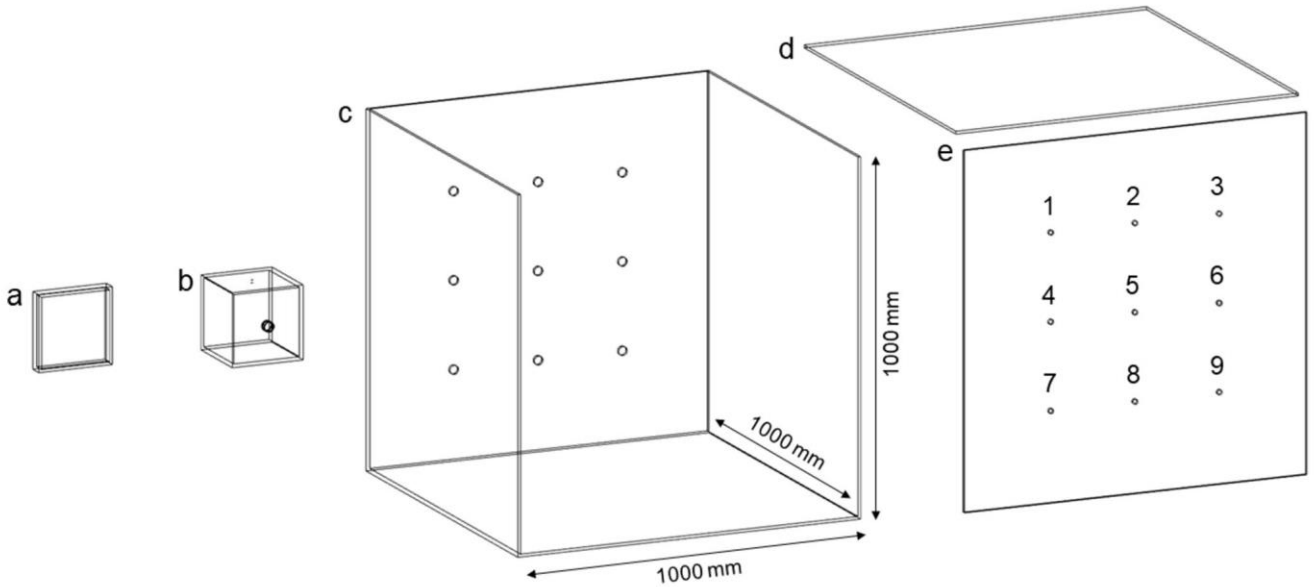


Fig. 1 Simplified illustration of the disassembled chamber setup for dust measurements, consisting of an emission chamber with a detachable lid and a modular detection chamber: **a** detachable lid, **b** emission chamber, **c** detection chamber, **d** interchangeable panel, **e** interchangeable panel with measurement spots 1–9

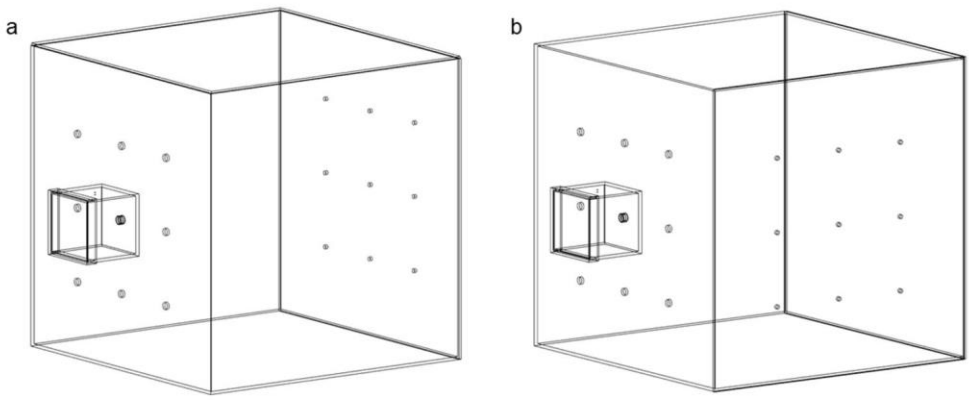


Fig. 2 Chamber setup in opposite (**a**) and orthogonal (**b**) arrangement

shown in Fig. 3. The lid of the emission chamber is detachable for cleaning purposes. A rubber seal is attached to the edges of the emission chamber and to the interchangeable panels of the detection chamber. The remaining four panels of the detection chamber are sealed with silicone to ensure tightness. The panels of both chambers consist of acrylic glass with a thickness of 0.8 cm. An outer framework of aluminum B type profiles is fastened to the panels of the detection chamber with polyurethane glue for stabilization. The aluminum framework is also used to mount various control and measuring instruments such as pneumatic valves, flowmeters and a programmable logic controller (PLC). A grounding cable is attached to the aluminum profiles to dissipate electrostatic charges. As shown in Fig. 3, a double-acting ball valve (KH 14 P, Pneumatikatlas, Lübeck, Germany), used for atomization of the powder samples, is positioned above the emission chamber. The ball valve is pneumatically controlled by a 5/2-way solenoid valve (VUVS-L25-M52-AD-G14-F8, Festo, Esslingen, Germany). 3/2-way solenoid valves (VUVS-LK25-M32C-14-B, Festo, Esslingen, Germany) are used to control two 3/2-way pneumatic valves (SFP4701, YPC, Jeongwang-Dong, South Korea). One of these two pneumatic valves controls the airflow through the IOM samplers. The other valve controls the flow of pressurized air used for atomization. A pressure reducing valve (Futura 1 RP14-2 F, Riegler, Bad Urach, Germany) and a flowmeter with a flow rate of 10–100 L/min (MR3000, Key Instruments, Croydon, USA) regulate the pressurized air for atomization. All valves of the chamber setup are controlled by a PLC (Siemens LOGO! 12/24 RCE, Munich, Germany). The PLC can be started via a simple toggle switch and the programmed sequence ensures that the complete measuring process takes place in a precise chronological order. The chamber setup is positioned in a climate room to control the environmental conditions during the experiments. Temperature in the climate room is set to 20°C and relative humidity to 40%.

Determination of the Evacuation Time with Fuming Sulfuric Acid

To determine the necessary evacuation time for gathering the complete aerosol content of the detection chamber fuming sulfuric acid was used for flow visualization. Therefore, a Dräger Air Flow Tester (Dräger, Lübeck, Germany), was inserted into the pressurized air tube between the source of compressed air and the double-acting ball valve. Subsequently, the 3/2-way pneumatic valve and the double-acting ball valve, controlled by the PLC and positioned above the emission chamber (Fig. 3), were opened. By this means, the white fume of sulfuric acid was introduced into the emission chamber for 60 s. Simultaneously, the 3/2-way pneumatic valve between the sampling pump and the nine IOM samplers attached to the measurement spots at the detection

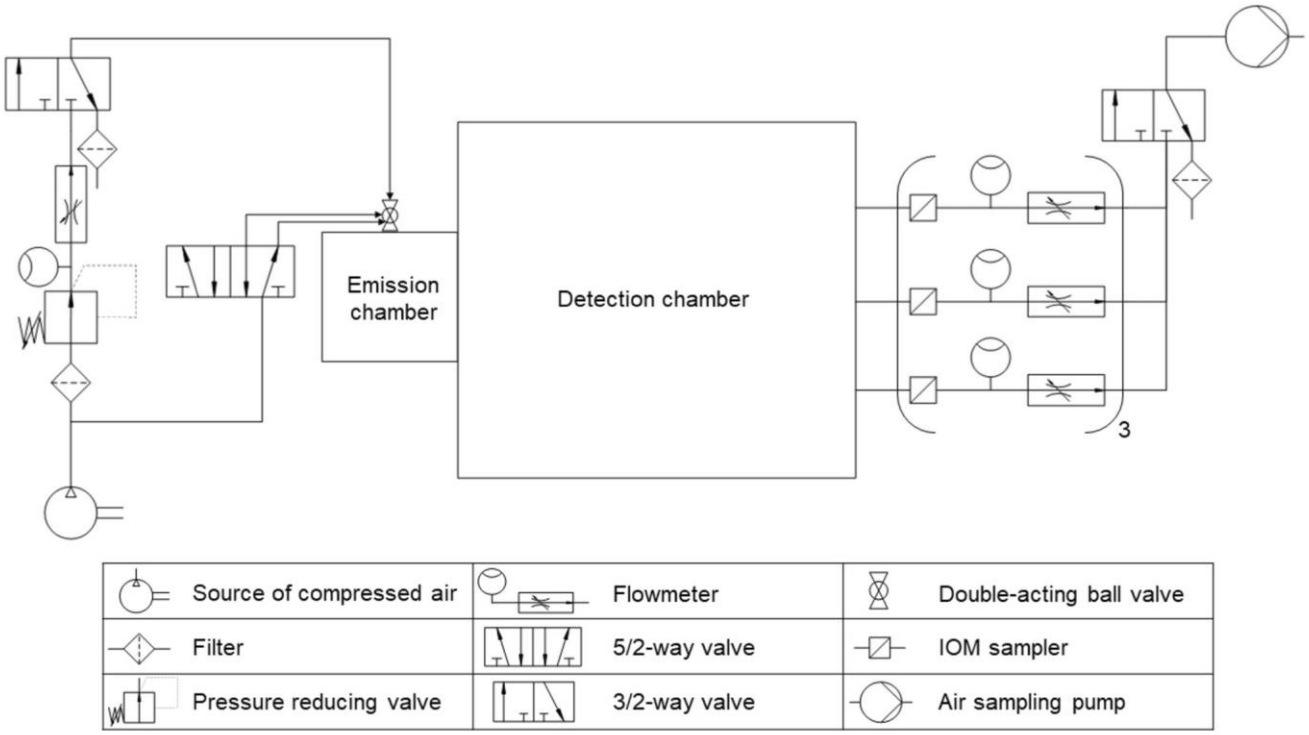


Fig. 3 Simplified piping and instrumentation diagram of the chamber setup

chamber was activated resulting in an airflow of 2 L/min through each of the glass microfiber filters (1820–025, Whatman, Little Chalfont, UK) located in the samplers. Through the connecting orifice the fume flowed from the emission into the detection chamber and was evacuated through the nine IOM samplers. During this experimental procedure the entire cross-sectional area of the detection chamber was monitored using a digital camera (ZV-1, Sony, Tokyo, Japan) positioned to the side of the detection chamber. Pictures were taken every 10 s for a time period of 5 h. The focus of the camera was manually set to the center of the detection chamber and the white balance, aperture, ISO value and shutter speed were adjusted to predefined values to minimize any optical bias, such as distortion. To increase the visual contrast of the fume, a black backdrop was placed behind the detection chamber and additionally a cold light source (CL 1500 ECO, Zeiss, Jena, Germany) was used for illumination. This series of pictures taken was subsequently examined via image analysis using the processing software ImageJ (US National Institute of Health, Bethesda, USA) [44]. For analysis of the evacuation of the fume, the optical fume density in the pictures was determined based on the mean gray value in four different zones (390 pixels × 390 pixels each) selected around the center of the side panel. This measure was taken to exclude picture areas with interfering effects such as reflections caused by the outer framework of aluminum profiles fastened to the panels. The values were then evaluated via nonlinear regression to determine the necessary evacuation time for the detection chamber.

Powder Characterization of the Surrogate Acetaminophen (ACAM)

Particle Size Distribution

The particle size distribution of ACAM was determined by laser diffractometry (Helos KR, Sympatec, Clausthal-Zellerfeld, Germany). Measurements ($n = 3$) were performed using a lens with an effective range of 0.5–875 µm. The ACAM powder was dispersed by compressed air at an air pressure of 1.5 bar. For analysis of the particle size distribution the Paqxos software (Version 2.0.3, Sympatec, Clausthal-Zellerfeld, Germany) was used.

Residual Moisture Content

The residual moisture content of samples with approximately 14 mg of ACAM ($n = 3$) was measured via thermal gravimetric analysis (TGA 2, Mettler Toledo, Germany). The temperature increase was set from 25°C to 160°C, with a heat rate of 10°C/min.

True Density

The true density of ACAM was determined with a helium pycnometer (Pycnomatic ATC EVO, Porotec, Hofheim am Taunus, Germany). For each sample of approximately 5 g ($n = 3$) ten measurement cycles were performed.

Bulk Density

The untapped bulk density and tapped bulk density were estimated according to the monograph 2.9.34, "Bulk Density of Powders" in the European Pharmacopoeia [45]. A graduated 250 mL measuring cylinder was filled with 100 g of ACAM and measured using a jolting volumeter (STAV 2003, J. Engelsmann, Ludwigshafen, Germany). The Hausner ratio was calculated using Eq. (1).

$$Hausner\ ratio = Untapped\ bulk\ volume / Tapped\ bulk\ volume \quad (1)$$

Dust Measurements with ACAM

For the determination of dustiness and spatial distribution of dust the safe surrogate substance ACAM (Caelo, Hilden, Germany) was selected, as it is commonly used for containment investigations [6, 15]. Powder samples of the surrogate substance ACAM at quantities of 65, 125, 250, 500 and 1000 mg were atomized. For each measurement the respective sample was transferred into the closed double-acting ball valve with a funnel. The measurement was started by actuating a toggle switch on the PLC. Subsequently, the double-acting ball valve was opened by the 5/2-way solenoid valve for a duration of 5 s (Fig. 3). By this means, compressed air with a gauge pressure of 1.5 bar and a flow rate of 100 L/min was directed through the double-acting ball valve and the powder sample inside. This expels the powder sample out of the ball valve and atomizes it via turbulent air and subsequent impact on the lower inner wall of the emission chamber. Simultaneously, the toggle switch activated the 3/2-way valve at the vacuum pump, leading to an airflow of 2 L/min through each of the glass microfiber filters within the IOM samplers for 278 min. Via convective and diffusive mass transport the aerosol passed through the connecting orifice from the emission to the detection chamber and eventually settled on the filters. The quantification of the settled amount of ACAM on the filters was performed by HPLC.

HPLC Assay

To quantify the amount of ACAM by HPLC (Chromaster 5000, VWR-Hitachi, Tokyo, Japan), the glass microfiber filters containing the collected ACAM dust were

transferred to individual iodine flasks. To also gather the ACAM amount deposited on the inside of the cassette fronts of each of the IOM samplers they were swabbed using additional glass microfiber filters which were transferred into the corresponding iodine flasks. The ACAM was extracted from the filters by adding 2 mL of the mobile phase, consisting of a mixture of acetonitrile and water (75:25 v/v), which was adjusted to a pH of 3.5 with phosphoric acid. Subsequently the flasks were shaken at 100 rpm for 30 min (Unimax 1010, Heidolph Instruments, Kelheim, Germany). These extracts were diluted with the mobile phase (1:15) and approximately 1.5 mL of the dilutions were transferred into HPLC vials. The HPLC flow rate was set to 1 mL/min and the injection volume was 20 µL. All measurements were carried out at a temperature of 22°C. ACAM quantification was performed by using a LiChroCART RP-18e 250–4 column (Merck, Darmstadt, Germany) with subsequent spectrophotometrical detection by a Diode Array Detector (Chromaster 5430, Hitachi, Tokyo, Japan) at 245 nm. The run time for each sample was 3.00 min and the retention time of ACAM was 1.92 min. The calibration of ACAM was linear between a concentration of 0.033 µg/mL and 2 µg/mL ($R^2 = 0.9999$). Based on the signal-to-noise ratio the detection limit (DL) for the assay was 0.0014 µg/L and the quantitation limit (QL) was 0.0047 µg/L [46].

Computational Fluid Dynamics (CFD) Simulations

Computational Fluid Dynamics simulations were performed to simulate the airflow in the form of air velocity, causing a convective mass transport of aerosol particles inside the chamber setup. These simulations were carried out with the SimScale CFD simulator (SimScale, Munich, Germany). The model used was the k-omega shear stress transport turbulence model (k-ω-SST) in a steady-state approach. In accordance to the Reynolds analogy the turbulent Schmidt number (Sc_t) was set to 1 and diffusion coefficients to 1×10^{-9} m^2/s. As initial conditions for the air, density was set to 1.196 kg/m^3 and the kinematic viscosity to 1.529×10^{-5} m^2/s applying a Newtonian viscosity model. The initial global air velocity was set to 0 m/s and the initial volumetric airflow through the inlet to 0 L/min. The initial global gauge pressure as well as the gauge pressures at the nine outlets (measurement spots) were set to 0 bar. Furthermore, the turbulence kinetic energy (k) was adjusted to 1.297×10^{-2} m^2/s^2 and the specific dissipation rate (ω) to 12.49 s^{-1}. A physics-based meshing was chosen, resulting in 271,600 cells and 66,000 nodes in the model. The simulated space was limited to the geometry of the chamber setup. In accordance with standard practice, the air was regarded as incompressible fluid, because the resulting flow velocities were significantly below mach 0.3 and therefore no relevant differences in density, pressure, or temperature were expected. Thus, no boundary limits were set for these parameters in the simulations numeric control. Nevertheless, to ensure a correct simulation it was tested for outliers and instabilities based on the convergence between individual iteration steps, the so-called residuals. A limitation of the simulation is the restricted resolution because of a maximum runtime of 24 h. To emulate the atomization process the orifice on top of the emission chamber was chosen as an inlet and a flow rate of 100 L/min was simulated for a duration of 5 s in increments of 0.005 s. For additional 2 s an inlet flow rate of 18 L/min was simulated to emulate the first seconds of the volume flow caused by the vacuum pump.

Results

Evacuation time of the Detection Chamber

To ensure that the complete content of the detection chamber is gathered for detection, the necessary evacuation time was determined with fuming sulfuric acid. The results of the evacuation time investigation are shown in Fig. 4. The maximum mean gray value of the fume density, determined photographically, was defined as 100% relative fume density and the corresponding time point was set to 0 s. The decrease of the fume density over time followed an exponential course and reached a value of less than 1% after 278 min [47].

Powder Characterization of the Surrogate ACAM

The dustiness of powders is influenced by various factors, such as particle size distribution, residual moisture content, true density as well as bulk density. These powder properties were determined for the investigated surrogate ACAM. Residual moisture was not detected. The respective values for the particle size distribution, true and bulk densities as well as flowability may be found in Table I.

Totally Settled Amount of ACAM (Dustiness)

To verify reproducible and precise dust measurements, experiments with the surrogate powder ACAM were carried out using the newly developed chamber setup. Different amounts of ACAM (65–1000 mg) were atomized and the totally settled amount, regarded as dustiness, as well as the spatial distribution were examined. In Fig. 5 the totally settled amounts of ACAM on all filters within the nine IOM samplers for both chamber arrangements are shown. It is evident, that the measurements in the orthogonal arrangement resulted in lower detected amounts of totally settled ACAM than in the opposite arrangement. In the

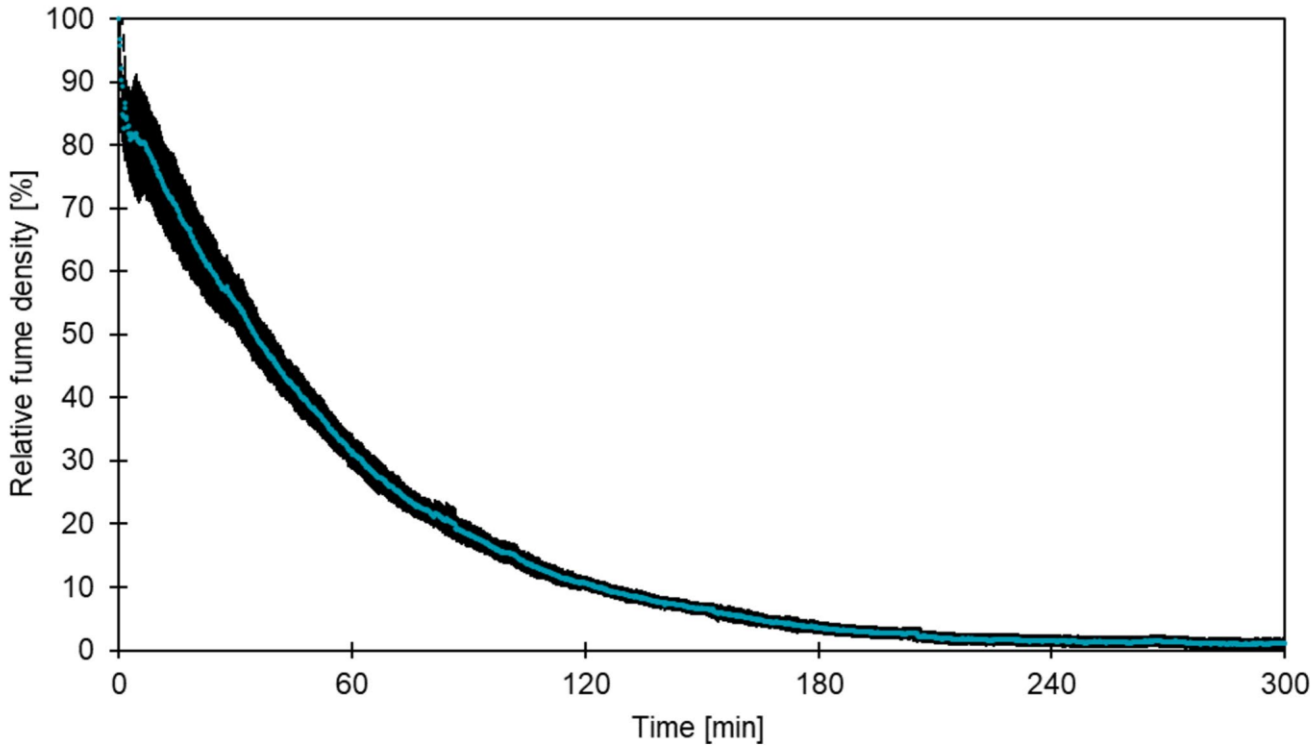


Fig. 4 Time course of the relative fume density of fuming sulfuric acid (means ± SD, $n = 3$) modified after [47]

Table I Physicochemical properties of the investigated surrogate ACAM (means ± SD, $n = 3$)

Powder properties	Values
Particle size [µm]	
x_{10}	3.23 ± 0.04
x_{50}	21.39 ± 0.36
x_{90}	128.85 ± 1.91
True density [g/cm^3]	1.290 ± 0.001
Untapped bulk density [g/mL]	0.401 ± 0.001
Tapped bulk density [g/mL]	0.586 ± 0.003
Hausner ratio	1.461 ± 0.007

opposite arrangement, values ranged from 26.62 ± 11.67 µg/m^3 up to 140.28 ± 18.32 µg/m^3 whereas in the orthogonal arrangement they ranged from 18.54 ± 2.89 µg/m^3 up to 81.98 ± 10.92 µg/m^3. At lower sample amounts of 65, 125, and 250 mg, the percentage of totally detected ACAM in the orthogonal arrangement amounted to 70, 78 and 73% (m/m), respectively, compared to the settled amounts in the opposite arrangement. For higher sample amounts of 500 and 1000 mg this percentage decreased to 58% (m/m).

Spatial Dust Distributions

Opposite Arrangement

The spatial distribution of the ACAM dust inside the detection chamber was investigated regarding the position of the nine IOM samplers. Only the results of the experiments with 500 mg ACAM are shown in the following 2 figures. In Fig. 6 the spatial distribution of the ACAM dust examined with the opposite arrangement is shown. It is noticed that the highest amount of ACAM (13.51 ± 0.84 µg) settled on the filter within the IOM sampler #5, which is positioned right in the middle of the detection site and directly opposite to the emission chamber. Significantly less ACAM settled on all surrounding IOM samplers ($p < 0.05$), except for IOM sampler #2. The lowest settled amount was found on IOM sampler #9 with 7.34 ± 0.88 µg.

Orthogonal Arrangement

The spatial distribution for the experiments with the orthogonal arrangement is shown in Fig. 7. The highest amount of ACAM was found within the IOM sampler #6, with 8.23 ± 1.76 µg, positioned on the right-hand side of the detection chamber. It is evident, that for all three horizontal IOM sampler rows, the corresponding highest amount of ACAM settled on the samplers which were positioned most

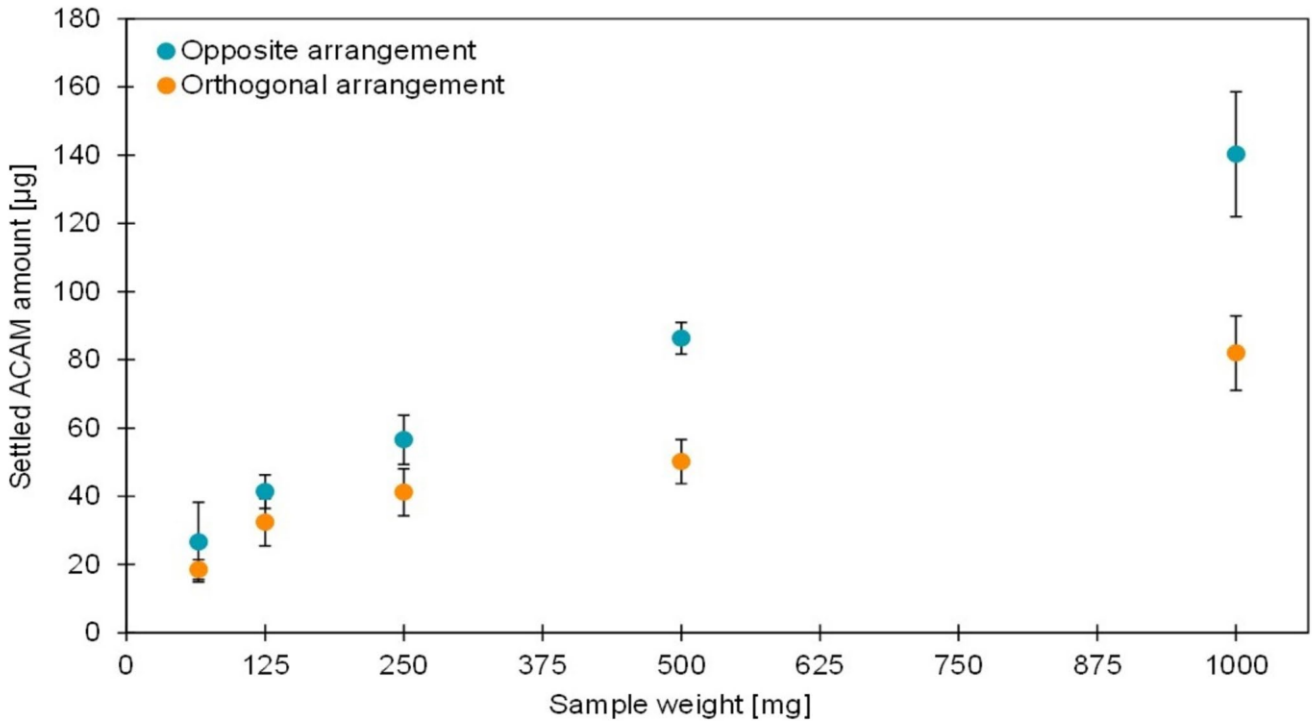


Fig. 5 Totally settled amount of ACAM on the filters within the IOM samplers for the opposite (blue) and the orthogonal (orange) arrangement (total of all nine samplers, means ± SD, $n = 3$); modified and extended from [48]

distant to the emission chamber, i.e. IOM samplers #3, #6 and #9. Moreover, the detected amount of ACAM decreases in a circular pattern with its origin at the position of sampler #6. The lowest amount of ACAM settled on the filter within IOM sampler #1 (3.98 ± 0.53 µg). The differences in the settled amount of ACAM is on a significance level of $p < 0.1$ for the IOM samplers on the right-hand side of the panel compared to their corresponding IOM samplers in the center column (IOM samplers #2, #5 and #8). The differences between the samplers on the right-hand side and their corresponding samplers on the left-hand side, closest to the emission chamber, are significant ($p < 0.05$).

Computational Fluid Dynamics (CFD) Simulations

The resulting air velocities inside the chamber setup during the 5 s of atomization and the two additional seconds thereafter were simulated with CFD and are shown in Figs. 8 and 9.

The resulting airflow for opposite arrangement is depicted in Fig. 8a) from a side view with the cutting plane positioned vertically in the middle of the chamber setup. After 0.2 s the airflow, caused by atomization of the powder sample, already passed through the emission chamber and through approximately one third of the detection chamber. The airflow reached the opposite wall in little more than 3 s. After 5 s the atomization process stops, but the increased airflow is still evident at 7 s. In Fig. 8b), from top view and a cutting plane located horizontally in the middle of the chamber setup, the airflow was directed in the same pattern as in Fig. 8a) through the chamber setup and towards the measurement spots located in the opposite panel of the detection chamber. In Fig. 8c) the airflow is shown in a cutting plane placed 2.5 cm inwards of the measurement spots. In this plane, the airflow increased uniformly during the first 0.2 s, but at 3 s it becomes evident, that the airflow raised to higher velocities in a circular pattern with its origin in the center of the panel.

In Fig. 9a), the airflow in the orthogonal arrangement is shown, again from side view with the cutting planes positioned vertically in the middle of the chamber setup. The resulting airflow is similar to that shown in Fig. 8a). In contrast, the simulated airflow in Fig. 9b) from top view, and cutting plane located horizontally in the middle of the chamber setup, shows an asymmetrical pattern. After approximately 3 s, the airflow is redirected sideways by the opposite panel and towards the measurement spots located in the side panel. This redirection is further supported by the simulation shown in Fig. 9c). The airflow first increases uniformly, but after 3 s the airflow increases to higher velocities on the right-hand side of the panel.

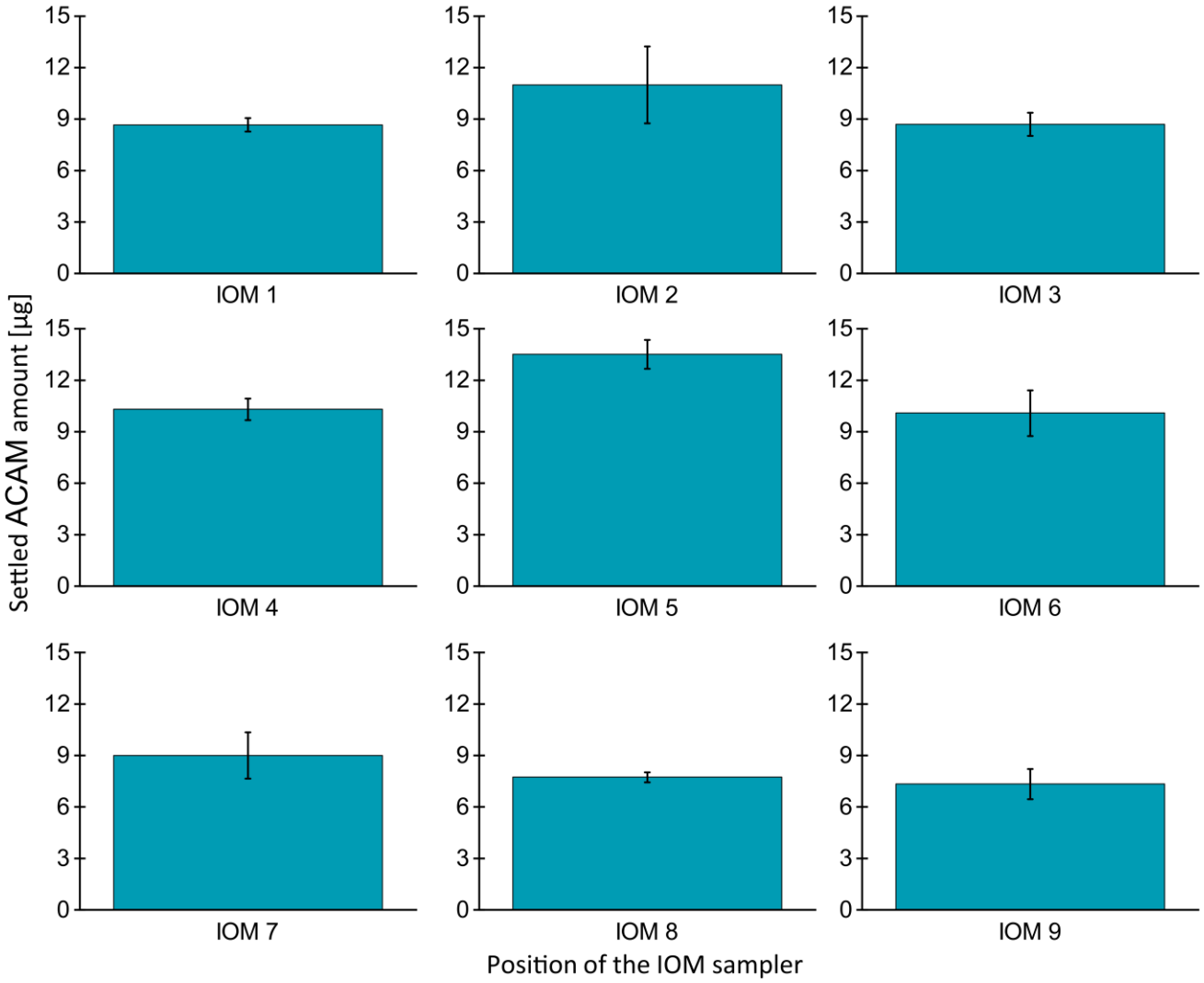


Fig. 6 Spatial distribution of the ACAM dust on the filters within the nine IOM samplers in opposite arrangement (means ± SD, $n = 3$)

Discussion

Evacuation Time of the Detection Chamber

An important parameter for dustiness measurements is the required sampling duration to gather the entire airborne dust content within the chamber setup, especially if dealing with very low sample amounts and resulting dust concentrations. For this purpose, Wirth *et al*. compared three methods for determination of the evacuation time: CFD simulations, flow visualizations with fuming sulfuric acid, and dustiness measurements with a surrogate substance [38]. The CFD simulations showed a relatively large deviation compared to the other two methods, whereas the results obtained with the surrogate and those obtained with the fume of sulfuric acid corresponded to each other [38]. As the evacuation time determination with fuming sulfuric acid proved to be an accurate and precise method, it was chosen for the present study. As shown in Fig. 4, the decrease of the fume density followed an exponential course. Based on a chosen cut off at 1% remaining relative fume density, the necessary evacuation time to gather the complete content of the detection chamber took 278 min. With a flow rate of 2 L/min through each of the nine IOM samplers and a detection chamber volume of 1 m^3, the evacuation time corresponds to an approximately fivefold air exchange. Wirth *et al*. also reported an exponential decrease of the fume density over time. In addition, Evans *et al*. reported a similar time-dependent decrease of the particle mass concentration in studies with the Venturi dustiness testing device, introduced by Boundy *et al*. [35, 49]. A study by Breum reported a non-linear accumulation of the particle mass arriving at an outlet of a rotating drum dustiness tester [50]. A similar result is presented in a study by Heitbrink for the MRI dustiness test, further underlining

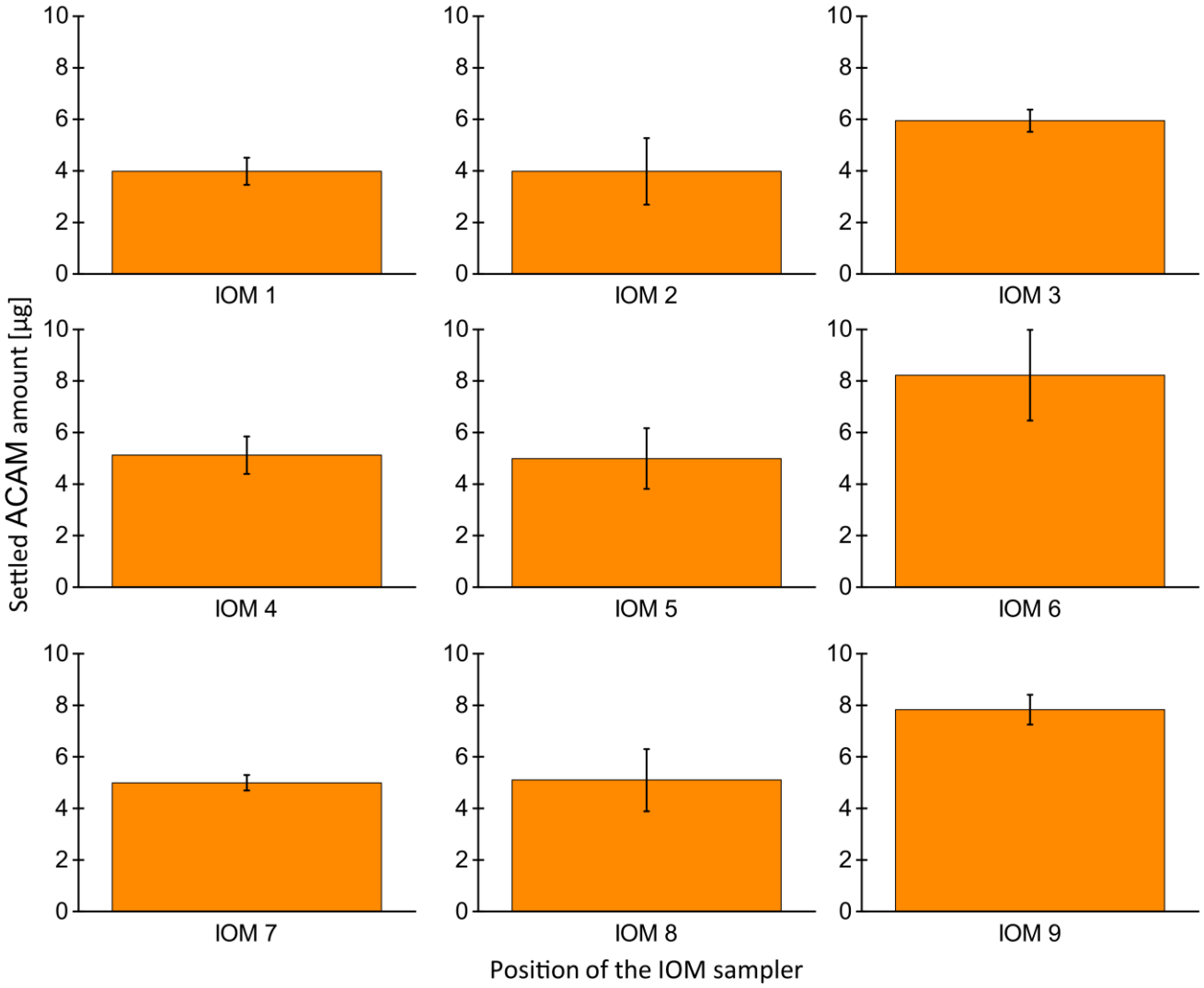


Fig. 7 Spatial distribution of the ACAM dust on the filters within the nine IOM samplers in orthogonal arrangement (means ± SD, $n = 3$)

the above-mentioned results [51]. Based on this knowledge, the detection time for the ACAM investigations was set to 278 min in the PLC for the surrogate experiments in the present study.

Powder Characterization of the Surrogate ACAM

The dustiness of a powder is defined as its propensity to generate airborne particles during its handling, such as mixing, milling or transferring [14, 25, 52]. Multiple physicochemical properties of powders may influence the propensity of particles to become airborne and thus powder dustiness. In one of the first investigations of this topic, Plinke *et al.* described the influence of moisture content and particle size of a powder sample on its dustiness [24]. Furthermore, Pujara and Kildsig identified powder sample mass, moisture content, bulk density as well as particle shape, size, and cohesion as the most important factors determining the dustiness of a powder [53]. In addition, Boundy *et al.* described the size and shape of powder particles as well as the moisture content as influencing factors for dustiness also considering factors such as prior handling of the powder [35]. In two studies, an increase in residual moisture content was found to cause a direct decrease of powder dustiness [30, 54]. As no residual moisture was detected by thermal gravimetric analysis in the present study, its influence on dustiness can be ruled out. The bulk densities and the resulting Hausner ratio of 1.46 indicate a very poor powder flowability [55].The particle size distribution and true density of ACAM in the present study, as shown in Table I, are comparable to other well-known APIs and thus ACAM represents a well suited surrogate to simulate occupational exposure and airborne spatial dust distributions in pharmaceutical production environments [56].

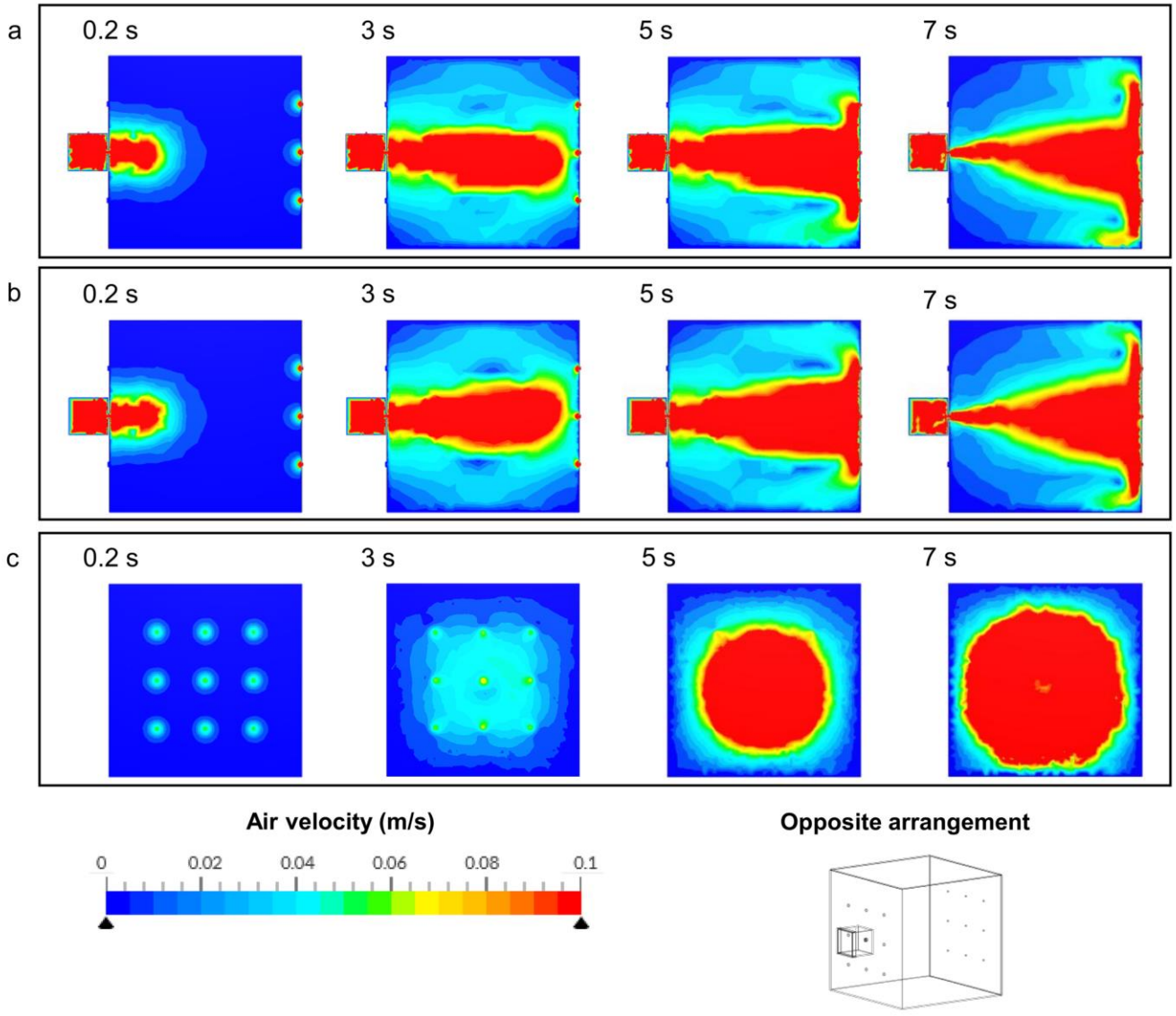


Fig. 8 Air velocities during the atomization process at different time points for the opposite arrangement: **a** centered cutting plane from side view, **b** centered cutting plane from top view, **c** cutting plane located 2.5 cm inwards of the measurement spots

Totally Settled Amount of ACAM (Dustiness)

Initial investigations with the chamber setup dealt with confirmation of a reproducible and precise atomization of small amounts of powders and the subsequent detection of low airborne dust concentrations as permitted in contained manufacturing of pharmaceuticals to ensure the highest possible transferability to industrial scenarios [7, 8, 15, 57]. This is of importance, as APIs are often of limited availability because of their high costs. Moreover, typical dustiness testers require high sample amounts, which would lead to exorbitantly high costs for the testing of pharmaceutical powders [26, 49, 58]. In the present study, IOM samplers were chosen as measurement devices of the detection chamber. These samplers consist of an enclosed housing with a 15 mm circular orifice and a protruding lip of 1.5 mm for entry of airborne dust particles eventually settling onto a 25 mm round filter. IOM samplers are usually worn at the lapel of workers to assess occupational exposure to airborne dust in the workers breathing region [59]. In addition, they are used for static sampling in the production environment, for example during factory acceptance tests of equipment [15, 60]. IOM samplers collect particles with a diameter of up to 90 µm, corresponding to the inhalable fraction of airborne dust, at wind speeds of up to 3 m/s [60]. Furthermore, IOM samplers are not limited by a specific minimum detectable airborne

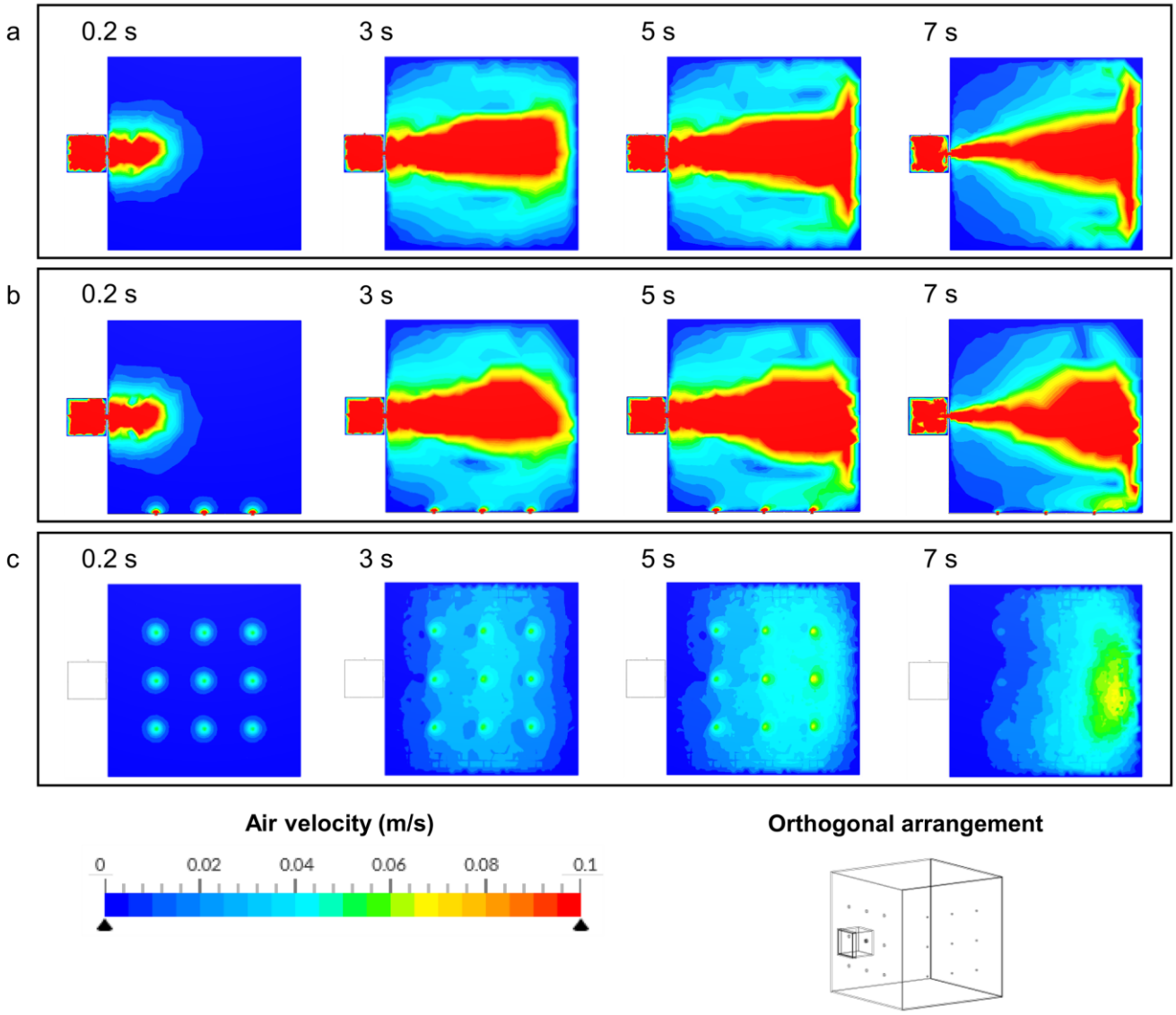


Fig. 9 Air velocities during the atomization process at different time points for the orthogonal arrangement: **a** centered cutting plane from side view, **b** centered cutting plane from top view, **c** cutting plane located 2.5 cm inwards of the measurement spots

dust concentration, as their detection limit is solely based on the volume of air sampled and the DL and QL of the subsequent analytical method.

The results of the totally settled amount on the filters within the IOM samplers, regarded as dustiness, were as low as 18.54 ± 2.89 µg at a sample mass of 65 mg (orthogonal arrangement) with single IOM sampler values as low as 3.98 ± 0.53 µg. These values do not only demonstrate the reproducibility of measurements with the newly developed chamber setup, but also its ability to generate and detect concentrations of airborne dust similar to the conditions in the contained manufacture of pharmaceuticals.

The totally settled amount followed a linear tendency depending on the sample mass in both, the opposite and the orthogonal arrangement. These results are in agreement with several studies dealing with the influence of the applied sample mass onto the detected dustiness with multiple dustiness testers, for example with a rotating drum tester as well as a chamber with dust generation by free falling powders [29, 37, 38, 50]. Whereas, the lowest settled amount of ACAM was found at a sample mass of 65 mg the highest ACAM amount was detected at a sample mass of 1000 mg for both arrangements. The opposite arrangement resulted in higher settled amounts of ACAM for every sample mass, but a significant difference between opposite and orthogonal arrangement ($p < 0.05$) was only detected at sample masses of 500 and 1000 mg. This difference may be explained by influencing factors affecting the measured dustiness, as not only the

physicochemical powder properties influence dustiness, but also the amount and type of energy applied as well as the measuring device itself. This is caused by the convective mass transport represented by the flight path of airborne particles from the atomization to the detection site defined by the geometry of the chamber setup [26]. The flight path in the opposite arrangement directs airborne particles straight from the emission site towards the measurement spots. In contrast, in the orthogonal arrangement the flight path of airborne particles includes a ninety degree turn to eventually settle on the filters. Thereby particles that cannot follow this turn because of their mass inertia are not captured on the filters. Moreover, a loss of airborne particles may be caused by gravitational settling or by wall effects in the chamber setup [61, 62].

Investigations on the Spatial Dust Distribution for Emission Site Localization

Since the beginning of the twenty-first century, more than 65 dustiness testing devices have been published and this number further increased in recent years [33, 35]. Nevertheless, only a small number of these devices is suitable for dustiness investigations of pharmaceutical powders at low sample quantities [26, 35, 36, 38]. In addition, all of these devices are equipped with only one measurement spot (in some cases two, but only to collect different particle size fractions of the airborne dust) and are therefore not able to detect the spatial distribution of airborne dust. Nevertheless, in some references it is suggested, that stationary location sampling may be used to identify areas of dust emission within a pharmaceutical production environment [6, 39]. To proof this suggestion, the spatial dust distribution within the newly developed chamber setup was investigated with nine measurement spots in two arrangements.

Transport mechanisms of airborne dust particles are categorized into diffusive and convective processes. Diffusion represents a process by which particles move from regions of higher concentration to those of lower concentration. This phenomenon is particularly significant for airborne dust particles < 0.5 µm, resulting from Brownian motion [63, 64]. However, diffusion should be negligible in measurements within the presented chamber setup because of the relatively large distance of 1 m from the emission site to the measurement spots. In contrast, the convective mass transport, caused by atomization of powder samples with compressed air and the subsequent airflow of 2 L/min through each of the IOM samplers plays a major role in the spatial distribution of airborne dust. This assumption is confirmed by the results in the opposite arrangement, where it is evident, that the convective airflow transports the airborne dust particles directly towards the opposite panel of the detection chamber and thus into the IOM samplers. As expected, this particle transport results in the highest settled ACAM amount on the filter within IOM sampler #5 and significantly less on all surrounding IOM samplers ($p < 0.05$), as this sampler represents the center measurement spot, directly located opposite to the connecting orifice of the emission chamber. These results confirm the localization of the emission chamber at the center position of the nine possible attachment points of the detection chamber, even at a relatively small distance of only 1 m between emission and detection site and a minimum distance of 25 cm between the individual measurement spots.

Assuming plain diffusive mass transport for particle distribution, the highest concentration should be expected close to the emission site. However, the opposite became evident during the measurements (orthogonal arrangement). The highest settled ACAM amount was found on the filters within IOM samplers #3, #6, and #9 on the right-hand side of the detection chamber and most distant to the emission chamber. Significantly lower amounts were detected with IOM samplers #1, #4, and #7 on the left-hand side of the detection chamber and closest to the emission chamber. These results confirm the assumption of a strong convective mass transport of the dust particles. Nevertheless, to identify the location of the attached emission chamber from the side view, additional knowledge of the airflow within the chamber setup is necessary. Therefore, CFD simulations were performed.

Computational Fluid Dynamics (CFD) Simulations

CFD simulations are a versatile tool for airflow visualizations, not only in production environments but also in dustiness test chambers [40]. Such simulations have been used by Dubey *et al*. to analyze the airflow in the Venturi dustiness tester and Chen *et al*. simulated aerosol behavior in the Heubach rotating drum dustiness tester [42, 43]. In addition, Wirth *et al*. investigated the required evacuation time of a dustiness test chamber as well as the relationship between dust emission and airflow with CFD simulations [38, 65]. In the present study, CFD simulations were performed to visualize the airflow in the chamber setup to confirm the assumption that the detected spatial dust distribution is caused by the convective mass transport. Regarding the simulations a few limitations have to be considered: It was only possible to simulate airflows but not the spatial distribution of particles with their corresponding particle interactions were simulated and it was impossible to simulate the flow resistance caused by the IOM samplers and the vacuum pump. Nevertheless, the simulations confirmed that with both arrangements the airflow resulting from atomization is directed straightly from the emission chamber towards the opposite panel of the detection chamber as depicted in Figs. 8 a) and 9 a). The simulations shown in Fig. 8 b) visualize an airflow

directed almost symmetrically through the chamber setup and the measurement spots located in the opposite panel of the detection chamber. In contrast, in Fig. 9 b) the visualized airflow shows an asymmetrical pattern. This asymmetrical airflow may be explained by the measurement spots representing the outlets of the chamber setup leading to a sideways redirection of the airflow of the pressurized air. The airflow causes a strong convective mass transport of ACAM particles from the emission through the detection chamber and onto the filters inside the IOM samplers in both arrangements. In Figs. 8 c) the airflow is shown in a cutting plane placed 2.5 cm inwards of the measurement spots. The simulations confirmed the spatial distribution of ACAM as observed in Fig. 6 with the highest settled ACAM amount on the filter in the middle of the panel (IOM sampler #5) is caused by the airflow in the detection chamber. Furthermore, the airflow simulated in Figs. 9 c) confirmed the spatial distribution of ACAM experimentally observed with the orthogonal arrangement (Fig. 7).

Three-Dimensional Localization of the Emission Site

The results of the spatial dust distribution measurements in the opposite arrangement clearly allowed a localization of the emission site in the center position of the nine available positions. These results were confirmed with the CFD simulations visualizing the airflow. The results of the dust distribution in the orthogonal arrangement also suggested the localization of the emission site to be in the horizontal center row. However, solely based on these results, it would be assumed that the emission chamber is positioned on the right-hand side of the panel equipped with the measurement spots. Only by combining the knowledge of the convective mass transport caused by the airflow in the chamber setup, visualized by the CFD simulations, and the results of the spatial dust distribution measurements it is possible to clearly localize the three-dimensional attachment position of the emission chamber and thus emission site (left-hand side and center position). This conclusion is based on the assumption that the airborne particles follow the simulated airflow of the CFD simulations. This is probably only true for a fraction of the atomized ACAM particles, because larger particles will not be able to follow the airflow from the emission to the detection site in the chamber setup, because of their inertia and resulting impaction on the panels of the emission chamber. Furthermore, sedimentation of particles > 10 µm, may prevent them from being collected at the measurement spots of the chamber setup. Several studies showed, that the measured dustiness of a powder tends to increase with decreasing particle size and that the polydispersity index (PDI) is negatively correlated with dustiness [24, 54, 56, 65–69]. These findings also indicate an influence of particle size and distribution on the spatial dust distribution. A direct analysis of collected ACAM particle sizes on the filters within the IOM samplers was not possible in this study because of the subsequent HPLC quantification. Another factor that has to be considered is the chosen size of the chamber setup, which is a compromise between its usability in a laboratory scale and the minimum required distance between measurement spots and number of measurement spots (resolution). In addition, the chamber setup represents a strictly confined space for reproducible investigations of the spatial dust distribution, but real world influences, such as controlled airflows in production environments and electrostatic charging of dust caused by production processes, directly affecting potential travelling distances of airborne dust particles are not taken into account, or only to a limited extent. For example, the selected material for the chamber setup panels is acrylic glass, a material which inherits a low conductivity [70, 71]. This choice was purposely made to mitigate any potential electrostatic interactions of the chamber setup with sample material. Nevertheless, ACAM shows a high tendency for electrostatic interactions and because of the limited space for its spatial distribution within the detection chamber in comparison to larger production environments, these interactions are more likely to occur than in real world scenarios [72]. The degree to which the chamber setup results may be transferred to real world scenarios therefore still needs to be verified. Nevertheless, the newly developed chamber setup represents the first system capable of substance-specific determination of spatial airborne particle distributions. The method requires only small sample amounts of API, has a low quantification limit, and due to the modular design of the chamber setup it represents a valuable tool suitable for a multitude of pharmaceutical containment investigations. With this chamber setup, the assumption, that an emission site localization is possible by means of stationary exposure data, even with extremely low amounts of airborne dust in single-digit microgram concentrations and minimum distances between the measurement spots was confirmed in the present study.

Conclusion

The newly developed chamber setup has shown to be capable of not only a reproducible atomization and detection of a surrogate powder but furthermore its capability for the investigation of the spatial powder distribution in the context of containment. The chamber setup allows a controlled and directed airflow from the emission to the detection chamber. According to the results of the fume experiments a fivefold air exchange was required for complete evacuation of the detection chamber. A linear tendency of the totally settled amount of the surrogate substance ACAM on the filters within the IOM samplers in dependence of the amount

of atomized substance was demonstrated. Furthermore, a spatial distribution of the ACAM dust within the detection chamber was detected and a convective mass transport caused by the flow of compressed air for atomization was suggested. This assumption was proven by Computational Fluid Dynamics simulations. The combined results allowed an exact three-dimensional localization of the emission site in the chamber setup. Future studies will deal with the comparison of APIs with different physicochemical properties as well as binary mixtures of APIs with excipients commonly used in tableting, regarding their dustiness and spatial distribution behavior. In addition, the chamber setup may be used in two arrangements to simulate real world scenarios such as the spatial dust distribution around a production device placed in the detection chamber. The results obtained with the laboratory scale chamber setup may eventually be useful as a training dataset for artificial intelligence thus allowing to localize potential leakages of a containment system in industrial production environments based on stationary exposure data. These investigations may provide valuable insights into factors affecting dustiness and especially the spatial distribution of pharmaceutical dusts and may thus significantly contribute to improve safety in the manufacture of pharmaceuticals containing HPAPIs.

Acknowledgements The authors express their gratitude to Petra Borbe and Kai Braunschweig for their technical and analytical assistance and to Steffen Wirth for his support in planning and construction of the chamber setup.

Author contributions Conceptualization, H.K., M.S. and C.S.L.; Data curation, H.K.; Formal analysis, H.K. and C.S.L.; Investigation, H.K.; Methodology, H.K.; Software, H.K. and J.B.; Supervision, C.S.L.; Validation, H.K., M.S. and C.S.L.; Visualization, H.K.; Writing—original draft, H.K.; Writing—review and editing, H.K., M.S., J.B. and C.S.L.

Funding Open Access funding enabled and organized by Projekt DEAL.

Data Availability The datasets generated and analyzed during this study are available from the corresponding author upon request.

Declarations

Conflict of Interest The authors declare that they have no known competing financial interests or personal relationships that could have appeared to influence the work reported in this paper.

Open Access This article is licensed under a Creative Commons Attribution 4.0 International License, which permits use, sharing, adaptation, distribution and reproduction in any medium or format, as long as you give appropriate credit to the original author(s) and the source, provide a link to the Creative Commons licence, and indicate if changes were made. The images or other third party material in this article are included in the article's Creative Commons licence, unless indicated otherwise in a credit line to the material. If material is not included in the article's Creative Commons licence and your intended use is not permitted by statutory regulation or exceeds the permitted use, you will need to obtain permission directly from the copyright holder. To view a copy of this licence, visit http://creativecommons.org/licenses/by/4.0/.

References

1. Broach JR, Thorner J. High-throughput screening for drug discovery. Nature. 1996;384(6604 Suppl):14–6.
2. Mari G, Moccaldi A, Ludovisi G. Handling of high potency drugs : process and containment. Trans Ecol Environ. 1999;85:257–65.
3. Paul D, Sanap G, Shenoy S, Kalyane D, Kalia K, Tekade RK. Artificial intelligence in drug discovery and development. Drug Discov Today. 2021;26:80–93.
4. Vemula D, Jayasurya P, Sushmitha V, Kumar YN, Bhandari V. CADD, AI and ML in drug discovery: a comprehensive review. Eur J Pharm Sci. 2023;181: 106324. https://doi.org/10.1016/j.ejps.2022.106324.
5. Heron RJL, Pickering FC. Health effects of exposure to active pharmaceutical ingredients (APIs). Occup Med (Chic Ill). 2003;53:357–62.
6. International Society for Pharmaceutical Engineering (ISPE). Good practice guide: assessing the particulate containment performance of pharmaceutical equipment. Tampa, FL, USA. 2012. https://onesearch.nihlibrary.ors.nih.gov/permalink/01NIH_INST/j8e6op/alma991000863809704686.
7. Graham JC, Hillegass J, Schulze G. Considerations for setting occupational exposure limits for novel pharmaceutical modalities. Regul Toxicol Pharmacol. 2020;118:104813. https://doi.org/10.1016/j.yrtph.2020.104813.
8. Ahuja V, Krishnappa M. Approaches for setting occupational exposure limits in the pharmaceutical industry. J Appl Toxicol. 2022;42:154–67.
9. Tiwari P, Chowdhury SR. Sustainable production of highly active pharmaceutical ingredients (HAPIs). Int J Sci Res Publ. 2014;4:2250–3153.
10. Glor M. Hazards due to electrostatic charging of powders. J Electrostat. 1985;16:175–91.
11. Eckhoff RK. Dust explosions: Fundamentals. In: Amyotte PR, Khan FI, editors. Dust Explosions [Internet]. Elsevier; 2019. p. 7–32. https://doi.org/10.1016/bs.mcps.2019.03.001.
12. Eckhoff RK. Understanding dust explosions. The role of powder science and technology. J Loss Prev Process Ind. 2009;22:105–16. https://doi.org/10.1016/j.jlp.2008.07.006.
13. International Society for Pharmaceutical Engineering (ISPE), ISPE D/A/CH Affiliate. Containment manual. Offenbach/Main: ISPE D/A/CH Working Group Containment of the International Society for Pharmaceutical Engineering; 2017. https://en.ispe-dach.org/the-containment-handbook-a-bestseller/.
14. Stein J, Fuchs T, Mattern C. Advanced milling and containment technologies for superfine active pharmaceutical ingredients. Chem Eng Technol. 2010;33:1464–70.
15. Nicolai R, Petroka GS, Whitaker K, et al. Good Practice Guide SMEPAC. 3rd ed. International Society for Pharmaceutical Engineering (ISPE); 2024. https://ispe.org/publications/guidance-documents/good-practice-guide-smepac-standardized-methodology-evaluation-pharmaceutical-airborne.
16. Luo Q, Huang L, Liu Y, Xue X, Zhou F, Hua J. Monitoring study on dust dispersion properties during earthwork construction. Sustain. 2021;13:1–21.
17. Smaoui N, Kim K, Gnawali O, Lee YJ, Suh W. Respirable dust monitoring in construction sites and visualization in building information modeling using real-time sensor data. Sens Mater. 2018;30:1775–86.
18. Wanjun T, Qingxiang C. Dust distribution in open-pit mines based on monitoring data and fluent simulation. Environ Monit Assess. 2018;190: 632.
19. Li J, Li H, Ma Y, Wang Y, Abokifa AA, Lu C, et al. Spatiotemporal distribution of indoor particulate matter concentration with

a low-cost sensor network. Build Environ. 2018;127:138–47. https://doi.org/10.1016/j.buildenv.2017.11.001.
20. Paolucci R, Rotilio M, Ricci S, Pelliccione A, Ferri G. A sensor-based system for dust containment in the construction site. Energies. 2022;15: 7272.
21. Alfano B, Barretta L, Giudice AD, De Vito S, Francia GD, Esposito E, et al. A review of low-cost particulate matter sensors from the developers' perspectives. Sensors. 2020;20:6819.
22. Ault AP, Axson JL. Atmospheric aerosol chemistry: spectroscopic and microscopic advances. Anal Chem. 2017;89:430–52.
23. Manikonda A, Zíková N, Hopke PK, Ferro AR. Laboratory assessment of low-cost PM monitors. J Aerosol Sci. 2016;102:29–40.
24. Plinke MAE, Maus R, Leith D. Experimental examination of factors that affect dust generation by using heubach and MRI testers. Am Ind Hyg Assoc J. 1992;53(5):325–30.
25. Lidén G. Dustiness testing of materials handled at workplaces. Ann Occup Hyg. 2006;50:437–9.
26. Bach S, Eickmann U, Schmidt E. Comparison of established systems for measuring the dustiness of powders with the UNC dustiness tester developed especially for pharmaceutical substances. Ann Occup Hyg. 2013;57:1078–86.
27. Davies KM, Hammond CM, Higman RW, Wells a. B. Progress in Dustiness Estimation. Ann Occup Hyg. 1988;32:535–44. http://annhyg.oxfordjournals.org/cgi/doi/10.1093/annhyg/32.4.535
28. Heitbrink WA, Tood WF, Cooper TC, O'Brien DM. The application of dustiness tests to the prediction of worker dust exposure. Am Ind Hyg Assoc J. 1990;51:217–23.
29. Heitbrink WA, Baron PA, Willeke K. An investigation of dust generation by free falling powders. Am Ind Hyg Assoc J. 1992;53:617–24.
30. Cawley B, Leith D. Bench-top apparatus to examine factors that affect dust generation. Appl Occup Environ Hyg. 1993;8:624–31.
31. Plinke MAE, Leith D, Boundy MG, Löffler F. Dust generation from handling powders in industry. Am Ind Hyg Assoc J. 1995;56(1):251–7.
32. Hamelmann F, Schmidt E. Methods of estimating the dustiness of industrial powders – a review. KONA Powder Part J. 2003;21:7–18.
33. Hamelmann F, Schmidt E. Methods for characterizing the dustiness estimation of powders. Chem Eng Technol. 2004;27:844–7.
34. Bach S, Schmidt E. Determining the dustiness of powders - a comparison of three measuring devices. Ann Occup Hyg. 2008;52:717–25.
35. Boundy M, Leith D, Polton T. Method to evaluate the dustiness of pharmaceutical powders. Ann Occup Hyg. 2006;50:453–8.
36. O'Shaughnessy PT, Kang M, Ellickson D. A novel device for measuring respirable dustiness using low-mass powder samples. J Occup Environ Hyg. 2012;9:129–39.
37. Ohta T, Maeda H, Kubota R, Koga A, Terada K. Establishment of powder dustiness evaluation method by dustmeter with small amount of pharmaceutical ingredients. Int J Pharm. 2014;472:251–6. https://doi.org/10.1016/j.ijpharm.2014.05.067.
38. Wirth S, Schöler M, Brügmann J, Leopold CS. A novel two-chamber setup for containment investigations with special focus on the dustiness of pharmaceutical powders depending on the airflow. Pharmaceutics. 2022;14: 2387.
39. Butler O, Forder J, Saunders J. Analytical protocol for the sensitive determination of mannitol, sorbitol and glucose containing powders in pharmaceutical workplaces by ion chromatography using a pulsed amperometric detector. J Pharm Biomed Anal. 2015;106:204–9. https://doi.org/10.1016/j.jpba.2014.10.006.
40. Lavanya N, Bhattacharyya S. Computational fluid dynamics-the futuristic innovation in pharmaceutical industry. Indian J Pharm Educ Res. 2021;55:930–8.
41. Milenkovic J, Alexopoulos AH, Kiparissides C. Deposition and fine particle production during dynamic flow in a dry powder inhaler: a CFD approach. Int J Pharm. 2014;461:129–36. https://doi.org/10.1016/j.ijpharm.2013.11.047.
42. Dubey P, Ghia U, Turkevich LA. Computational fluid dynamics analysis of the Venturi Dustiness Tester. Powder Technol. 2017;312:310–20. https://doi.org/10.1016/j.powtec.2017.02.030.
43. Chen H, Jog MA, Turkevich LA. Computational fluid dynamics simulations of aerosol behavior in a high-speed (Heubach) rotating drum dustiness tester. Particuology. 2023;72:68–80. https://doi.org/10.1016/j.partic.2022.02.010.
44. Schneider CA, Rasband WS, Eliceiri KW. NIH image to ImageJ: 25 years of image analysis. Nat Methods. 2012;9:671–5.
45. European Pharmacopoeia 11.5; 2.9.34. Bulk Density of Powders. Strasbourg, France: European Directorate for the Quality of Medicines & Health Care (EDQM); 2024. p. 5830–3. https://www.edqm.eu/en/european-pharmacopoeiaph.-eur.-11th-edition.
46. European Medicines Agency (EMA). ICH Q2(R2) Validation of analytical procedures guideline. Amsterdam; 2023. https://www.ema.europa.eu/en/ich-q2r2-validation-analytical-procedures-scientific-guideline.
47. Küllmar H, Schöler M, Leopold CS. Determination of the evacuation time of a newly developed chamber setup for the investigation of the spatial dust distribution of pharmaceutical powders. In: AAPS 2022 PharmSci 360.
48. Küllmar H, Schöler M, Leopold CS. Pneumatic Aerosolization of the Surrogate Acetaminophen in a Newly Developed Chamber Setup for Containment Investigations with Special Focus on Spatial Dust Distribution. In: AAPS 2023 PharmSci 360.
49. Evans DE, Turkevich LA, Roettgers CT, Deye GJ, Baron PA. Dustiness of fine and nanoscale powders. Ann Occup Hyg. 2013;57:261–77.
50. Breum NO. The rotating drum dustiness tester: variability in dustiness in relation to sample mass, testing time, and surface adhesion. Ann Occup Hyg. 1999;43:557–66.
51. Heitbrink WA. Factors affecting the Heubach and MRI dustiness tests. Am Ind Hyg Assoc J. 1990;51:210–6.
52. World Health Organization. Hazard Prevention and Control in the Work Environment: Airborne Dust. Geneva, Switzerland; 1999. (Occupational and environmental health series). https://iris.who.int/handle/10665/66147. Accessed 15 Jul 2021.
53. Pujara CP, Kildsig DO. Effect of Individual Particle Characteristics on Airborne Emissions. In: Containment in the Pharmaceutical Industry. 2020. p. 29–53. https://doi.org/10.1201/9780429074943-4.
54. Shandilya N, Kuijpers E, Tuinman I, Fransman W. Powder intrinsic properties as dustiness predictor for an efficient exposure assessment? Ann Work Expos Health. 2019;63:1029–45.
55. European Pharmacopoeia 11.5; 2.9.36. Powder Flow. Strasbourg, France: European Directorate for the Quality of Medicines & HealthCare (EDQM); 2024. p. 5834–6. https://www.edqm.eu/en/european-pharmacopoeiaph.-eur.-11th-edition.
56. Ribalta C, Viana M, López-Lilao A, Estupiñá S, Minguillón MC, Mendoza J, et al. On the relationship between exposure to particles and dustiness during handling of powders in industrial settings. Ann Work Expo Health. 2019;63:107–23.
57. Ku RH. An overview of setting occupational exposure limits (OELs) for pharmaceuticals. Chem Heal Saf. 2000;9098:34–7.
58. Chakravarty S, Le Bihan O, Fischer M, Morgeneyer M. Dust generation in powders: Effect of particle size distribution. EPJ Web Conf. 2017;140:1–4.
59. Mark D, Vincent JH. A new personal sampler for airborne total dust in workplaces. Ann Occup Hyg. 1986;30:89–102.
60. Mark D, Vincent JH, Gibson H, Lynch G. A new static sampler for airborne total dust in workplaces. Am Ind Hyg Assoc J. 1985;46:127–33.

61. Kanig JL. Pharmaceutical aerosols. Pharm Sci. 1963;52:513–34.
62. Jin H, He C, Lu L, Fan J. Numerical investigation of the wall effect on airborne particle dispersion in a test chamber. Aerosol Air Qual Res. 2013;13:786–94.
63. Li A, Ahmadi G. Deposition of aerosols on surfaces in a turbulent channel flow. Int J Eng Sci. 1993;31:435–51.
64. Chang TJ, Hu TS. Transport mechanisms of airborne particulate matters in partitioned indoor environment. Build Environ. 2008;43:886–95.
65. Wirth S, Schöler M, Brügmann J, Leopold CS. An investigation on the relationship between dust emission and air flow as well as particle size with a novel containment two-chamber setup. Pharmaceutics. 2024;16: 1088.
66. Likitwattanasade T, Barringer SA. The influence of particle size on separation and dustiness in powder mixtures during nonelectrostatic and electrostatic coating. J Electrostat. 2015;77:44–50. https://doi.org/10.1016/j.elstat.2015.07.001.
67. Wirth S, Schöler M, Leopold CS. Investigations on the dustiness of binary acetaminophen - lactose monohydrate powder blends. Powder Technol. 2024;448:120317.
68. Küllmar H, Schöler M, Leopold CS. Optimization of a newly developed chamber setup for spatial dust measurements in the context of containment. Pharmaceutics. 2025;17(5): 565.
69. Hurychová H, Kuentz M, Šklubalová Z. Fractal aspects of static and dynamic flow properties of pharmaceutical excipients. J Pharm Innov. 2018;13:15–26.
70. Czech Z, Kowalczyk A, Shao L, Cheng XQ, Quan S, Bai YP. Novel acrylic pressure-sensitive adhesive (PSA) containing silver particles. J Adhes Sci Technol. 2013;27:1446–54.
71. Devikala S, Kamaraj P, Arthanareeswari M. Conductivity and dielectric studies of PMMA composites. Chem Sci Trans. 2013;2:129–34.
72. Jallo LJ, Dave RN. Explaining electrostatic charging and flow of surface-modified Acetaminophen powders as a function of relative humidity through surface energetics. J Pharm Sci. 2015;104:2225–32. https://doi.org/10.1002/jps.24479.

Publisher's Note Springer Nature remains neutral with regard to jurisdictional claims in published maps and institutional affiliations.

3.2 Optimization of a newly developed chamber setup for spatial dust measurements in the context of containment

In a second study, the cleaning method of the chamber setup and the effect of particle characteristics on the detected dustiness were investigated. In addition, atomization parameters ‘volume flow rate for atomization’, ‘atomization duration’ as well as ‘sample mass’ were investigated by means of a design of experiments approach.

Because of the appearance of wipe marks of deposited dust on the panels of the emission and detection chamber during the first study, the cleaning method of the setup was reviewed. Even though the chamber setup was attached to a grounding cable, the wipe marks were assumed to be caused by electrostatic charging resulting from friction during the cleaning procedure of the panels with laboratory wipes. This assumption was confirmed by measurement of the surface charge of the panels prior to and after cleaning. Therefore, the cleaning procedure was modified to achieve a friction-free method, leading to higher detectable amounts of airborne dust.

Two ACAM types, differing in particle size distribution and particle shape, were investigated to determine the influence of these powder characteristics on the detected dustiness. It became evident, that the ACAM type with smaller particles and a more granular, almost spherical particle shape exhibited a higher dustiness than ACAM with larger, elongated and needle-like particle shape, indicating an influence of the particle properties on dust emission.

To extend the investigated design space of the design of experiments approach for the investigation of the atomization parameters, the chamber setup was modified to allow higher air pressures and thus higher volume flow rates for atomization. The results confirmed the linear relationship of sample mass and detected dust emission of sample masses up to 400 mg. In addition, a two-factor interaction of the atomization volume flow rate and atomization duration was observed with regard to the detected dustiness.

Interestingly, the same two-factor interaction became obvious for the spatial dust distribution. Thereby, the atomization effectiveness of the chamber setup can be predicted and optimized regarding the dustiness and the spatial dust distribution.

A visual summary of the study results is presented in Figure 15.

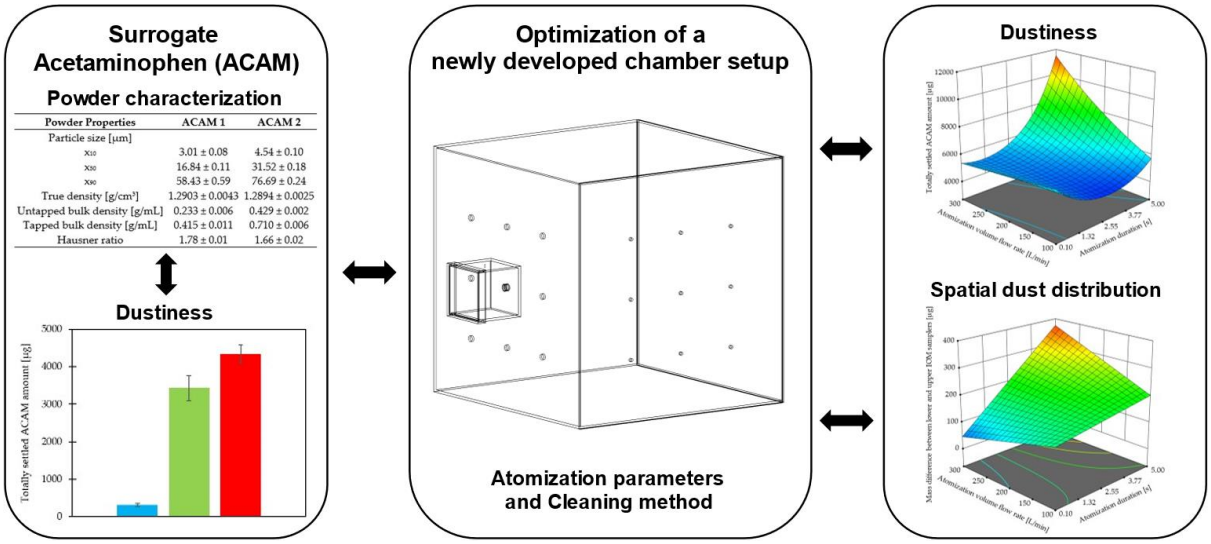


Figure 15: Visual description of the main findings and results of the study [85].

In summary, multiple strategies for influencing dust emissions on a laboratory scale were identified. These strategies may be applied to reduce dust emissions in industrial environments. Moreover, the influence of the atomization parameters on the detected dustiness and the spatial dust distribution were determined. Based on the obtained results, in a further study, the detection chamber was equipped with optical sensors, allowing a real-time spatiotemporal detection of airborne dust.

pharmaceutics

MDPI

Article

Optimization of a Newly Developed Chamber Setup for Spatial Dust Measurements in the Context of Containment

Hendrik Küllmar [1], Martin Schöler [2] and Claudia S. Leopold [1,*]

[1] Division of Pharmaceutical Technology, University of Hamburg, Bundesstr. 45, 20146 Hamburg, Germany; hendrik.kuellmar@uni-hamburg.de
[2] Fette Compacting GmbH, Grabauer Straße 24, 21493 Schwarzenbek, Germany; mschoeler@fette-compacting.com
* Correspondence: claudia.leopold@uni-hamburg.de; Tel.: +49-40-42838-3479

Abstract: Background/Objectives: A specially designed chamber setup for containment investigations of pharmaceutical dusts was recently developed. The aim of the present study was to optimize the measurement procedure with this chamber setup, focusing on the atomization parameters. The optimization was aimed at a maximization of the amount of detected dust and a minimization of the required sample mass. **Methods:** For this purpose, the safe surrogate substance acetaminophen was used for dust measurements. In addition to the atomization parameters investigated by a design of experiments, the cleaning of the chamber setup and the selection of two different types of acetaminophen with different physicochemical properties were examined. **Results:** By altering the cleaning method of the chamber setup, more than a tenfold increase of detected acetaminophen was observed. In addition, by selecting the more appropriate acetaminophen type, the totally detected acetaminophen amount was further increased by more than 25%. By means of the design of experiments two models were developed, one dealing with the atomization parameters with regard to the atomization effectiveness and the other describing their influence on the spatial dust distribution of acetaminophen. Based on the model for atomization effectiveness, the totally detected acetaminophen amount may be increased by more than double at a constant sample mass. **Conclusions:** In summary, the measurement procedure of the chamber setup was optimized in terms of the cleaning method, surrogate choice, and the adjustment of the atomization parameters, giving valuable insights to deepen our understanding of dustiness and the spatial distribution of dust in the context of containment.

Keywords: containment; dustiness chamber; IOM sampler; spatial dust distribution design of experiments

check for updates

Academic Editor: Ruggero Bettini

Received: 14 March 2025
Revised: 19 April 2025
Accepted: 23 April 2025
Published: 25 April 2025

Citation: Küllmar, H.; Schöler, M.; Leopold, C.S. Optimization of a Newly Developed Chamber Setup for Spatial Dust Measurements in the Context of Containment. *Pharmaceutics* **2025**, *17*, 565. https://doi.org/10.3390/pharmaceutics17050565

Copyright: © 2025 by the authors. Licensee MDPI, Basel, Switzerland. This article is an open access article distributed under the terms and conditions of the Creative Commons Attribution (CC BY) license (https://creativecommons.org/licenses/by/4.0/).

1. Introduction

Highly potent active pharmaceutical ingredients (HPAPIs) have lately become increasingly important in therapeutic fields such as oncology or the treatment of autoimmune diseases [1]. With high-throughput screening and the application of artificial intelligence, an increasing number of innovative and highly effective compounds have been developed [2–5]. Because of their high pharmacological and toxicological potential, HPAPIs often pose a risk for the personnel in the pharmaceutical industry during manufacturing [3,6]. To control the exposure of personnel to HPAPIs, so-called Occupational Exposure Limits (OELs) are implemented to ensure that this exposure does not exceed a tolerable level [7–10]. In addition, cross-contamination during manufacturing must be prevented,

and environmental protection is of concern [6,11,12]. Because of the high risks posed by HPAPIs during the manufacturing of pharmaceuticals, containment measures have to be implemented at production sites, machines, and devices. These measures involve barrier concepts such as airlocks or housings for production machines as well as pressure differentials and high performance filter systems for ambient air [6,13–15].

The dustiness of a powder is defined as its propensity to generate airborne particles during processes such as mixing, milling, or transferring, which may lead to the generation of inhalable dust [14,16,17]. Airborne dust comprises particles with an aerodynamic diameter of up to 100 µm. The largest inhaled particles with an aerodynamic diameter of 100–30 µm are deposited between the point of entry (lips or nares) and the larynx. Smaller particles with a size of less than 10 µm may reach the thoracic region, and maximum deposition occurs with particles of approximately 2 µm aerodynamic diameter in the alveolar region. Particles smaller than 0.5 µm are usually exhaled without being deposited [17].

As dustiness with its associated health risks is of concern in different industries, various chambers for dustiness measurements of powders have been described in recent years [18–26]. Most of these systems require a relatively high amount of powder sample. As most active pharmaceutical ingredients (APIs) are of high production costs and thus of limited quantity, devices suitable for small sample quantities and/or pharmaceutical powders have been developed [27–30].

Dustiness is dependent on various physicochemical powder properties such as moisture content, particle morphology, density, and particle size distribution [28,31–33]. In addition, the type and amount of energy input needed for atomization as well as the flight path from the atomization to the detection site may influence the measured dustiness [18,32].

Because of the above-mentioned health risks associated with the handling of HPAPIs, the International Society for Pharmaceutical Engineering (ISPE) recommends safe surrogate substances such as lactose, naproxen sodium, or acetaminophen for tests of containment equipment and pharmaceutical dustiness investigations in the laboratory [10,13,34]. The choice of the surrogate substance should be based on its limits of analytical quantification as well as its physicochemical powder properties. For example, acetaminophen is a suitable surrogate for HPAPIs of low molecular weight. Furthermore, the quantification limit of acetaminophen by HPLC with subsequent spectrophotometrical detection is low, making it an industry-accepted standard for dustiness investigations [10,35,36]. If no suitable surrogate exists for dustiness investigations of a specific HPAPI, the risk posed for employees by handling this HPAPI has to be assessed. The risk assessment includes the identification of any potential hazards, defining who may be harmed, and the verification of whether existing precautions are adequate or need improvements [1]. These precautions may include, among others, the use of bottles with split butterfly valve connectors, handling of HPAPIs in isolators, as well as personal protective equipment [1,13].

In a previous study, a newly developed chamber setup was introduced, being the first of its kind, allowing not only the investigation of the dustiness of an API but also the determination of its spatial dust distribution. The results of these investigations were verified with computational fluid dynamics [37]. As the detected amount of generated airborne dust was low compared to the applied sample amount, the objective of this study was to optimize the presented chamber setup regarding its atomization effectiveness. This was performed by alteration of the cleaning method and by surrogate choice. As mentioned above, the type and amount of energy input applied for atomization of a powder sample is of major concern in dustiness investigations. To our knowledge, most investigations and comparisons of dustiness chambers comprised different methods for atomization of powder samples (for example, a rotating drum or a single-drop method). In addition, these studies only focused on experimental parameters such as sample mass, sampling duration,

or volume flow rate for filter-based sampling, while none of these chambers were capable of measuring the spatial distribution of pharmaceutical dust [18,26,27,29,30,32]. Therefore, in the present study, the influence of the atomization parameters for pneumatic atomization with a newly developed chamber setup on the detected dustiness was investigated by application of a design of experiments approach.

2. Materials and Methods

2.1. Materials

The determination of the spatial distribution of dust was carried out with two different types of acetaminophen as safe surrogate substances (ACAM 1: Caelo, Hilden, Germany; ACAM 2: Fagron, Glinde, Germany), differing in their particle size and shape.

2.2. Methods

2.2.1. Chamber Setup

The experimental setup was described in detail in a previous publication [37]. Briefly, the chamber setup consisted of two connected chambers, a small emission chamber and a larger detection chamber made of acrylic glass (Plexiglas XT, Polyvantis, Weiterstadt, Germany), as depicted in Figure 1. The emission chamber showed a volume of approximately 7.3 L and was connected to the detection chamber at one of nine possible positions by a protruding tube fixed to the emission chamber. The detection chamber with a volume of 1 m^3 was set up in two different arrangements, either with oppositely or with orthogonally positioned measurement spots. In the present study all experiments were carried out with the orthogonal arrangement as displayed in Figure 1.

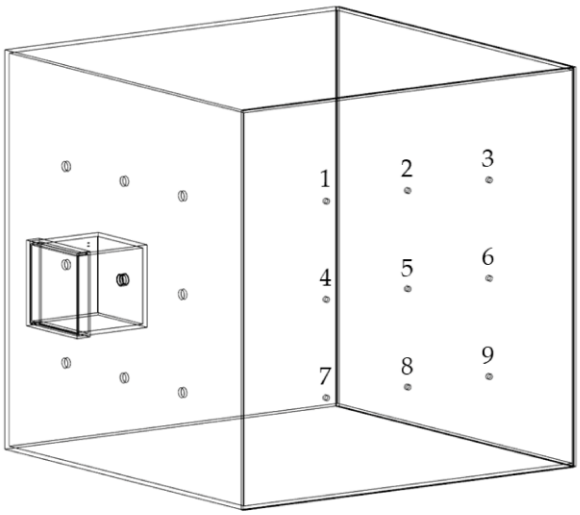


Figure 1. Simplified illustration of the chamber setup for dust measurements in orthogonal arrangement with measurement spots 1–9, modified after [37].

The measurement spots for dust detection were equipped with nine IOM samplers (I.O.M. Multi-Dust samplers, SKC, Blandford Forum, UK), each connected to an air sampling pump (Flite 4, SKC, Blandford Forum, UK) with independent flowmeters being located in the tube connections, as shown in Figure 2. A double-acting ball valve was connected to an orifice with an attachment point located in the top plate of the emission chamber and used for atomization of the powder samples. The ball valve was pneumatically controlled by a 5/2-way solenoid valve. An arrangement of two 3/2-way solenoid valves and two 3/2-way pneumatic valves controlled the duration of the airflow through the IOM samplers and the flow of pressurized air used for atomization (Figure 2). For the present study, three modifications with regard to the initial chamber setup were made.

A compressor (Metabo Mega 400-50W, Nürtingen, Germany) was used as a source for compressed air for atomization to generate pre-pressures of up to 10 bar. To regulate the high pressures, the pressure-reducing valve (Futura 1 RP14-10 F, Riegler, Bad Urach, Germany) had to be exchanged. To make use of these pressures for high atomization volume flow rates, the flowmeter (FR4500, Key Instruments, Croydon, PA, USA) installed upstream of the double-acting ball valve also had to be exchanged. A Programmable Logic Controller (PLC: Siemens LOGO! 12/24 RCE, Munich, Germany) controlled all valves of the chamber setup. To dissipate electrostatic charges, a grounding cable was attached to the chamber setup.

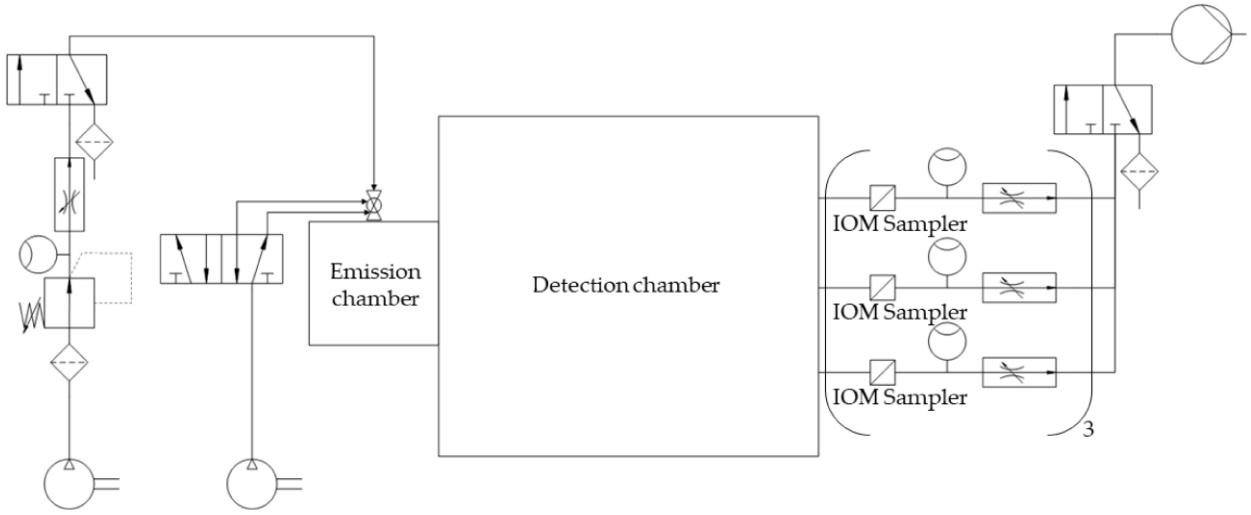


Figure 2. Simplified piping and instrumentation diagram of the optimized chamber setup.

2.2.2. Dust Measurements

For each dust measurement, the respective sample was transferred into a small tube above the double-acting ball valve. After starting the measurement by actuating a toggle switch on the PLC, the programmed sequence led to the immediate opening of the double-acting ball valve (Figure 2). Thereby, the sample was atomized with compressed air, introduced into the emission chamber, and passed through the connecting orifice from the emission to the detection chamber. As the lag time between atomization and detection was set to 0 s, the 3/2-way solenoid valve between the IOM samplers and the vacuum pump was activated simultaneously. By this measure, an immediate airflow through each of the glass microfiber filters (1820-025, Whatman, Little Chalfont, UK) fixed within the IOM samplers with a flow rate of 2 L/min was realized for 278 min. Thereby, the ACAM dust moved via convective and diffusive mass transport and eventually settled on the filters. This settled amount was quantified by HPLC.

2.2.3. HPLC Assay

The quantification of the settled amount of ACAM on the glass microfiber filters was performed by HPLC (Chromaster 5000, VWR-Hitachi, Tokyo, Japan) using a LiChroCART RP-18e 250-4 column (Merck, Darmstadt, Germany). Therefore, the filters were withdrawn from the IOM samplers and transferred to individual iodine flasks. The cassette fronts of each of the IOM samplers were swabbed with additional glass microfiber filters. These filters were also transferred to the corresponding iodine flasks. ACAM was extracted from the filters with 2 mL of the mobile phase, consisting of a mixture of acetonitrile and water (75:25 v/v), and adjusted to a pH of 3.5 with phosphoric acid. Therefore, the flasks were shaken for 30 min at 100 rpm (Unimax 1010, Heidolph Instruments, Kelheim, Germany). The obtained extracts were diluted with the mobile phase (1:150), and approximately

1.5 mL of the dilutions were transferred to HPLC vials. 20 µL of each diluted sample was injected into the sample loop, and the HPLC flow rate was set to 1 mL/min. The measurements were carried out at a temperature of 22 °C, and the spectrophotometrical detection was performed with a Diode Array Detector (Chromaster 5430, Hitachi, Tokyo, Japan). Because of the higher ACAM load on the filters, caused by the optimization of the dust measurements performed in the present study, the calibration range had to be extended compared to a previous study [37] and was linear between 0.033 µg/mL and 19.99 µg/mL (R^2 = 0.9999).

2.2.4. Cleaning of the Chamber Setup

Two different methods for cleaning the chamber setup were investigated. In "Cleaning method I", the residual ACAM dust deposited on the inner panel surfaces was removed with a vacuum cleaner (Nilfisk GM 80, Bellenberg, Germany). Subsequently, the surfaces were wiped with a moistened microfiber cloth. The residual moisture was removed with Kimtech Science Precision Wipes (Kimberly-Clark, Koblenz, Germany). In "Cleaning method II", the residual ACAM dust was directly removed with a moistened microfiber cloth. The residual moisture was removed with a conventional hair dryer (ThermoProtect 2200 W, Philips, Hamburg, Germany) to prevent electrostatic charging of the chamber setup as a result of friction. The electrostatic potential of the acrylic panel surfaces of the emission and detection chamber was measured with an IZH10 Handheld Electrostatic Meter (SMC Corporation, Tokyo, Japan) prior to cleaning and after Cleaning method I and II.

To evaluate the influence of the cleaning methods on the dust measurements, samples of ACAM 2 with a mass of 250 mg each were measured. The compressor was set to 10 bar, and the pre-pressure at the pressure reducing valve was reduced to 6 bar. The volume flow rate for atomization was set to 300 L/min with a duration of 0.2 s.

2.2.5. Sieving of the Surrogate

Both ACAM types were sieved with 90 µm mesh size (LINKER Industrie-Technik, Kassel, Germany), as this step may improve the reproducibility of dust measurements [38]. By this means a coarse and a fine fraction were obtained for each ACAM type. The coarse fractions were discarded, and only the fine fractions were used in this study.

2.2.6. Particle Size Distribution

The particle size distributions of both ACAM types were determined in triplicate by laser diffractometry (Helos KR, Sympatec, Clausthal-Zellerfeld, Germany). The measurements were performed with a lens with an effective range of 0.5–875 µm. Compressed air at a pressure of 1.5 bar was used to disperse the ACAM powder samples. The particle size distribution was analyzed with the Paqxos software (Version 2.0.3, Sympatec, Clausthal-Zellerfeld, Germany).

2.2.7. Residual Moisture Content

The residual moisture contents of both ACAM types were measured in triplicate via thermal gravimetric analysis (Pyris 1 TGA, PerkinElmer, Waltham, MA, USA). Therefore, approximately 15 mg of ACAM were heated up with a heat rate of 10 °C/min to 105 °C and were kept at this temperature for 30 min to remove the residual moisture.

2.2.8. True Density

The true densities of the two ACAM types were measured with a helium pycnometer (Pycnomatic ATC EVO, Porotec, Hofheim am Taunus, Germany). For this purpose, approximately 4 g of each ACAM type, measured in triplicate, were used, and five measurement cycles per sample were performed.

2.2.9. Bulk Density

In accordance with the monograph 2.9.34, "Bulk Density of Powders" in the European Pharmacopoeia [39], the untapped and tapped bulk densities of both ACAM types were determined with a jolting volumeter (STAV 2003, J. Engelsmann, Ludwigshafen, Germany) in triplicate. Therefore, approximately 22 g of ACAM 1 and approximately 40 g of ACAM 2 were transferred into a 100 mL graduated measuring cylinder and subjected to the specified number of taps. The determined volumes were used to calculate the Hausner ratios.

2.2.10. Scanning Electron Microscopy (SEM)

To investigate the particle shape of the two ACAM types, SEM images of the particles were taken with a Scanning Electron Microscope (Zeiss EVO MA10, Carl Zeiss, Oberkochen, Germany). The measurements were carried out in a high vacuum with an acceleration voltage of 5 kV.

2.2.11. Atomization Parameters (DoE)

The experimental design for the statistical and factorial analysis of the atomization parameters was created with the software Design-Expert (Version 11.1.2.0, Stat-Ease Inc., Minneapolis, MN, USA). An I-optimal design was chosen to analyze the effect of three atomization parameters (atomization duration, atomization volume flow rate, and ACAM sample mass). A custom optimal design had to be chosen because the volume flow rate of the flowmeter used for atomization could only be set in increments of 10 L/min. From the given options, the I-optimal design was selected, as designs based on the I-optimality criterion minimize the integral of the prediction variance across the design space [40,41]. This design is commonly used if the response surface has to be modeled with good precision and if the significance of the investigated factors has been determined [40,42,43]. For analysis of the three atomization parameters mentioned above, for the basic model, ten model points were required. Five additional lack-of-fit points were added if a higher-order model, such as a quadratic model, was required to describe the response surface. Eight replicate points were added to estimate the precision of the model. Another eight additional model points were added to improve the statistical power (>80%) of potential two-factor interactions.

The choice of the factor limits for the DoE design is based on preliminary tests and a previous study and is shown in Table 1 [37]. Based on this previous study, the upper limit for the atomization duration was set to 5 s, as with this duration it was possible to obtain sufficient airborne dust concentrations in the detection chamber of the setup. The lower duration was set to 0.1 s because a synchronization of the double-acting ball valve and the 3/2-way pneumatic valve was not possible with shorter atomization durations due to switching delays. The upper limit for the atomization volume flow rate was set to 300 L/min, representing the maximum adjustable flow rate for the flowmeter. The lower limit was set to 100 L/min, as already applied in the above-mentioned previous study. ACAM 1 (50 to 500 mg) was selected for the DoE because of its higher dustiness (see Section 3.3). The compressor was set to its maximum pressure of 10 bar, which was subsequently reduced to 4 bar by the pressure-reducing valve. In a preliminary study, the reduction to 4 bar turned out to be best suited to achieve a constant volume flow over several seconds for both high and low atomization volume flow rates with the flowmeter. With a pressure reduction to values lower than 4 bar, the pressurized air was insufficient to achieve a volume flow rate of 300 L/min, and with a reduction to values higher than 4 bar, the compressed air of the compressor was not sufficient to maintain a constant volume flow for a duration of 5 s.

Table 1. Selected factor limits for the DoE.

Factor	Lower Limit	Upper Limit
Atomization duration [s]	0.1	5
Atomization volume flow rate [L/min]	100	300
ACAM 1 sample mass [mg]	50	500

A model for the atomization effectiveness of the chamber setup was created by selecting the totally settled amount of ACAM 1 on all nine filters within the IOM samplers as a response. A further model for the spatial dust distribution in the detection chamber was created by selecting the mathematical difference of the settled amount of ACAM 1 between the lower row of IOM samplers (#7–#9) and the upper row of IOM samplers (#1–#3) as response, named 'Mass difference between lower and upper IOM samplers' throughout this paper.

Both models were statistically evaluated based on an analysis of variance (ANOVA). With the ANOVA, the significance of the models, their lack-of-fit, their R^2, adjusted R^2, and predicted R^2 were determined. Non-significant model terms were omitted unless required for support of the factor hierarchy.

For the validation of both models, two additional measurements (confirmation runs) each were performed in triplicate at factor combinations different than those used to calculate the models. One confirmation run was carried out at the center point of the design space with an atomization duration of 2.55 s, an atomization volume flow rate of 200 L/min, and an ACAM 1 sample mass of 275 mg. For the other confirmation run, the atomization parameters were randomly chosen in the design space with an atomization duration of 3 s, an atomization volume flow rate of 100 L/min, and an ACAM 1 sample mass of 500 mg.

3. Results and Discussion

3.1. Powder Characterization

Various factors may influence the dustiness of powders. The particle size distribution and the residual moisture content play a major role; however, other parameters such as the bulk density and particle shape may also be of importance [28,32,33]. These relevant powder properties were determined for both investigated ACAM types used as surrogates in this study. The respective values are shown in Table 2. Even though both ACAM types were sieved with 90 µm mesh size, they differed in their particle size distribution. ACAM 2 showed larger particle sizes than ACAM 1.

Table 2. Physicochemical properties of the investigated surrogate ACAM (means ± SD, $n = 3$).

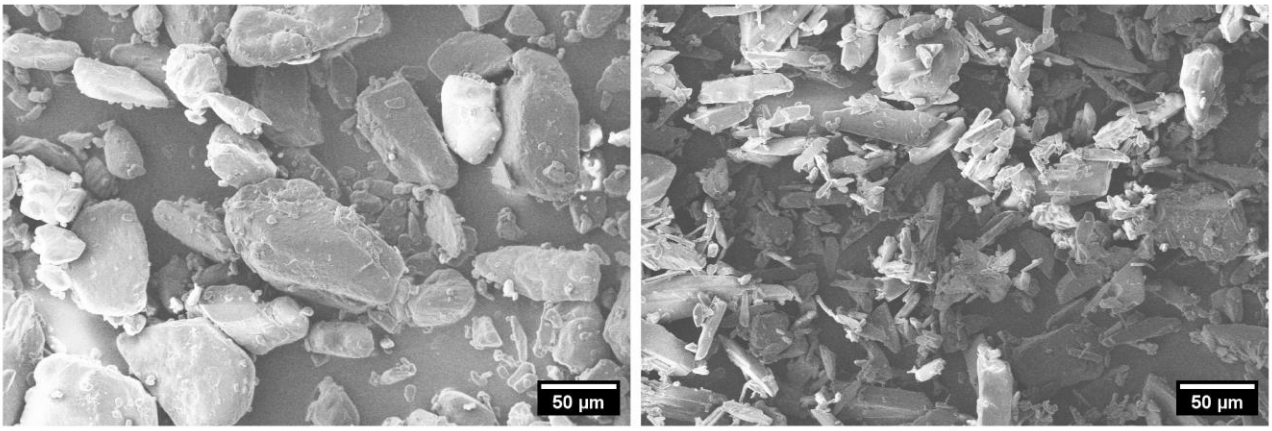
Powder Properties	ACAM 1	ACAM 2
Particle size [µm]		
x_{10}	3.01 ± 0.08	4.54 ± 0.10
x_{50}	16.84 ± 0.11	31.52 ± 0.18
x_{90}	58.43 ± 0.59	76.69 ± 0.24
True density [g/cm^3]	1.2903 ± 0.0043	1.2894 ± 0.0025
Untapped bulk density [g/mL]	0.233 ± 0.006	0.429 ± 0.002
Tapped bulk density [g/mL]	0.415 ± 0.011	0.710 ± 0.006
Hausner ratio	1.78 ± 0.01	1.66 ± 0.02

For both ACAM types, no residual moisture content was detectable, and therefore, its supposedly high influence on dustiness was ruled out. The same applied to the true density, which did not show a significant difference ($p < 0.05$) regarding both ACAM types. Hausner ratios of 1.78 for ACAM 1 and 1.66 for ACAM 2 indicated a very, very poor

powder flowability of both ACAM types [44]. ACAM 2 showed higher untapped and tapped bulk densities than ACAM 1.

In Figure 3, SEM images of ACAM 1 (a) and ACAM 2 (b) are shown. It is clearly visible that the particles of the two different types of ACAM exhibited different shapes.

The particles of ACAM 1 showed a more granular, almost spherical shape, whereas the particles of ACAM 2 exhibited a more elongated, irregular, needle-like shape.



(**a**) (**b**)

Figure 3. SEM images of ACAM 1 (**a**) and ACAM 2 (**b**).

3.2. Influence of the Cleaning Method

The totally settled amount of ACAM 2 after each of the two cleaning methods was measured, and the results are shown in Figure 4. A highly significant difference ($p < 0.0001$) was evident, with a more than tenfold higher totally settled amount of ACAM 2 if the chamber setup was cleaned with Cleaning method II as compared to Cleaning method I. This result demonstrated a strong influence of the cleaning method on the dustiness measurements. By drying the acrylic glass panels of the chamber setup with Kimtech Science Precision Wipes as described in Cleaning method I, electrostatic charging of the panels, especially with the attached grounding cable, was not expected. However, dust traces remained on the panels in the form of wipe marks after each experiment. ACAM itself shows a high tendency for electrostatic interactions with processing vessels, and acrylic glass exhibits a low conductivity [45–47]. Therefore, the presence of wipe marks combined with the results of the cleaning experiments strongly suggests electrostatic charging of the acrylic panels, resulting in a loss of airborne dust. Generally, electrostatic charging is described as one major factor influencing powder dustiness [31]. The lower dustiness detected after application of Cleaning method I was therefore assumed to be caused by electrostatic charging. Thus, the electrostatic potential of the emission and detection chamber was determined prior to cleaning, after Cleaning method I, and after Cleaning method II. The electrostatic potential of the emission chamber surface prior to cleaning amounted to 0.16 ± 0.12 kV, after Cleaning method I to 7.34 ± 0.49 kV, and after Cleaning method II to -2.40 ± 0.21 kV ($n = 5$). Similar values were measured at the surface of the detection chamber. The electrostatic potential prior to cleaning resulted in -0.01 ± 0.01 kV, after Cleaning method I in -1.56 ± 0.32 kV, and after Cleaning method II in 7.52 ± 0.61 kV ($n = 5$). The results demonstrated a significant difference ($p < 0.0001$) in the electrostatic potential between the two cleaning methods, verifying their influence on the detected settled amount of ACAM in this study.

With the change to a friction-free cleaning method, it was possible to mitigate electrostatic charges on the panels. To further reduce electrostatic charges, Sayahi et al. described an anti-static system consisting of a helical pattern of grounded copper strips and wire at-

tached to their chamber setup, which was also made of acrylic glass [48]. With the modified cleaning method, a potential bias of the chamber setup when comparing electrostatically chargeable powders with non-chargeable substances is reduced, thereby improving its reliability. The results underline the importance of mitigating electrostatic charges when investigating dustiness in a laboratory environment. However, electrostatic charging only plays a minor role in pharmaceutical manufacturing under contained conditions, as production machines are usually grounded. Furthermore, tablet presses or isolators for the manufacture of dosage forms containing HPAPIs may be washed in place.

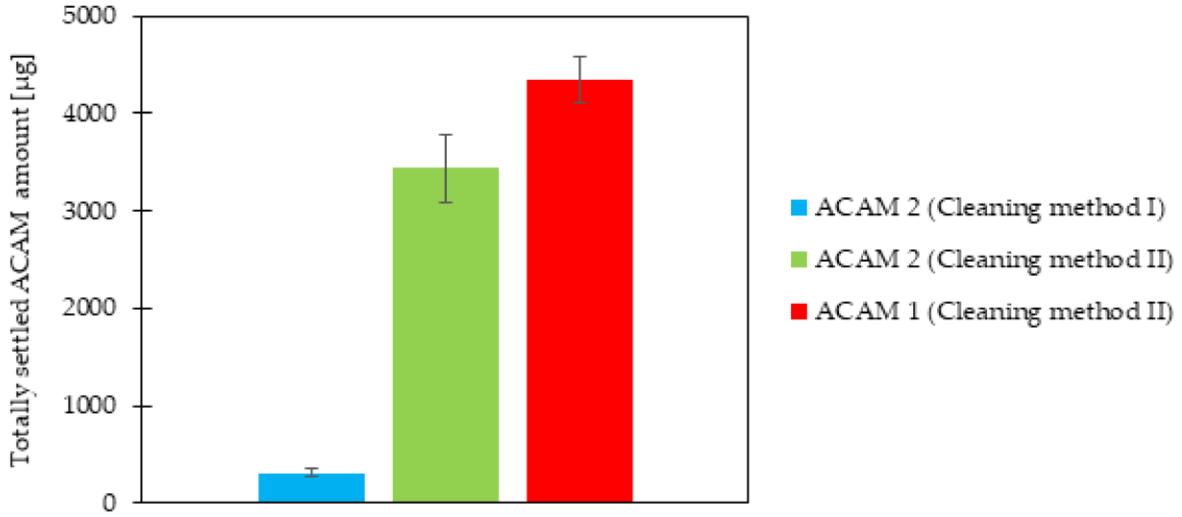


Figure 4. Totally settled amount of ACAM 2 after Cleaning methods I and II as well as that of ACAM 1 after Cleaning method II, on all nine filters within the IOM samplers (means ± SD, $n = 3$).

3.3. Comparison of the ACAM Types

The difference in the totally settled amount of ACAM 1 and ACAM 2, obtained with the same atomization parameters as used for the cleaning evaluation, is also shown in Figure 4. As the Cleaning method II led to higher dustiness values, as mentioned above, it was selected for the comparison of the two ACAM types. A significant difference ($p < 0.05$) between the totally settled amount of ACAM 1 and ACAM 2 was evident. As mentioned in the introduction, if investigating the dustiness of powders, the energy input needed for atomization must be taken into consideration [18]. As the atomization parameters for the comparison of both ACAM types were identical and no residual moisture content as well as no significant difference in their true density was detectable, the observed dustiness results were caused most likely by their different particle size distributions, particle shapes, and bulk densities.

Several authors identified the particle size distribution as one of the most important powder characteristics affecting dustiness [28,32,36,38,49,50]. Regarding the particle size, Plinke et al. postulated that the size-specific dust generation rate increases with the particle diameter d. They explained this observation in their experiments with the fact that the separation forces, such as impaction, increase with d^3, whereas binding forces based on van der Waals attraction and capillary forces are proportional to d [32]. This influence of binding and separation forces is overlaid by the particle transport away from the atomization site. Larger particles (>10 µm) are affected by gravity and thus sedimentation, preventing the transport from the atomization site to the measuring site [32]. Results of coating experiments with powder particles on an aluminum tray indicated that with decreasing particle size, dustiness tended to increase [49]. This observation is supported by findings of Wirth et al. in two studies, where different particle size fractions of ACAM were investigated regarding their dustiness. A significant decrease in dust emission

was observed with increasing particle size [36,51]. This is in accordance with the detected differences in dustiness observed with the two ACAM types in the present study.

Beyond that, the particle morphology may affect the measured dustiness because of its influence on interparticular adherence as well as attraction to or repulsion from surfaces [24,28,51]. As shown in Figure 3, ACAM 2 showed a more elongated, irregular, needle-like shape. In experiments with nanoparticles carried out by O'Shaughnessy et al., a lower dustiness for fibrous particles in comparison to granular particles was demonstrated [28]. This result supports the lower dustiness of ACAM 2 observed in this study. Furthermore, a significantly higher untapped bulk density ($p < 0.01$) of ACAM 2 than that of ACAM 1 was observed (Table 2). This also may have contributed to the lower dustiness of ACAM 2 [31].

3.4. Results of the DoE

An I-optimal design was used to analyze the effect of the three atomization parameters on the atomization effectiveness and spatial dust distribution within the detection chamber of the newly developed chamber setup. The results are shown in Table 3. The non-significant lack of fit showed that both models described the original data well. One value had to be excluded from the data set of the spatial dust distribution model because of a sampling error. This did not affect the totally settled ACAM amount and thus the model for the atomization effectiveness. For this model, the high values for R^2, adjusted R^2, and predicted R^2, as well as the high adequate precision value, indicated a good model for correlation and prediction. These values were lower for the spatial dust distribution model, but the predicted R^2 was still in reasonable agreement with the adjusted R^2 (difference <0.2), and the adequate precision was higher than 4. Therefore, the model was used to navigate the design space. As shown in Table 3, non-significant model terms and higher-order models were excluded, if possible, to simplify the models.

The results for the confirmation runs are listed in Table 4. The predicted values of the statistical models were compared to the measured values of the confirmation runs. For the atomization effectiveness model, a good overall prediction was achieved with deviations of only 3.49 and 16.67%, respectively. However, the second model for the spatial dust distribution failed in terms of the confirmation runs at the center point of the model with a deviation of 120.59% from the predicted value. This was caused by slightly more settled dust on the filters in the upper IOM row than in the lower IOM row. The second combination of atomization parameters resulted in a deviation of 47.12%, indicating an imprecise overall model prediction. Therefore, predictions based on this model should only be made with keeping the quality of the model in mind. On the one hand, the imprecise prediction was caused by the chosen factor limits. These limits were selected based on preliminary studies with the optimization of the atomization effectiveness in mind. On the other hand, as the main goal of this study was the optimization of the atomization effectiveness, ACAM was sieved to improve the reproducibility of the dustiness measurements [38]. This sieving step narrowed the particle size distribution (Table 2) by removing the coarse fraction of the particles. Consequently, the fraction of particles affected by sedimentation within the detection chamber was reduced, and thus the spatial dust distribution with regard to the mass difference between lower and upper IOM samplers was less pronounced.

In Figure 5 the results of the response surface model for the atomization effectiveness are shown. As the sample mass did not show any factor interactions (Table 3), its direct influence on the totally settled ACAM amount is shown in Figure 5a. It is obvious that the curve profile of the settled ACAM amount shows a linear tendency from 50 mg up to approximately 300 mg with a peak maximum of 410 mg. A similar effect was observed with

a different chamber setup for dustiness investigations using an identical double-acting ball valve for atomization [30]. This observation indicates that with this ball valve geometry, the atomization of even low sample amounts is possible, which is advantageous with regard to reduced experimental costs. Furthermore, by adjusting the atomization duration and volume flow rate according to the results of the DoE, the totally settled ACAM amount may be more than doubled at a constant sample mass (Figure 5b). This poses a major advantage compared to a previous study [37].

Table 3. ANOVA results of the DoE models.

Model	Atomization Effectiveness (Totally Settled Amount) *p*-Value	Spatial Dust Distribution (Lower–Upper IOM Row) *p*-Value
Model	0.0001	0.0001
Sample mass (A)	0.0001	0.0004
Atomization duration (B)	0.0204	0.0009
Atomization volume flow rate (C)	0.0357	Nonsignificant
Interaction AB	Nonsignificant	Nonsignificant
Interaction AC	Nonsignificant	Nonsignificant
Interaction BC	0.0103	0.0312
A^2	0.0027	Nonsignificant
B^2	0.0079	Nonsignificant
C^2	Nonsignificant	Nonsignificant
Lack of fit	Nonsignificant	Nonsignificant
R^2	0.8455	0.6525
Adjusted R^2	0.8069	0.5969
Predicted R^2	0.7381	0.4268
Adequate precision	15.7408	13.1658

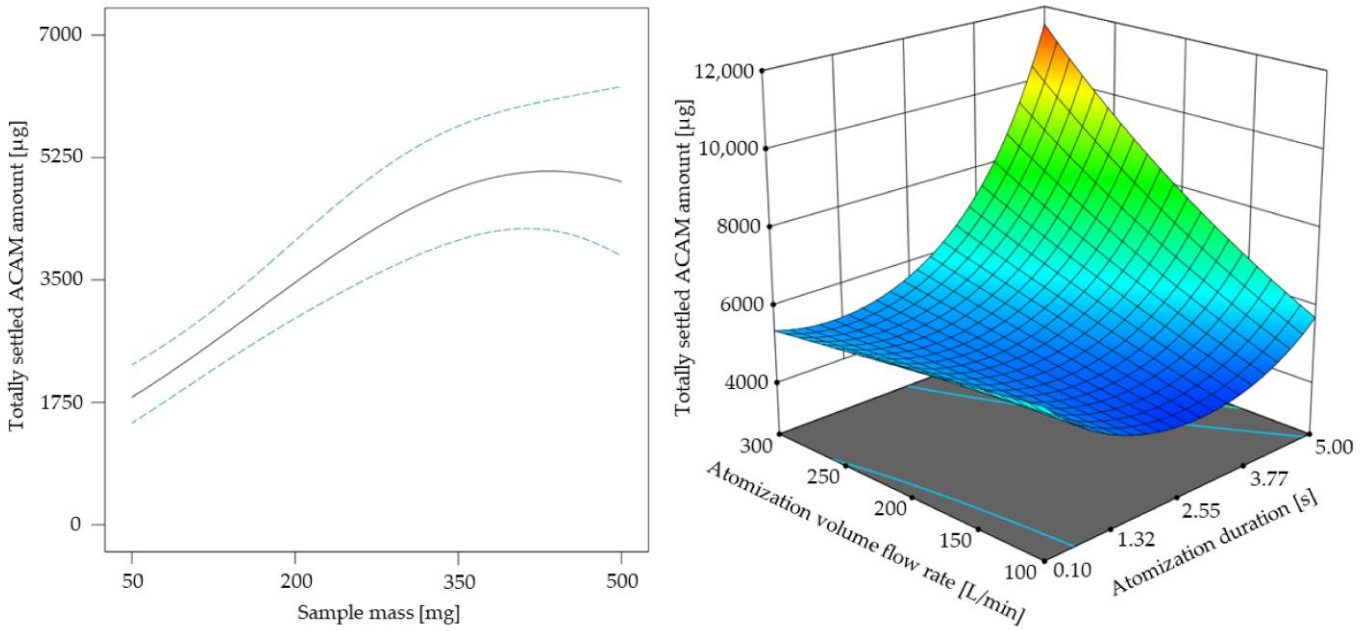
Table 4. Confirmation of the DoE models.

Model	Atomization Effectiveness		Spatial Dust Distribution	
Atomization duration [s]	2.55	3	2.55	3
Atomization volume flow rate [L/min]	200	100	200	100
Sample mass [mg]	275	500	275	500
Predicted mean [µg]	4245.83	4294.13	133.95	220.26
Measured mean ± SD [µg] (n = 3)	4394.02 ± 184.32	5010.07 ± 359.31	−27.58 ± 2.54	116.48 ± 11.63
Deviation [%]	3.49	16.67	120.59	47.12

The response surface shown in Figure 5b describes the two-factor interaction of the atomization volume flow rate and the atomization duration. It is evident that the totally settled ACAM amount clearly increases if an atomization duration of over 2 s is combined with an atomization volume flow rate of more than 150 L/min. By combining these results, a high, totally settled ACAM amount may be achieved with sample masses as low as possible.

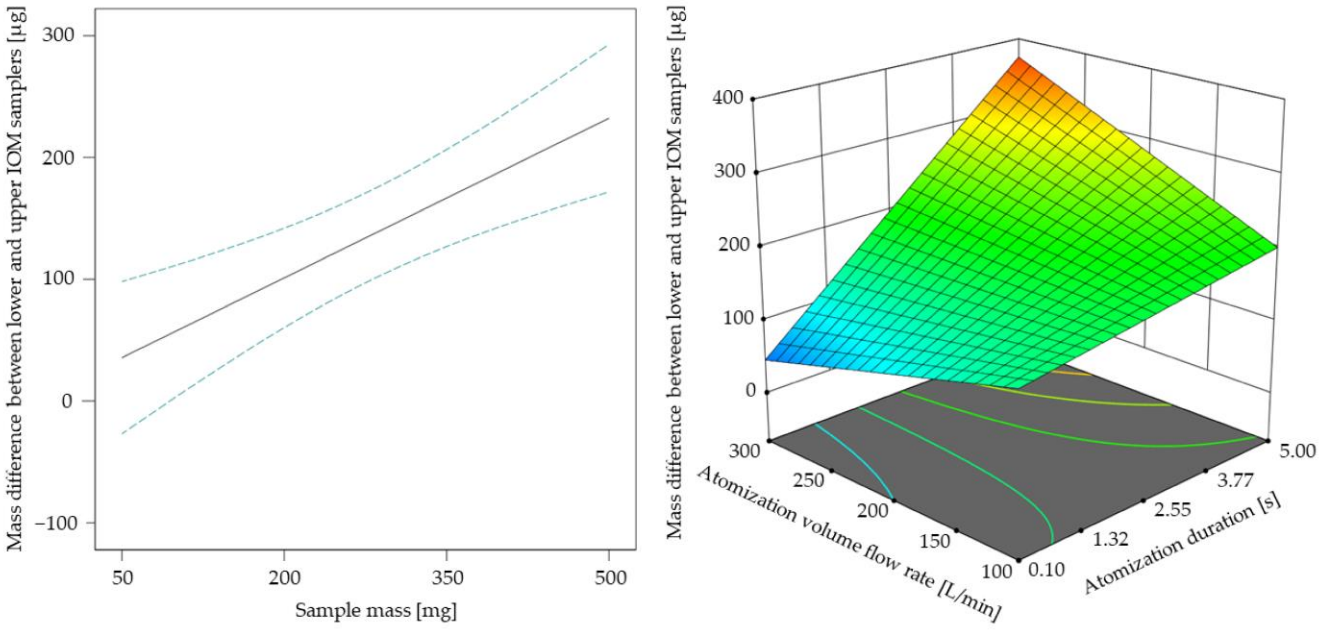
The results of the response surface model for the mass difference between lower and upper IOM samplers are shown in Figure 6. In Figure 6a, a linear relationship between the sample mass and the corresponding mass difference becomes apparent, similar to the linear tendency of the totally settled ACAM amount up to a sample mass of 410 mg, as shown in Figure 5a. This observation is especially of interest, as both the atomization effectiveness and the spatial dust distribution may be increased by selecting higher sample amounts. With the ANOVA of the spatial dust distribution model, the same two-factor interaction of atomization volume flow rate and atomization duration as with the ANOVA of the atomization effectiveness model was recognized (Table 3). The two-factor interaction shown

in Figure 6b indicates that the spatial dust distribution may be increased by increasing both the atomization duration and the atomization volume flow rate. Thus, both models highlight the strong influence of the type and amount of applied energy for atomization—in this case compressed air—on dustiness and spatial dust distribution.



(**a**) (**b**)

Figure 5. Totally settled amount of acetaminophen [µg] in dependence of the sample mass with its 95% CI bands at an atomization duration of 2.55 s and an atomization volume flow rate of 200 L/min (**a**). Response surface for the totally settled ACAM amount [µg] in dependence of the two-factor interaction at a sample mass of 410 mg (**b**).



(**a**) (**b**)

Figure 6. Mass difference between lower and upper IOM samplers [µg] in dependence of the sample mass with its 95% CI bands at an atomization duration of 2.55 s and an atomization volume flow rate of 200 L/min (**a**). Response surface for the mass difference between lower and upper IOM samplers [µg] in dependence of the two-factor interaction at a sample mass of 410 mg (**b**).

4. Conclusions

A newly developed chamber setup has been optimized with regard to the atomization parameters and other experimental factors. The detected amount of the surrogate acetaminophen was increased more than tenfold by an alteration of the cleaning method comprising a friction-free thermal drying. In addition, the choice of an appropriate acetaminophen type with regard to the particle size distribution and particle morphology resulted in a further increase of the detected surrogate amount. With an I-optimal design of experiments, a response surface model for the atomization parameters (atomization duration, atomization volume flow rate, and sample mass) and the resulting atomization effectiveness was created. According to this model, the atomization effectiveness may be improved by longer atomization durations, higher volume flow rates, and sample masses up to 400 mg. These results allow a significant decrease in the required sample mass and thus cost for dust investigations by increasing the atomization duration and volume flow rate. A second model with regard to the spatial dust distribution was designed based on the same dataset gathered for the optimization of the atomization effectiveness. However, it became apparent that the parameter limits for the design space selected to maximize the atomization effectiveness were poorly suited for the investigation of spatial dust distributions. This selection of factor limits and the use of sieved acetaminophen powder resulted in an imprecise response surface model. As the measurement procedure and the atomization parameters were optimized with regard to the detected surrogate amount in the present study, future studies will deal with the optimization of the determination of spatial dust distributions. For this purpose, non-sieved acetaminophen as well as more appropriate factor limits for the design space will be selected, and the results will be analyzed with a machine learning approach to better capture the complexity of spatial dust distribution. The chamber setup will then be used to investigate and compare the dustiness and spatial dust distribution of APIs with different physicochemical properties, such as particle morphology or particle size distribution. Beyond that, binary mixtures of an API and different excipients will be investigated. These studies may provide valuable insights into dustiness and especially the spatial distribution of pharmaceutical dusts, and based on this knowledge, the classification of HPAPIs to OELs is going to be more accurate and will further improve safety in the manufacturing of pharmaceutical dosage forms.

Author Contributions: Conceptualization, H.K., M.S. and C.S.L.; Data curation, H.K.; Formal analysis, H.K. and C.S.L.; Investigation, H.K.; Methodology, H.K.; Software, H.K.; Supervision, C.S.L.; Validation, H.K., M.S. and C.S.L.; Visualization, H.K.; Writing—original draft, H.K.; Writing—review and editing, H.K., M.S. and C.S.L. All authors have read and agreed to the published version of the manuscript.

Funding: This research received no external funding.

Institutional Review Board Statement: Not applicable.

Informed Consent Statement: Not applicable.

Data Availability Statement: Data is contained within the article.

Acknowledgments: The authors express their gratitude to Petra Borbe and Kai Braunschweig for their technical and analytical support. Furthermore, the authors would like to thank the Electron Microscopy Service Unit of the University of Hamburg, especially Charlotte Ruhmlieb, for the SEM data.

Conflicts of Interest: Author Martin Schöler was employed by the company Fette Compacting GmbH. The remaining authors declare that the research was conducted in the absence of any commercial or financial relationships that could be construed as a potential conflict of interest.

Abbreviations

The following abbreviations are used in this manuscript:

HPAPI	Highly potent active pharmaceutical ingredient
OEL	Occupational exposure limit
API	Active pharmaceutical ingredient
ACAM	Acetaminophen
IOM	Institute of Occupational Medicine
PLC	Programmable logic controller
HPLC	High performance liquid chromatography
SEM	Scanning electron microscopy
DoE	Design of experiments
ANOVA	Analysis of variance

References

1. Dunny, E.; O'Connor, I.; Bones, J. Containment Challenges in HPAPI Manufacture for ADC Generation. *Drug Discov. Today* **2017**, *22*, 947–951. [CrossRef] [PubMed]
2. Broach, J.R.; Thorner, J. High-Throughput Screening for Drug Discovery. *Nature* **1996**, *384*, 14–16. [PubMed]
3. Mari, G.; Moccaldi, A.; Ludovisi, G. Handling of High Potency Drugs: Process and Containment. *Trans. Ecol. Environ.* **1999**, *85*, 257–265.
4. Mak, K.-K.; Wong, Y.-H.; Pichika, M.R. Artificial Intelligence in Drug Discovery and Development. In *Drug Discovery and Evaluation: Safety and Pharmacokinetic Assays*; Hock, F.J., Pugsley, M.K., Eds.; Springer: Cham, Switzerland, 2024; pp. 1463–1492.
5. Vemula, D.; Jayasurya, P.; Sushmitha, V.; Kumar, Y.N.; Bhandari, V. CADD, AI and ML in Drug Discovery: A Comprehensive Review. *Eur. J. Pharm. Sci.* **2023**, *181*, 106324. [CrossRef] [PubMed]
6. Wollowitz, S. Managing High-Potency Active Pharmaceutical Ingredients—A Drug Sponsor's Guide. *Drug Dev. Res.* **2010**, *71*, 420–428. [CrossRef]
7. Ku, R.H. An Overview of Setting Occupational Exposure Limits (OELs) for Pharmaceuticals. *Chem. Health Saf.* **2000**, *7*, 34–37. [CrossRef]
8. Naumann, B.D.; Sargent, E.V.; Starkman, B.S.; Fraser, W.J.; Becker, G.T.; Kirk, G.D. Performance-Based Exposure Control Limits for Pharmaceutical Active Ingredients. *Am. Ind. Hyg. Assoc. J.* **1996**, *57*, 33–42. [CrossRef]
9. Heron, R.J.L.; Pickering, F.C. Health Effects of Exposure to Active Pharmaceutical Ingredients (APIs). *Occup. Med.* **2003**, *53*, 357–362. [CrossRef]
10. International Society for Pharmaceutical Engineering (ISPE). *Good Practice Guide: Assessing the Particulate Containment Performance of Pharmaceutical Equipment*; ISPE: Tampa, FL, USA, 2012; ISBN 978-1-936379-35-4.
11. Becker, J.; Industries, E.; Pohlmann, T.; Industries, E. Development and Implementation of a Large-Scale HPAPI Manufacturing Process. *Chim. Oggi-Chem. Today* **2019**, *35*, 20–24.
12. Tiwari, P.; Chowdhury, S.R. Sustainable Production of Highly Active Pharmaceutical Ingredients (HAPIs). *Int. J. Sci. Res. Publ.* **2014**, *4*, 2250–3153.
13. International Society for Pharmaceutical Engineering (ISPE). *ISPE D/A/CH Affiliate: Containment Manual*; ISPE D/A/CH: Offenbach/Main, Germany, 2017; ISBN 9781936379354.
14. Stein, J.; Fuchs, T.; Mattern, C. Advanced Milling and Containment Technologies for Superfine Active Pharmaceutical Ingredients. *Chem. Eng. Technol.* **2010**, *33*, 1464–1470. [CrossRef]
15. Adams, N.J.; Johnson, D.L.; Lynch, R.A. The Effect of Pressure Differential and Care Provider Movement on Airborne Infectious Isolation Room Containment Effectiveness. *Am. J. Infect. Control* **2011**, *39*, 91–97. [CrossRef] [PubMed]
16. Lidén, G. Dustiness Testing of Materials Handled at Workplaces. *Ann. Occup. Hyg.* **2006**, *50*, 437–439. [CrossRef]
17. WHO. Dust Definition and Concepts. In *Hazard Prevention and Control in the Work Environment: Airborne Dust*; WHO: Geneva, Switzerland, 1999; WHO/SDE/OEH/99.14.
18. Bach, S.; Eickmann, U.; Schmidt, E. Comparison of Established Systems for Measuring the Dustiness of Powders with the UNC Dustiness Tester Developed Especially for Pharmaceutical Substances. *Ann. Occup. Hyg.* **2013**, *57*, 1078–1086. [CrossRef] [PubMed]
19. Davies, K.M.; Hammond, C.M.; Higman, R.W.; Wells, A.B. Progress in Dustiness Estimation. *Ann. Occup. Hyg.* **1988**, *32*, 535–544.
20. Heitbrink, W.A.; Tood, W.F.; Cooper, T.C.; O'BRIEN, D.M. The Application of Dustiness Tests to the Prediction of Worker Dust Exposure. *Am. Ind. Hyg. Assoc. J.* **1990**, *51*, 217–223. [CrossRef]
21. Heitbrink, W.A.; Baron, P.A.; Willeke, K. An Investigation of Dust Generation by Free Falling Powders. *Am. Ind. Hyg. Assoc. J.* **1992**, *53*, 617–624. [CrossRef]

22. Cawley, B.; Leith, D. Bench-Top Apparatus to Examine Factors That Affect Dust Generation. *Appl. Occup. Environ. Hyg.* **1993**, *8*, 624–631. [CrossRef]
23. Plinke, M.A.E.; Leith, D.; Boundy, M.G.; Löffler, F. Dust Generation from Handling Powders in Industry. *Am. Ind. Hyg. Assoc. J.* **1995**, *56*, 251–257. [CrossRef]
24. Hamelmann, F.; Schmidt, E. Methods of Estimating the Dustiness of Industrial Powders—A Review. *KONA Powder Part. J.* **2003**, *21*, 7–18. [CrossRef]
25. Hamelmann, F.; Schmidt, E. Methods for Characterizing the Dustiness Estimation of Powders. *Chem. Eng. Technol.* **2004**, *27*, 844–847. [CrossRef]
26. Bach, S.; Schmidt, E. Determining the Dustiness of Powders—A Comparison of Three Measuring Devices. *Ann. Occup. Hyg.* **2008**, *52*, 717–725. [CrossRef] [PubMed]
27. Boundy, M.; Leith, D.; Polton, T. Method to Evaluate the Dustiness of Pharmaceutical Powders. *Ann. Occup. Hyg.* **2006**, *50*, 453–458. [CrossRef] [PubMed]
28. O'Shaughnessy, P.T.; Kang, M.; Ellickson, D. A Novel Device for Measuring Respirable Dustiness Using Low-Mass Powder Samples. *J. Occup. Environ. Hyg.* **2012**, *9*, 129–139. [CrossRef]
29. Ohta, T.; Maeda, H.; Kubota, R.; Koga, A.; Terada, K. Establishment of Powder Dustiness Evaluation Method by Dustmeter with Small Amount of Pharmaceutical Ingredients. *Int. J. Pharm.* **2014**, *472*, 251–256. [CrossRef]
30. Wirth, S.; Schöler, M.; Brügmann, J.; Leopold, C.S. A Novel Two-Chamber Setup for Containment Investigations with Special Focus on the Dustiness of Pharmaceutical Powders Depending on the Airflow. *Pharmaceutics* **2022**, *14*, 2387. [CrossRef]
31. Shandilya, N.; Kuijpers, E.; Tuinman, I.; Fransman, W. Powder Intrinsic Properties as Dustiness Predictor for an Efficient Exposure Assessment? *Ann. Work Expo. Health* **2019**, *63*, 1029–1045. [CrossRef]
32. Plinke, M.A.E.; Maus, R.; Leith, D. Experimental Examination of Factors That Affect Dust Generation by Using Heubach and Mri Testers. *Am. Ind. Hyg. Assoc. J.* **1992**, *53*, 325–330. [CrossRef]
33. Pujara, C.P.; Kildsig, D.O. Effect of Individual Particle Characteristics on Airborne Emissions. In *Containment in the Pharmaceutical Industry*; CRC Press: Boca Raton, FL, USA, 2020; pp. 29–53.
34. International Society for Pharmaceutical Engineering (ISPE). *Good Practice Guide SMEPAC*; ISPE: Tampa, FL, USA, 2024; ISBN 978-1-946964-81-6.
35. Butler, O.; Forder, J.; Saunders, J. Analytical Protocol for the Sensitive Determination of Mannitol, Sorbitol and Glucose Containing Powders in Pharmaceutical Workplaces by Ion Chromatography Using a Pulsed Amperometric Detector. *J. Pharm. Biomed. Anal.* **2015**, *106*, 204–209. [CrossRef]
36. Wirth, S.; Schöler, M.; Brügmann, J.; Leopold, C.S. An Investigation on the Relationship between Dust Emission and Air Flow as Well as Particle Size with a Novel Containment Two-Chamber Setup. *Pharmaceutics* **2024**, *16*, 1088. [CrossRef]
37. Küllmar, H.; Schöler, M.; Brügmann, J.; Leopold, C.S. A Newly Developed Chamber Setup for the Investigation of the Spatial Dust Distribution of Pharmaceutical Powders—A Proof of Concept. *Adv. Powder Technol.* 2025, *submitted*.
38. Evans, D.E.; Turkevich, L.A.; Roettgers, C.T.; Deye, G.J.; Baron, P.A. Dustiness of Fine and Nanoscale Powders. *Ann. Occup. Hyg.* **2013**, *57*, 261–277. [CrossRef] [PubMed]
39. 2.9.34. Bulk Density of Powders. In *European Pharmacopoeia 11.5*; European Directorate for the Quality of Medicines & Health Care (EDQM): Strasbourg, France, 2024; pp. 5830–5833.
40. Hardin, R.H.; Sloane, N.J.A. A New Approach to the Construction of Optimal Designs. *J. Stat. Plan. Inference* **1993**, *37*, 339–369. [CrossRef]
41. Anderson-Cook, C.M.; Borror, C.M.; Montgomery, D.C. Response Surface Design Evaluation and Comparison. *J. Stat. Plan. Inference* **2009**, *139*, 629–641. [CrossRef]
42. Jones, B.; Goos, P. I-Optimal Versus D-Optimal Split-Plot Response Surface Designs. *J. Allergy Clin. Immunol.* **2010**, *130*, 556. [CrossRef]
43. Bondi, R.W.; Igne, B.; Drennen, J.K.; Anderson, C.A. Effect of Experimental Design on the Prediction Performance of Calibration Models Based on Near-Infrared Spectroscopy for Pharmaceutical Applications. *Appl. Spectrosc.* **2012**, *66*, 1442–1453. [CrossRef]
44. 2.9.36. Powder Flow. In *European Pharmacopoeia 11.5*; European Directorate for the Quality of Medicines & Health Care (EDQM): Strasbourg, France, 2024; pp. 5834–5836.
45. Jallo, L.J.; Dave, R.N. Explaining Electrostatic Charging and Flow of Surface-Modified Acetaminophen Powders as a Function of Relative Humidity Through Surface Energetics. *J. Pharm. Sci.* **2015**, *104*, 2225–2232. [CrossRef]
46. Czech, Z.; Kowalczyk, A.; Shao, L.; Cheng, X.Q.; Quan, S.; Bai, Y.P. Novel Acrylic Pressure-Sensitive Adhesive (PSA) Containing Silver Particles. *J. Adhes. Sci. Technol.* **2013**, *27*, 1446–1454. [CrossRef]
47. Transactions, C.S.; Devikala, S.; Kamaraj, P.; Arthanareeswari, M. Conductivity and Dielectric Studies of PMMA Composites. *Chem. Sci. Trans.* **2013**, *2*, 129–134. [CrossRef]

48. Sayahi, T.; Kaufman, D.; Becnel, T.; Kaur, K.; Butterfield, A.E.; Collingwood, S.; Zhang, Y.; Gaillardon, P.E.; Kelly, K.E. Development of a Calibration Chamber to Evaluate the Performance of Low-Cost Particulate Matter Sensors. *Environ. Pollut.* **2019**, *255*, 113131. [CrossRef]
49. Likitwattanasade, T.; Barringer, S.A. The Influence of Particle Size on Separation and Dustiness in Powder Mixtures during Nonelectrostatic and Electrostatic Coating. *J. Electrostat.* **2015**, *77*, 44–50. [CrossRef]
50. Chakravarty, S.; Le Bihan, O.; Fischer, M.; Morgeneyer, M. Dust Generation in Powders: Effect of Particle Size Distribution. *EPJ Web Conf.* **2017**, *140*, 13018. [CrossRef]
51. Wirth, S.; Schöler, M.; Leopold, C.S. Investigations on the Dustiness of Binary Acetaminophen—Lactose Monohydrate Powder Blends. *Powder Technol.* **2024**, *448*, 120317. [CrossRef]

Disclaimer/Publisher's Note: The statements, opinions and data contained in all publications are solely those of the individual author(s) and contributor(s) and not of MDPI and/or the editor(s). MDPI and/or the editor(s) disclaim responsibility for any injury to people or property resulting from any ideas, methods, instructions or products referred to in the content.

3.3 Low-cost particulate matter sensors for real-time spatiotemporal detection of pharmaceutical dust in containment

In the two previous studies, the detection of the atomized powder samples was carried out with IOM samplers and subsequent quantification via HPLC. However, this procedure requires a considerable amount of time and effort. Furthermore, an instantaneous and temporally resolved detection of airborne dust for real-time visualization of spatial dust distributions is impossible. To overcome these problems, the IOM samplers were exchanged by laser-based low-cost particulate matter sensors for dust detection of particles < 2.5 µm. Based on the results of the second study, the atomization parameters were customized during a third study and investigated with regard to a reproducible and precise spatiotemporal detection of airborne dust by these PM sensors. The measurements with the modified chamber setup demonstrated the ability of the sensors to determine the spatiotemporal dust distribution. Moreover, the spatial dust distributions detected with PM sensors resembled those of the first two studies carried out with IOM samplers. However, it became evident that the spatial distribution of the particle fraction < 2.5 µm occurs during the first minutes after atomization until a concentration balance in the detection chamber is reached. This observation not only resulted in a significant reduction of the experimental runtime but also gave valuable insights into the time-dependent distribution of airborne dusts.

The handling and processing of plain APIs only play a minor role in the manufacture of pharmaceuticals, such as direct compression tableting. Therefore, the frequently used excipient lactose and a binary blend of lactose and ACAM were characterized with regard to dustiness and spatial dust distributions. As expected, coarse lactose exhibited a significantly lower dustiness in comparison to fine ACAM. The binary blend of the coarse and the fine powder showed a reduced, yet higher than expected dustiness, indicating

particle interactions of the API particles with those of the excipient which may influence dust generation.

In Figure 16, a simplified illustration of the modified chamber setup and essential outcomes of the third study are shown.

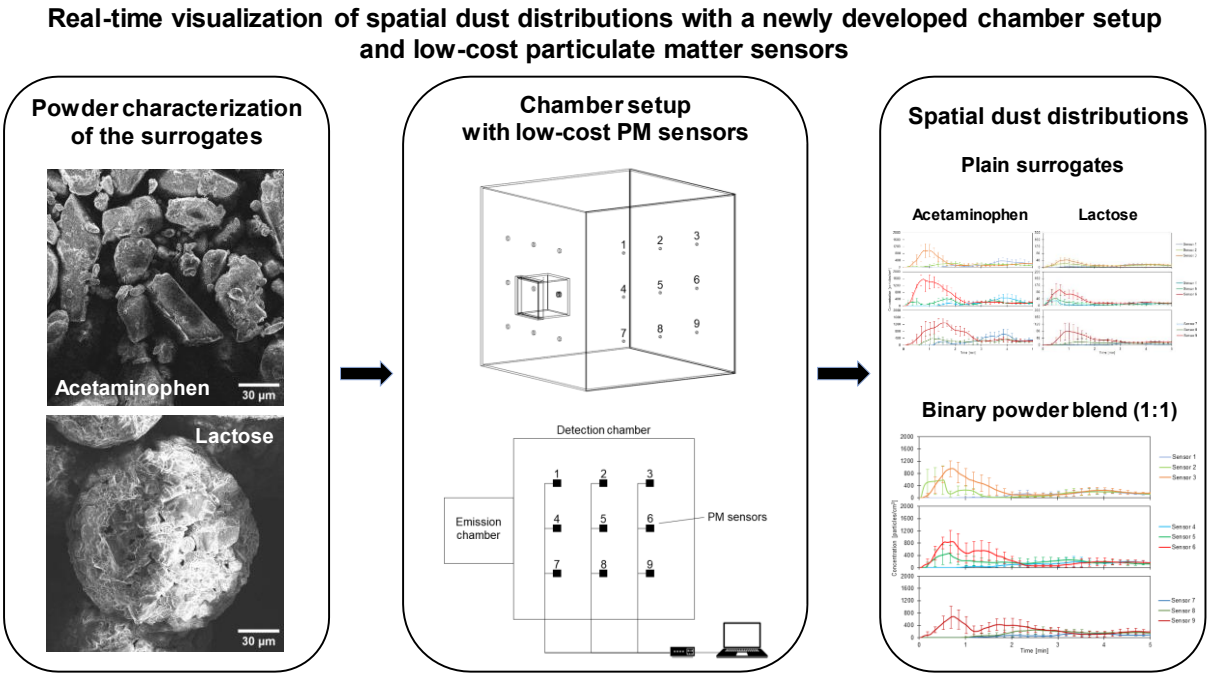


Figure 16: Overview of the methodology and the main results of the study [222].

In summary, the results of the study not only confirmed the feasibility of low-cost particulate matter sensors for dustiness investigations but also suggest a potential application for industrial containment monitoring. Moreover, first insights into the detection of airborne dust resulting from an API-excipient blend were obtained.

European Journal of Pharmaceutics and Biopharmaceutics 223 (2026) 115069

Contents lists available at ScienceDirect

European Journal of Pharmaceutics and Biopharmaceutics

journal homepage: www.elsevier.com/locate/ejpb

Research paper

Low-cost particulate matter sensors for real-time spatiotemporal detection of pharmaceutical dust in containment

Hendrik Küllmar [a], Martin Schöler [b], Kai U. Braunschweig [a], Claudia S. Leopold [a,*]

[a] University of Hamburg, Division of Pharmaceutical Technology, Bundesstraße 45, Hamburg 20146, Germany
[b] Fette Compacting GmbH, Grabauer Straße 24, Schwarzenbek 21493, Germany

ARTICLE INFO

Keywords:
Containment
Dustiness
Low-cost particulate matter sensors
Spatial dust distribution
Real-time visualization
Spatiotemporal detection

ABSTRACT

Highly potent active pharmaceutical ingredients pose a risk with regard to dustiness and spatial distribution of dust in the manufacture of pharmaceuticals. Traditional filter-based methods for dust investigations, for example based on IOM samplers have several disadvantages, such as the gravimetrical or wet chemical analysis of the collected samples, neither allowing the detection of airborne dust concentrations in real-time, nor time-resolved. Therefore, a recently developed chamber setup was equipped with low-cost particulate matter sensors to investigate their feasibility to detect and visualize the spatiotemporal distribution of pharmaceutical dusts in real-time. Experiments with the surrogate substance acetaminophen revealed that with a suitable adjustment of the atomization parameters, reproducible dust concentrations and the spatiotemporal dust distribution within the chamber setup were detectable with the sensors in real-time. Based on these results, lactose as a typical excipient in tableting blends for direct compression and a binary powder blend of acetaminophen and lactose were also investigated. The binary blend as well as plain lactose showed a reduced dustiness when compared to plain acetaminophen, indicating particle interactions between both substances which influence their tendency to become airborne. In conclusion, the particulate matter sensors allow investigations of spatiotemporal dust distributions in real-time.

1. Introduction

Lately, in the therapy of autoimmune disorders, cancer, or hormone imbalances, Highly Potent Active Pharmaceutical Ingredients (HPAPIs) have become increasingly important [1,2]. To the benefit of patients, an increasing number of innovative compounds with high efficacy have been developed by combinatorial chemistry, high-throughput screening, and the application of artificial intelligence [3–6]. During the manufacture of pharmaceutical dosage forms, HPAPIs often pose a risk to the personnel because of their high pharmacological and toxicological potential [4,7]. The acceptable exposure of personnel to HPAPIs is limited by Occupational Exposure Limits (OEL) [8–11]. Furthermore, cross-contamination during manufacturing as well as the release of HPAPIs into the environment have to be prevented [7,12,13]. To effectively minimize these risks, containment measures are implemented at production sites and machines, such as airlocks, isolators, and/or housings, as well as high-performance filter systems for ambient air [7,14–16].

The performance of containment systems may be assessed according to the 'Standardized Methodology for the Evaluation of Pharma Airborne Particle Emissions from Containment Systems' (SMEPAC) [17]. For the determination of airborne particles, filter-based IOM samplers (Institute of Occupational Medicine), DIS (Disposable Inhalable Samplers), as well as CFC (Closed-Face Cassettes) may be used. Based on the risk assessment of potential contamination hazards at critical spots of production machines, such as the product in- and outlets of a tablet press, the samplers are positioned in the production environment. With these samplers, the amount of airborne dust during a preliminary test prior to production may be determined to detect any malfunctions or leakages in containment systems [17]. An advantage of the IOM samplers is that they exclusively capture the inhalable fraction of airborne dust and offer the possibility to analyze the samples with regard to a specific substance, for example, an API. However, a major disadvantage is that they detect airborne particles neither in real-time nor time-resolved [18,19]. Moreover, the filters have to be analyzed in a laboratory and the analysis often takes days or even weeks. These disadvantages result in a major limitation of the SMEPAC methodology:

* Corresponding author.
E-mail addresses: hendrik.kuellmar@uni-hamburg.de (H. Küllmar), mschoeler@fette-compacting.com (M. Schöler), kai.braunschweig@uni-hamburg.de (K.U. Braunschweig), claudia.leopold@uni-hamburg.de (C.S. Leopold).

https://doi.org/10.1016/j.ejpb.2026.115069
Received 29 September 2025; Received in revised form 21 February 2026; Accepted 27 March 2026
Available online 27 March 2026
0939-6411/© 2026 The Authors. Published by Elsevier B.V. This is an open access article under the CC BY license (http://creativecommons.org/licenses/by/4.0/).

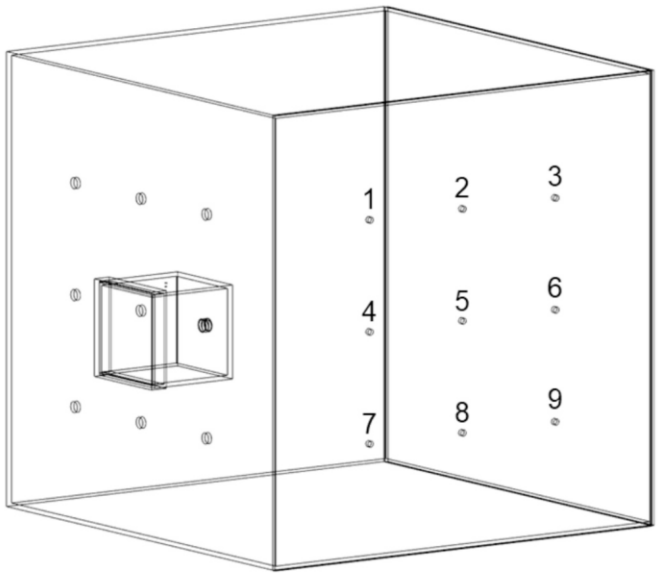


Fig. 1. Simplified illustration of the chamber setup used for dust measurements in orthogonal arrangement with measurement spots 1–9, modified after [47].

Defects or maloperation of containment systems leading to an unwanted release of dust during production cannot be detected. Therefore, real-time dust monitoring during production is desirable.

The International Society for Pharmaceutical Engineering (ISPE) recommends the use of safe surrogate substances such as lactose, insulin, naproxen sodium, or acetaminophen for performance tests of containment equipment and pharmaceutical dustiness investigations, to reduce the above-mentioned health risks associated with the handling of HPAPIs [11,14,17]. The surrogate should be selected based on various factors, such as its limits for analytical quantification and its physicochemical powder properties [11,20].

The dustiness of a powder is defined as its propensity to generate airborne particles during handling and is dependent on various physicochemical powder properties, such as particle size distribution, particle shape, density, as well as moisture content [15,21–25]. For dustiness investigations, the type and amount of energy input needed for atomization, along with the sample mass, must be considered. Furthermore, the flight path from the atomization to the detection site, defined by the geometry of the measuring system, may influence the measured dustiness [22,26].

As dustiness with its associated health risks is of concern in various research and manufacturing environments, several systems for dustiness investigation have been described over the last decades [26–34]. Most of these systems require a relatively high sample quantity, which might pose a problem, as many HPAPIs are expensive and sometimes of limited availability. Therefore, devices for dustiness investigations of small sample quantities have been developed in recent years [23,35–37].

In containment, three particle size fractions of airborne dust are of interest: The inhalable fraction consisting of particles with an aerodynamic diameter of up to 100 µm, the thoracic fraction of particles < 10 µm, and the respirable fraction of particles between 0.5 – 5 µm [25,38]. Because of the alveolar deposition, not only fine airborne particles of HPAPIs pose a health risk, but also fine particulate matter < 10 µm (PM_{10}) and < 2.5 µm ($PM_{2.5}$) in general [38,39]. Therefore, the detection and especially quantification of fine particulate matter in ambient air became a topic of interest in recent years, with high priority in environmental hygiene [40,41]. To make affordable monitoring of pollution with particulate matter possible, several low-cost particulate matter sensors have been developed [42,43]. Most of these sensors represent optical particle counters (OPCs) and their principle of detection is based on the Mie scattering theory [44–46].

In two previous studies, a chamber setup for the investigation of the dustiness of the surrogate substance acetaminophen as well as of its spatial distribution was introduced. In these studies, the detection of the atomized aerosol samples was carried out with IOM samplers and subsequent quantification via HPLC [47,48]. As expected, this measurement procedure showed the same disadvantages as the SMEPAC methodology. Therefore, in the present study, the chamber setup was equipped with low-cost particulate matter sensors. With these sensors, the real-time detection and visualization of spatiotemporal dust distributions within the chamber setup were investigated.

2. Materials and methods

2.1. Materials

The determination of spatial dust distributions was carried out with acetaminophen (ACAM; Caelo, Hilden, Germany) and spray-dried agglomerates of α-lactose monohydrate crystals bound by amorphous lactose (LAC; FlowLac 90, Meggle, Wasserburg am Inn, Germany) as safe surrogate substances commonly used for containment investigations [11].

2.2. Methods

2.2.1. Chamber setup

In Fig. 1, a modified version of the chamber setup already used in previous studies is shown [47,48]. The chamber setup consisted of a small emission chamber with inner dimensions of 19.4 cm × 19.4 cm × 19.4 cm and a larger detection chamber, which showed inner dimensions of 100 cm × 100 cm × 100 cm. The panels of both chambers were made of acrylic glass (Plexiglas® XT, Polyvantis, Weiterstadt, Germany) with a thickness of 0.8 cm. The emission chamber may be connected to the detection chamber at one of nine available positions by a protruding tube with an inner diameter of 2.54 cm fixed to the emission chamber. In the present study, the emission chamber was positioned at the attachment point to the right-hand side of the middle row, as depicted in Fig. 1. The eight unused positions were closed with specially designed seals. For cleaning purposes, the lid of the emission chamber was detachable. The detection chamber was set up in two different arrangements, either with oppositely or with orthogonally positioned measurement spots, because two of the panels of the chamber were interchangeable. All experiments were carried out with the orthogonal arrangement, as only this arrangement allowed different distances between emission chamber and measurement spots to be investigated (Fig. 1). In contrast to the previous studies, the nine measurement spots for dust detection were equipped with low-cost particulate matter sensors (PM sensors; SPS30, Sensirion, Staefa, Switzerland) instead of IOM samplers. The number and layout of the sensors according to Fig. 1 were chosen to obtain the highest possible resolution of the detected spatiotemporal dust distribution. The maximum number of sensors is limited by the minimum distance required between individual measurement spots to detect statistically significant differences in dust concentration. The 3x3 sensor layout enables the detection of concentration differences resulting from the spatial dust distribution in three horizontal and three vertical planes in relation to the emission site. In addition, three measurement spots in each plane allow a determination of not only linear but also nonlinear spatial dust distributions.

The PM sensors were connected to the detection chamber with 3D-printed adapters, made of electrostatic discharging acrylonitrile–butadiene–styrene filament. For the atomization of powder samples, a double-acting ball valve was connected to an orifice located in the top plate of the emission chamber, as shown in Fig. 2. A 5/2-way solenoid valve pneumatically opened and closed the ball valve. A 3/2-way pneumatic valve, actuated by a 3/2-way solenoid valve, controlled the flow of pressurized air used for atomization as well as ambient air for pressure compensation. A compressor (Metabo Mega 400–50 W,

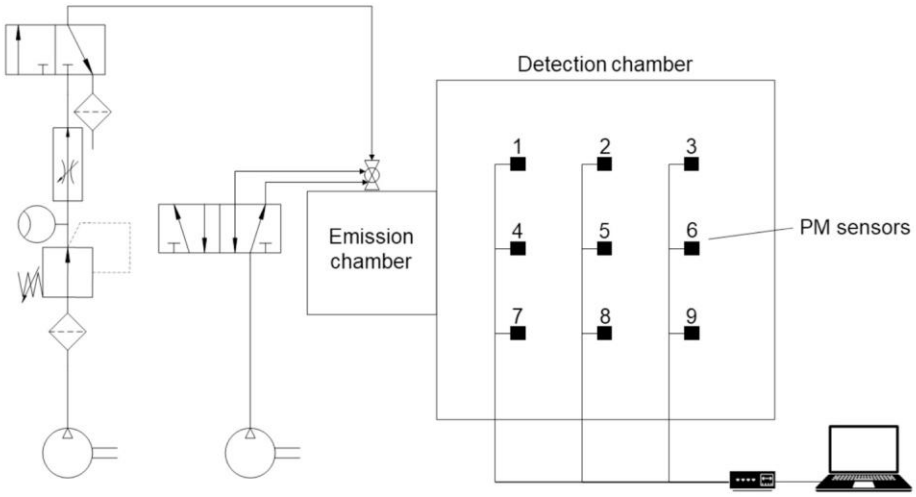


Fig. 2. Simplified piping and instrumentation diagram of the chamber setup equipped with SPS30 sensors.

Table 1
Physicochemical properties of the investigated surrogates ACAM and LAC (means ± SD, $n = 3$).

Powder properties	ACAM	LAC
Particle size [µm]		
x_{10}	2.73 ± 0.08	60.92 ± 0.97
x_{50}	14.32 ± 0.55	141.92 ± 1.39
x_{90}	46.27 ± 2.40	231.03 ± 2.13
Residual moisture content [%]	0.016 ± 0.004	4.95 ± 0.01
True density [g/cm^3]	1.2830 ± 0.0030	1.5278 ± 0.0008
Untapped bulk density [g/mL]	0.252 ± 0.001	0.593 ± 0.003
Tapped bulk density [g/mL]	0.448 ± 0.004	0.721 ± 0.005
Hausner ratio	1.78 ± 0.02	1.22 ± 0.01

Nürtingen, Germany) generated compressed air with a pre-pressure of up to 10 bar. This pre-pressurized air was down-regulated to a defined pressure (between 1 and 8 bar) by a pressure reducing valve and to a defined volume flow with a flowmeter, both installed upstream of the double-acting ball valve, to obtain the pressurized air for atomization. The panels of the detection chamber were attached to an outer framework of aluminum B-type profiles, which was also used to mount various control and measuring instruments, such as the flowmeter, pneumatic valves, and a Programmable Logic Controller (PLC; Siemens LOGO! 12/24 RCE, Munich, Germany). The PLC controlled all valves of the chamber setup. A grounding cable was attached to the chamber setup to dissipate electrostatic charges.

2.2.2. Dust measurements

Based on recent studies, powder samples of the surrogate substances ACAM, LAC, as well as a binary blend of both substances in the quantities of 500 mg each were investigated [47,48]. For each measurement, the respective sample was transferred into a small tube, the bottom end of which was closed by the double-acting ball valve. The measurements were started by actuating a toggle switch on the PLC. Thereby, the programmed sequence led to the immediate opening of the double-acting ball valve. By this means, compressed air was directed through the sample present in the double-acting ball valve, thereby atomizing the sample and introducing it into the emission chamber. Subsequently, the dust moved through the connecting orifice into the detection chamber via convective and diffusive mass transport. The spatial dust distribution (particle sizes between 0.3 and 2.5 µm) was registered with the PM sensors. Experiments were run over a time period of 33 min, whereby the first 3 min served for background measurements to ensure that the setup was aerosol free. For real-time visualization, the signals of the PM sensors were directly transferred to a laptop (Fig. 2). To reduce signal noise, the sensor signals were smoothed by means of a moving average with a length of 30 data points.

All of the experiments in the present study were carried out at an

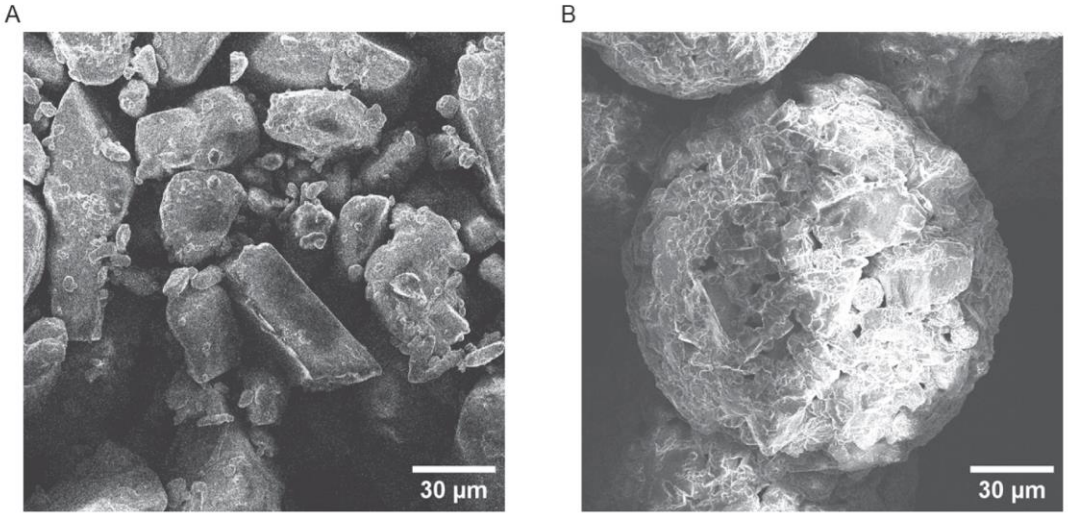


Fig. 3. SEM images of ACAM (A) and LAC (B).

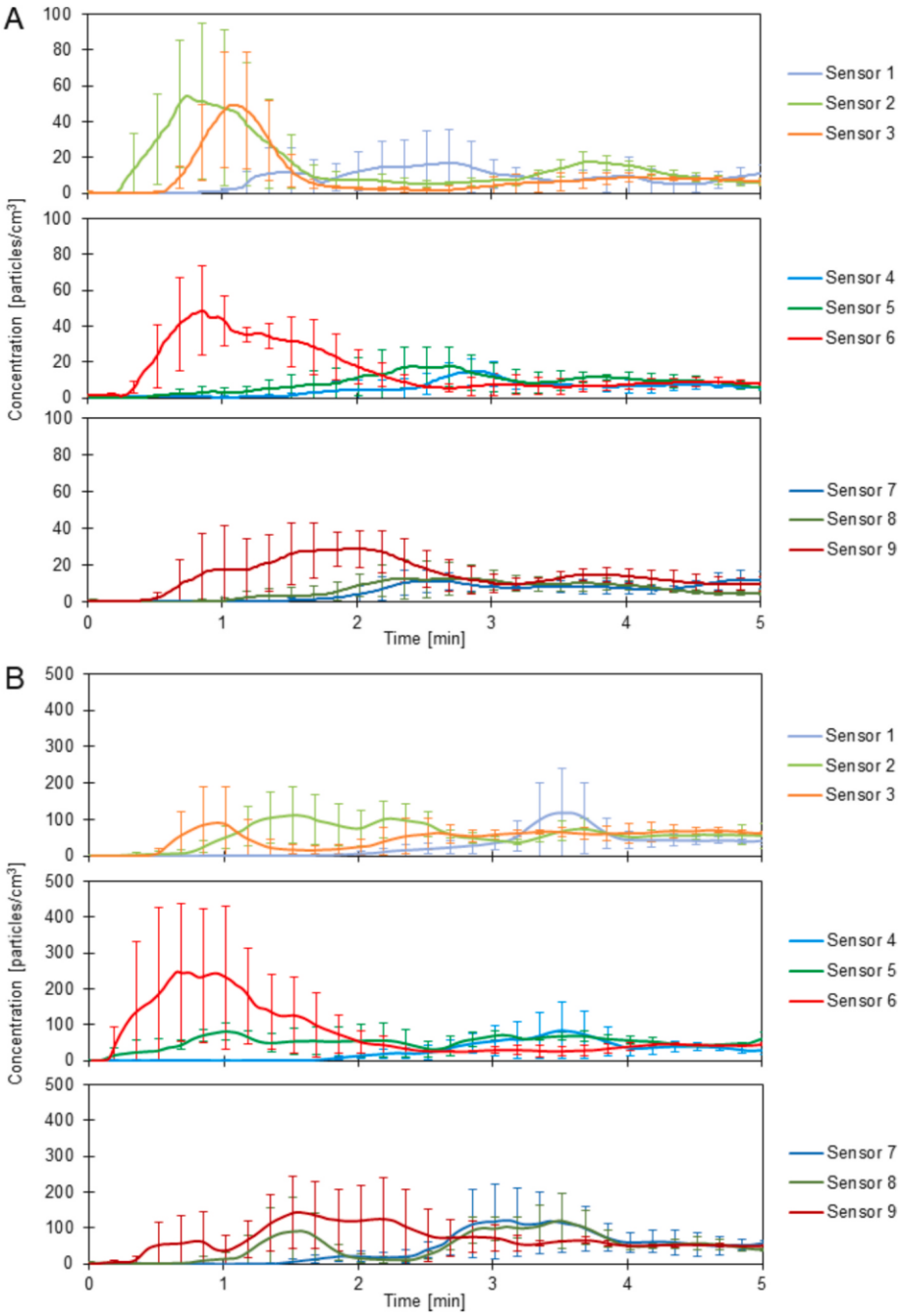


Fig. 4. Sensor-position dependent ACAM particle concentration at gauge pressures of 1 bar (A) and 3 bar (B) at an atomization duration of 1 s (means ± SD, $n = 3$).

atomization volume flow rate of 30 L/min. The influence of the gauge pressure (1, 3, 4.5, 6, and 8 bar, controlled by the pressure reducing valve) was investigated at an atomization duration of 1 s. Subsequently, atomization durations of 1, 2, and 3 s at a gauge pressure of 4.5 bar were examined. Finally, for measurements of binary blends of ACAM and LAC, a gauge pressure of 4.5 bar and an atomization duration of 2 s were selected.

2.2.3. Sieving

To improve the reproducibility of the dust measurements, the ACAM powder was sieved at 90 µm mesh size (LINKER Industrie-Technik, Kassel, Germany) [49]. The obtained coarse fraction was discarded and only the fine fraction was used for this study.

2.2.4. Blending

For dust investigations, binary powder blends at a ratio of 1:1 (m/m) of ACAM and LAC were prepared by adding 250 mg of each powder to a stainless steel cup. Subsequently, the powders were carefully mixed by hand to avoid electrostatic charging of the samples. Each sample was then directly transferred into the tube above the double-acting ball valve for immediate dust measurement.

2.2.5. Particle size distribution

The particle size distributions of ACAM and LAC were determined in triplicate by laser diffractometry (Helos KR, Sympatec, Clausthal-Zellerfeld, Germany). The lens used for the measurements had an effective range of 0.5–875 µm. The powder samples were dispersed by compressed air at an air pressure of 1.5 bar. With the Paqxos software (Version 2.0.3, Sympatec, Clausthal-Zellerfeld, Germany) the particle

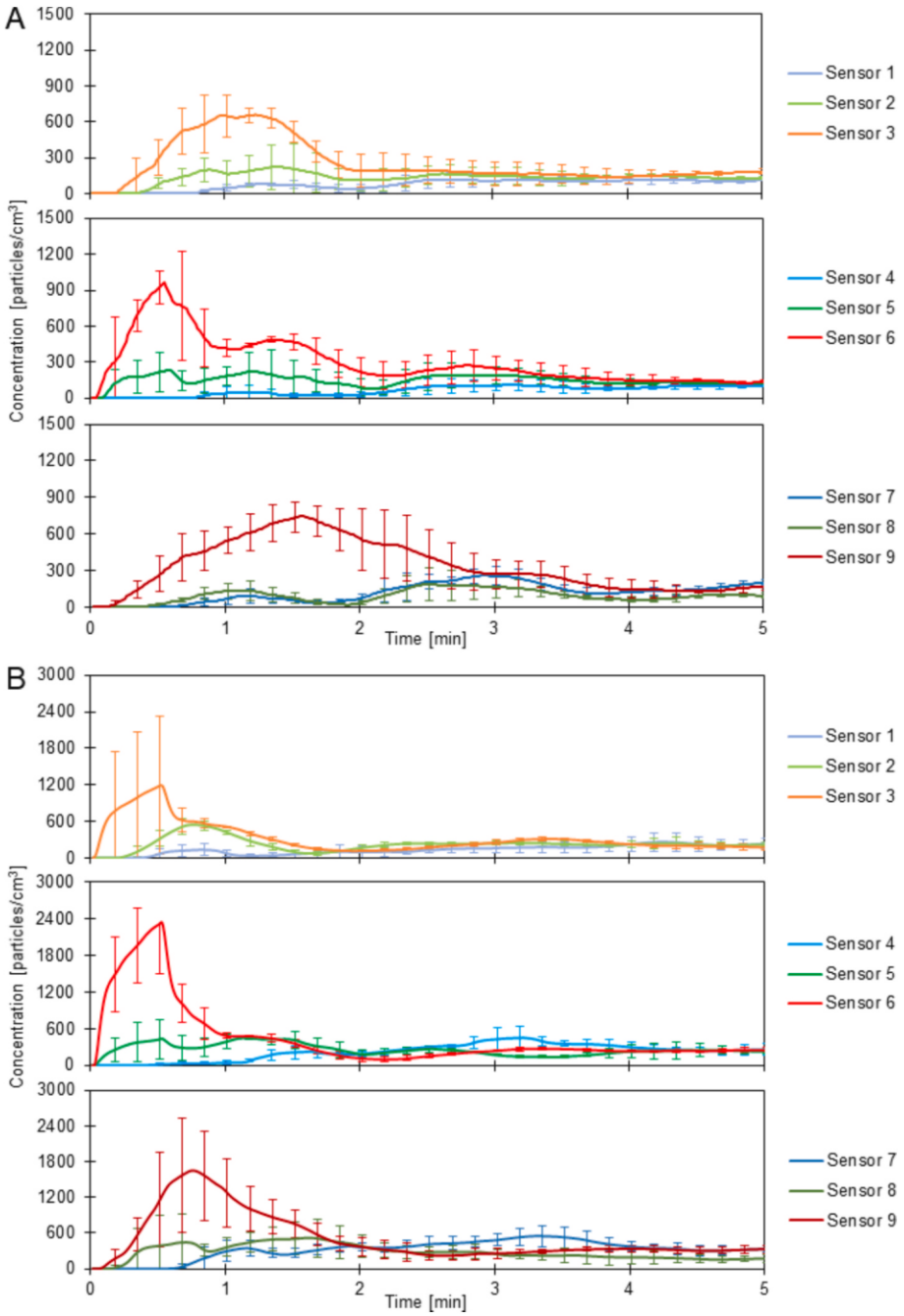


Fig. 5. Sensor-position dependent ACAM particle concentration at gauge pressures of 4.5 bar (A) and 6 bar (B) at an atomization duration of 1 s (means ± SD, $n = 3$).

size distributions were analyzed.

2.2.6. Residual moisture content

The residual moisture content of ACAM and LAC was measured by thermal gravimetric analysis (Pyris 1 TGA, PerkinElmer, Waltham, USA) with sample masses of approximately 15 mg in triplicate. Therefore, the temperature was increased from 22 °C to 160 °C with a heating rate of 10 K/min.

2.2.7. True density

The true densities of ACAM and LAC were determined by helium pycnometry (Pycnomatic ATC EVO, Porotec, Hofheim am Taunus, Germany). For this purpose, approximately 4 g of each sample ($n = 3$) were used and five measurement cycles were performed.

2.2.8. Bulk density

The untapped and tapped bulk densities were estimated according to the monograph 2.9.34, "Bulk density of powders" in the European Pharmacopoeia with a jolting volumeter (STAV 2003, J. Engelsmann, Ludwigshafen, Germany) [50]. Therefore, samples with a mass of 23 g of ACAM as well as samples of 50 g of LAC were transferred to a graduated 100 mL measuring cylinder and subjected to the specified number of tapping cycles. The Hausner ratios as well as the bulk densities were calculated from the resulting volumes.

2.2.9. Scanning Electron Microscopy (SEM)

To investigate the shape and surface structure of the ACAM and LAC particles, SEM images were taken with a Scanning Electron Microscope (Quanta 3D FEG, FEI Company, Hillsboro, USA). The measurements were carried out with an acceleration voltage of 5 kV in high vacuum.

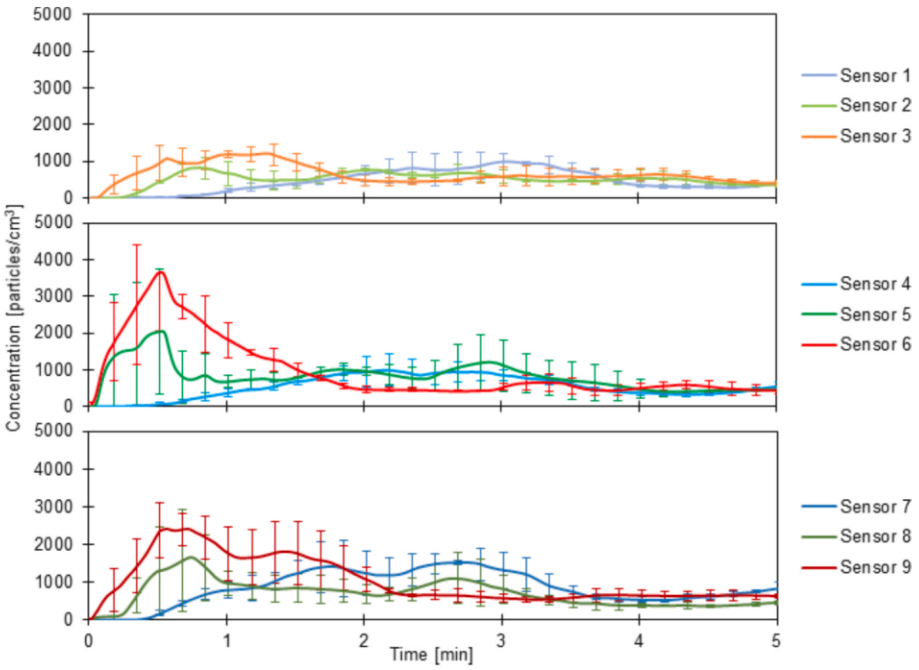


Fig. 6. Sensor-position dependent ACAM particle concentration at a gauge pressure of 8 bar and an atomization duration of 1 s (means ± SD, $n = 3$).

3. Results and discussion

3.1. Powder Characterization

The dustiness of a powder is influenced by various factors. Hereby, the particle size distribution as well as the residual moisture content play a major role. However, other parameters such as powder density and flowability may also influence dustiness [22,23,51]. Therefore, all of these powder properties were determined for ACAM and LAC, which were used as surrogates in this study. The results are shown in Table 1. The effect of the sieving procedure (90 µm mesh) of ACAM became evident by its x_{90} value of 46.27 µm. In comparison to ACAM, LAC showed larger particles (> 2.5 µm), which were undetectable by the sensors. Its residual moisture content was high (4.95 %) compared to ACAM (0.016 %).

The Hausner ratios, resulting from the bulk densities, indicated a very, very poor flowability of ACAM (1.78) and a fair flowability of LAC (1.22) [52]. This combination of ACAM and LAC has been chosen by purpose to investigate a binary blend of a fine, poorly flowing API and a coarse excipient.

In Fig. 3, the SEM images of ACAM particles (A) and LAC particles (B) are shown.

The ACAM particles exhibited an angular shape in contrast to the granular, almost spherical shape of the LAC particles. The surface of the ACAM particles appeared quite smooth and distinct variations in their particle size were apparent. Fine particles with only a few micrometers in size were noticeable. The LAC particles are larger in size and they exhibit a rough surface with prominent angled recesses as well as protruding areas. The observations regarding the particle sizes were confirmed by the results of laser diffractometry, shown in Table 1.

3.2. Influence of the gauge pressure on the dust measurements

In a previous study, it was shown that the PM sensors were capable to visualize the spatial distribution of dust in the chamber setup [53]. In this study, two sensors were attached to the chamber setup in position #4 and #6, and position-dependent concentration maxima of the respective sensor signals at different time points provided proof of the spatial distribution of airborne dust in the detection chamber of the setup. It was noticeable that immediately after atomization, the sensor signal at position #6 increased to a high maximum concentration. This could be explained by the results of another previous study where the spatial distribution in the detection chamber was determined with IOM samplers. These results and CFD simulations showed that the airflow caused by atomization was directed to the opposite panel of the detection chamber. There the airflow was redirected sideways towards the panel equipped with the samplers [48]. To investigate the influence of the gauge pressure on the concentration of airborne dust in the detection chamber, experiments with gauge pressures of 1, 3, 4.5, 6, and 8 bar were carried out and the results are shown in Fig. 4, 5 and 6. For better visualization, the time point of atomization was set to 0 s (the prior 3 min of background measurement were cut off) and only the first 5 min of the 30 min measurement time are shown. During these 5 min the main differences between the measured concentrations at the sensors as well as the concentration changes at each individual sensor were already evident and the concentrations approximated a constant level within this time span. To be able to present all graphs in Fig. 4, 5 and 6 in an assessable manner, the y-axes had to be scaled accordingly.

In Fig. 4, the detected concentrations at all nine sensor positions are shown for gauge pressures of 1 bar (A) and 3 bar (B). The PM sensors have a precision of ± 100 particles/cm^3 for measured values of up to 1000 particles/cm^3 [44]. Regarding this precision as well as the SDs of the graphs, it is obvious that low gauge pressures of 1 and 3 bar were not able to produce sufficient airborne dust concentrations in the detection chamber. Furthermore, these low gauge pressures seemed to result in a slow distribution of the dust towards the measurement spots, becoming apparent as a lag time of 10–30 s between time point of atomization and beginning increase of dust concentrations. Even though the dust concentrations were too low for inter-sensor differences regarding the spatial distribution, the increase of the gauge pressure from 1 to 3 bar led to an increase in the airborne dust concentration.

The detected concentrations at all nine sensor positions for gauge pressures of 4.5 bar (A) and 6 bar (B) are shown in Fig. 5. It is evident that an increase of the gauge pressure to 4.5 bar resulted in higher concentration maxima directly after atomization and sufficiently high airborne dust concentrations for the determination of inter-sensor differences. Similar to a previous study in which the highest amount of ACAM settled on the filter within the IOM sampler at position #6, the

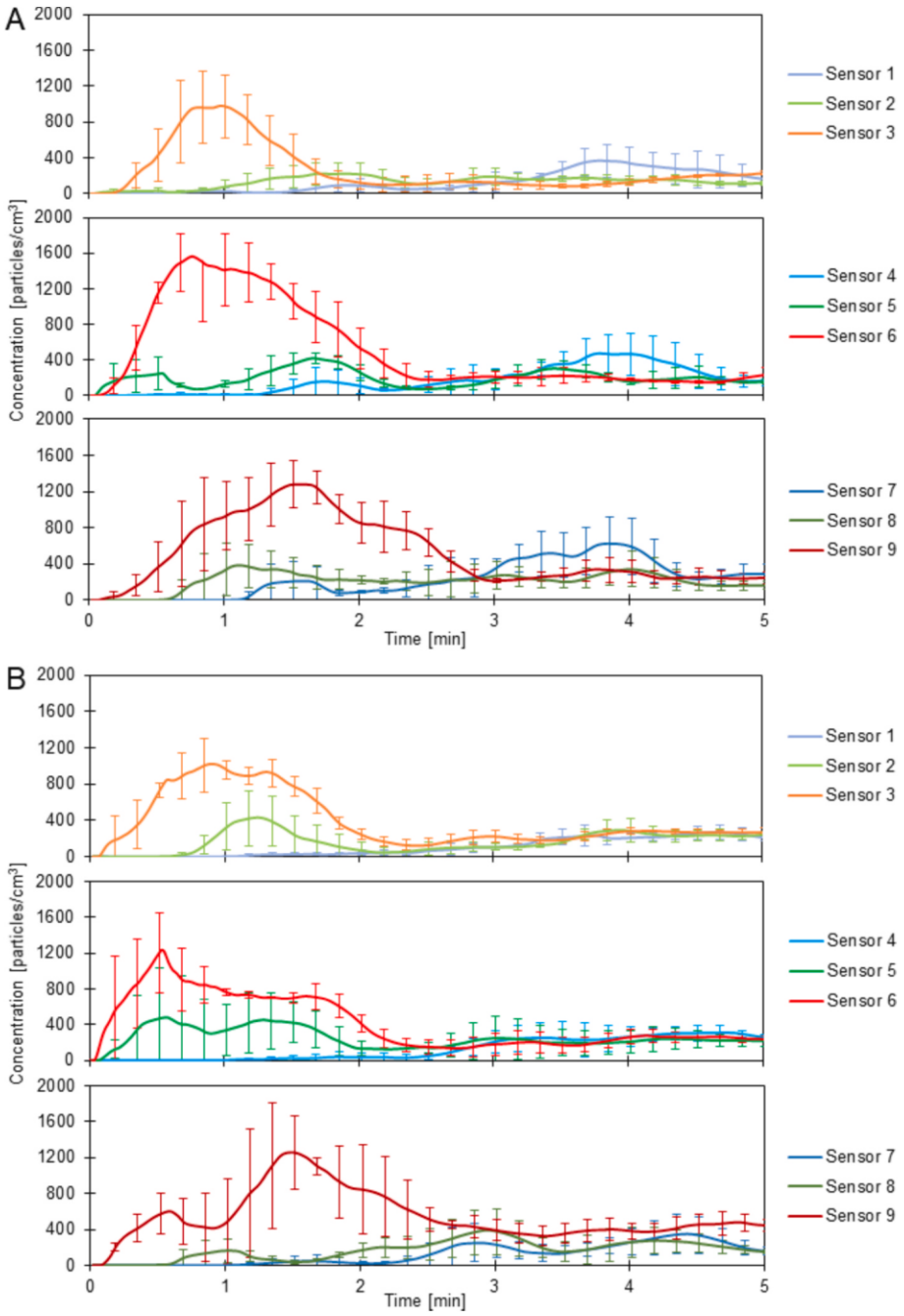


Fig. 7. Sensor-position dependent ACAM particle concentration at atomization durations of 2 s (A) and 3 s (B) (means ± SD, n = 3).

concentration maximum in the present study was also observed at sensor position #6 [48]. Moreover, the spatial dust distribution determined with the IOM samplers was comparable to the concentration signals of the sensors at all nine positions [48].

As expected, a further increase of the gauge pressure to 6 bar led to even higher dust concentrations. Unfortunately, the concentration maxima of the unsmoothed signals without noise reduction (data not shown) exceeded the upper limit of the calibration range of the PM sensors specified in the datasheet (3000 particles/cm^3) [44]. Nevertheless, any signals exceeding the upper threshold of the sensor calibration range were processed in the same manner as signals within the range.

As shown in Fig. 6, a gauge pressure of 8 bar led to a further increase of the airborne dust concentrations. However, the maximum values also exceeded the upper threshold of the sensor calibration range. The next lower pressure step below 6 bar (4.5 bar) resulted in a pronounced spatiotemporal dust distribution (Fig. 5A), with all detected concentration values within the calibration range of the sensors. Therefore, this pressure was selected as the optimum for the further investigations.

Even though not all experiments with different gauge pressures led to data within the desired concentration range, a similar spatial distribution pattern was noticeable with almost all gauge pressures. The highest dust concentration was measured at sensor #6 and the concentration decreased in a circular pattern from this position. As mentioned above, this observation is consistent with the results of a previous study using IOM samplers for dust detection [48].

These new time-resolved results obtained with the PM sensors showed that the spatial dust distribution was predominantly affected by the atomization process and the convective transport of dust into the detection chamber. This spatial distribution is subsequently evened out

Table 2
AUC values of the concentration vs. time profiles at different atomization durations (means ± SD, $n = 3$).

Sensor position	Atomization 1 s	Atomization 2 s	Atomization 3 s
	AUC [particles·min/cm^3]	AUC [particles·min/cm^3]	AUC [particles·min/cm^3]
1	371.7 ± 87.5	644.5 ± 204.8	512.3 ± 141.1
2	663.8 ± 285.8	662.3 ± 191.8	809.9 ± 362.4
3	1276.6 ± 381.1	1351.9 ± 443.9	1959.6 ± 166.2
4	309.0 ± 82.2	849.1 ± 308.8	634.8 ± 219.7
5	747.4 ± 279.6	989.5 ± 64.7	1248.7 ± 325.4
6	1519.5 ± 298.6	2604.5 ± 232.2	2108.1 ± 175.7
7	588.7 ± 26.5	1148.8 ± 445.9	618.7 ± 362.3
8	459.9 ± 142.8	1063.5 ± 383.7	863.8 ± 213.4
9	1689.6 ± 487.5	2618.9 ± 708.9	2733.7 ± 353.3
Total dustiness	**7626.1 ± 1908.8**	**11932.9 ± 487.5**	**11489.5 ± 1243.9**

after a few minutes, probably by particle diffusion. As the sensors are only able to detect particles < 2.5 µm, sedimentation should not become apparent in the signals and the detected concentration decrease may only be caused by 'dilution' of the airborne dust with ambient air resulting from the flow through the sensors and out of the detection chamber.

3.3. Influence of the atomization duration on the dust measurements

In a previous study, it was shown that the atomization duration has a significant influence on the resulting dust concentration (totally settled amount on all filters in the IOM samplers) as well as on the spatial distribution of the dust in the detection chamber [47]. Therefore, the atomization duration was increased stepwise from 1 to 3 s at a gauge pressure of 4.5 bar, and the results are shown in Fig. 5A (1 s), 7A (2 s), and 7B (3 s).

All unsmoothed concentration values were below the upper limit of the calibration range of the PM sensors. For better comparability of the signals, the Areas Under the Curve (AUC) of all graphs were calculated by integration and are shown in Table 2. The influence of the atomization duration on the resulting particle concentration in the detection chamber was investigated based on the total dustiness of the samples. The total dustiness was regarded as the sum of all nine sensor AUCs of each measurement in this study. The increase of the atomization duration from 1 to 2 s led to a significantly elevated dustiness ($p < 0.02$), whereas from 2 to 3 s no further increase in dustiness was observed ($p > 0.5$). Apparently, an atomization duration of 2 s is sufficient for the atomization of the powder samples and for convective particle transport from the emission into the detection chamber.

To investigate the horizontal difference of the spatial dust distribution for the three atomization durations, the AUCs of the sensor signals on the left-hand side (#1, #4, and #7) were compared to those on the right-hand side (#3, #6, and #9). For the investigation of the vertical difference, the AUCs of the sensor signals in the upper row (#1, #2, and #3) were compared to those of the lower row (#7, #8, and #9).

For an atomization duration of 1 s, the AUCs of the sensor signals on the left-hand side made up 16.6 % of the total AUC, whereas the signals on the right-hand side 58.8 %, resulting in a difference of 42.2 %. The sensor signals of the upper row amounted to 30.3 % and the signals of the lower row to 35.9 %, resulting in a difference of only 5.6 %, thus leading to a total difference of 47.8 %.

In the experiments with an atomization duration of 2 s, the horizontal difference of the sensor signal AUCs revealed a difference of 33 % (22.1 % to the left and 55.1 % to the right). The vertical difference was 18.2 % (22.3 % upper row and 40.5 % lower row), resulting in a total difference of 51.2 %.

The experiments with an atomization duration of 3 s showed a percentage of 15.4 % for the signal AUCs to the left and of 59.2 % for those to the right, making up a horizontal difference of 43.8 %. The vertical difference between the signals of the upper row (28.6 %) and those of the lower row (36.7 %) was 8.1 %, accounting for a total difference of 51.9 %. Thus, the resulting total differences, as measures of the heterogeneity of the spatial dust distributions, were very similar for all three atomization durations. However, the vertical difference was highest at an atomization duration of 2 s. As the horizontal difference at this duration was sufficient to detect statistically significant differences in the dust concentrations, it led to the best combination for the examination of differences in both, the horizontal and the vertical spatial dust distributions.

In summary, an atomization duration of 2 s was the most effective time span regarding atomization, resulting in the highest total amount of dust as well as the best combination for the investigation of horizontal and vertical concentration differences in spatial dust distributions. Therefore, it was chosen for the investigation of the binary blend of ACAM and LAC.

3.4. Dust measurements with the binary blend of ACAM and LAC

Binary powder blends of an API with an excipient play a major role in powder tableting. In contrast to previous studies, where IOM samplers were used to investigate the settled amount of ACAM, in the present study, the chamber setup was operated with PM sensors to allow investigations of the total dust concentration of a binary blend [47,48]. As excipient, LAC with a low content of fine particles (Table 1) was chosen. When comparing the results of plain ACAM (Fig. 7A) with those of LAC (Fig. 8A), both atomized with the same parameters of 30 L/min, a gauge pressure of 4.5 bar and an atomization duration of 2 s, it became obvious that LAC led to a comparably lower detectable dust concentration. The sensor signals of LAC were below the sensor precision of 100 particles/cm^3, whereas those of the binary blend (Fig. 8B) were all above the precision of the sensors, as well as within the calibration range [44].

Comparing the total dustiness of ACAM and LAC (Table 3), LAC accounted for only 5.5 % of the ACAM dustiness. On the one hand, this observation may be explained by the low fine particle fraction of LAC, detectable with the PM sensors, and on the other hand by the higher residual moisture content of LAC (Table 1), reducing its dustiness [22].

The binary blend of ACAM and LAC shows a significantly lower total dustiness than plain ACAM ($p < 0.02$) and a significantly higher dustiness than plain LAC ($p < 0.002$). Considering the detected dust concentrations of each plain component, the expected percentage of the total dustiness of the binary blend should have amounted to 52.75 % of the dustiness of plain ACAM. However, the actual percentage was 66.2 %. Wirth et al. (2024) postulated a similar effect, observing a higher ACAM dustiness if combined with the coarse fraction of lactose-monohydrate in contrast to a combination with its fine fraction [54]. The higher than expected dustiness in the present study may be caused by interacting effects of the ACAM and LAC particles. It is widely known, that the particle size with its resulting specific surface area as well as factors such as particle shape, surface roughness, and adsorption phenomena influence the flow, the mixing behavior, and the dustiness of binary powder mixtures [51,54–59].

For investigation of the spatial dust distribution, the vertical and horizontal differences of the corresponding sensor signal AUCs were again calculated as described above. Plain LAC led to AUC values with a horizontal difference of 40.6 % (16.6 % to the left and 57.2 % to the right). The vertical difference was 6.5 %, with 27.0 % in the upper sensor row and 33.5 % in the lower row. Comparing these results to the AUCs obtained with plain ACAM, it becomes apparent that the horizontal AUC difference of LAC was higher than that of ACAM (40.6 vs. 33.0 %). This may be caused by the larger particles of LAC: these coarse particles are probably more affected by the convective transport into the detection chamber and are taking the smaller particles along with them, as a result of adhesion. In contrast, the vertical AUC difference was more pronounced with plain ACAM (6.5 vs. 18.2 %). As sedimentation should not

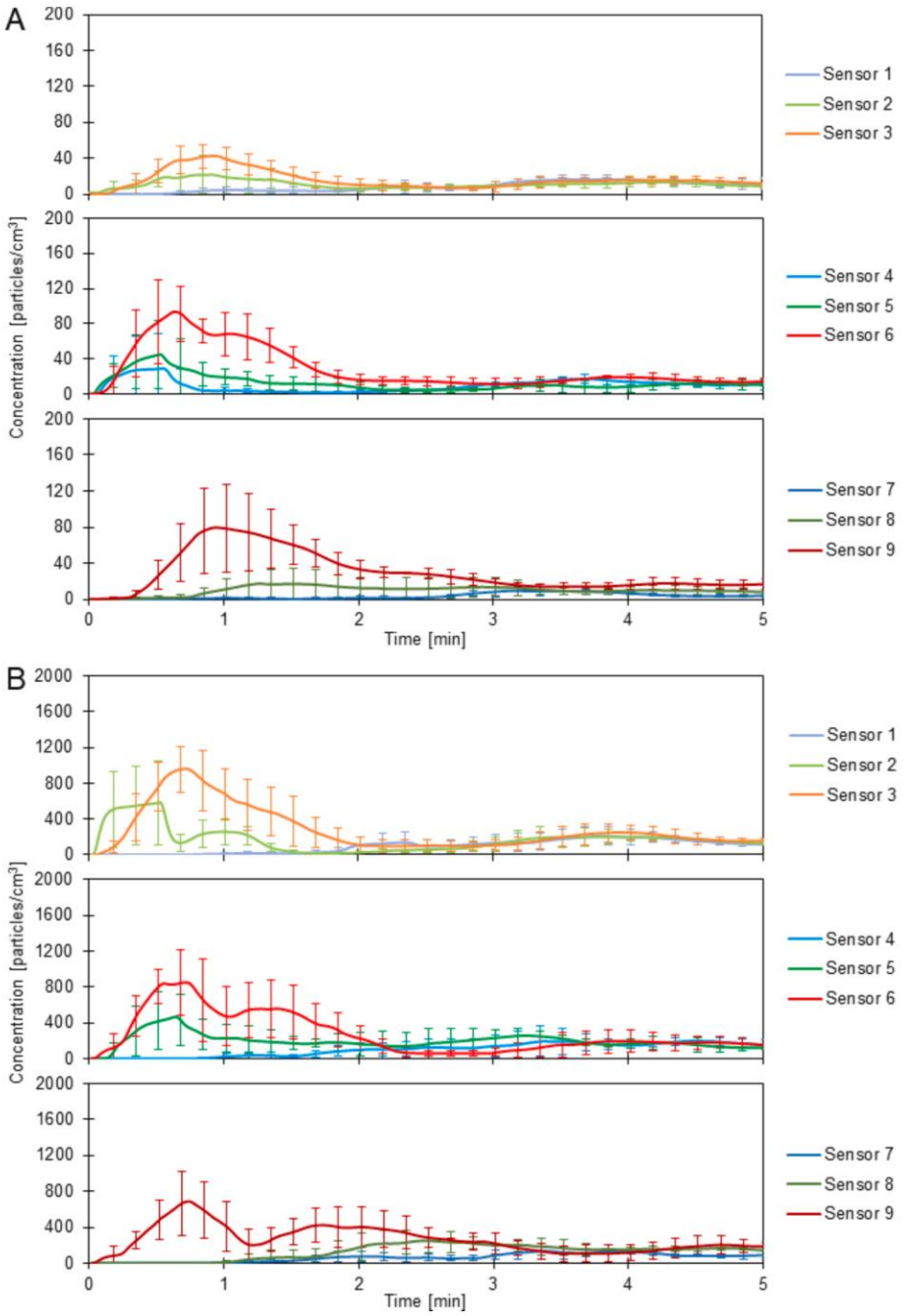


Fig. 8. Sensor-position dependent particle concentration of LAC (A) and binary blend (B) at a gauge pressure of 4.5 bar and an atomization duration of 2 s (means ± SD, $n = 3$).

play a role in this case, the vertical AUC difference cannot be explained yet and needs to be investigated with sensors able to detect larger particles.

In the experiments with the binary blend, the horizontal difference was 35.5 % (16.6 % to the left and 52.1 % to the right). This value is close to the mean of the horizontal differences of the plain two surrogates (ACAM: 33 %, LAC: 40.6 %). The vertical difference was 5.8 % (34.7 % upper row and 28.9 % lower row). However, previous studies based on IOM samplers, which are able to detect particles up to 100 μm, showed larger vertical differences with higher amounts of particles detected in the lower row than in the upper row [47,48]. As mentioned above, these discrepancies still have to be further investigated.

Vertical differences in the spatial dust distribution and the decrease in dust concentrations over the time course of the measurements are assumed to be higher if particles of up to 100 μm were detectable with the sensors. These larger particles are also of interest, as all particles < 100 μm pose a threat to personnel in the industry with regard to inhalability [25,38]. Also, the horizontal differences of the determined spatial distribution of larger particles are expected to deviate from those of smaller particles < 2.5 μm, as particle size directly affects binding and separation forces. Whereas binding forces based on van der Waals attraction and capillary forces are proportional to the particle diameter d, separation forces such as aggregate impaction increase with d^3 [22,60]. Depending on the geometry of the chamber setup, either smaller or larger particles are better suited to follow the flight path from the atomization to the detection site. In addition, larger particles may take smaller particles along with them as a result of adhesion [22,26]. Combining all of the above-mentioned factors, it is assumed, that a

Table 3
AUC values of the concentration vs. time profiles for ACAM, LAC, and the 1:1 (m/m) binary blend (means ± SD, $n = 3$).

Sensor position	ACAM	LAC	Binary blend
	AUC [particles·s/cm^3]	AUC [particles·s/cm^3]	AUC [particles·s/cm^3]
1	644.5 ± 204.8	40.4 ± 11.8	476.9 ± 200.4
2	662.3 ± 191.8	56.0 ± 22.2	857.2 ± 166.3
3	1351.9 ± 443.9	81.2 ± 18.9	1410.3 ± 242.3
4	849.1 ± 308.8	50.1 ± 22.5	514.9 ± 187.7
5	989.5 ± 64.7	65.0 ± 34.6	987.0 ± 389.1
6	2604.5 ± 232.2	145.1 ± 38.3	1374.3 ± 393.5
7	1148.8 ± 445.9	18.7 ± 5.0	316.5 ± 108.4
8	1063.5 ± 383.7	51.5 ± 35.2	636.1 ± 182.6
9	2618.9 ± 708.9	150.5 ± 46.1	1328.9 ± 460.5
Total dustiness	**11932.9 ± 487.5**	**658.6 ± 224.9**	**7901.8 ± 1588.6**

spatial dust distribution detected with multi-channel sensors, capable to detect particles of up to 100 µm, might be less uniform and particle interactions influencing the spatial distribution of the inhalable particle fractions should be investigated in further studies.

Nevertheless, the modification of the chamber setup with PM sensors proved to be suitable for the detection of dust as well as its spatiotemporal distribution. Each experiment of the present study showed that the spatial distribution took place within the first few minutes after atomization, reducing the duration of the experiments by more than four hours compared to previous studies with IOM samplers [47,48]. Furthermore, the real-time spatiotemporal detection allowed the determination of optimum atomization parameters, not only taking the total dustiness into consideration but also the time-resolved dust concentrations. Although the sensors have the drawback of not being able to detect substance-specific dust, they are suitable to assess the combination of both, dustiness and spatiotemporal dust distribution of powder blends. In addition, because of their ability to detect spatiotemporal dust distributions in real-time, the sensors allow dust monitoring in production environments during pharmaceutical processing. With the PM sensors, a major limitation of the SMEPAC methodology based on IOM samplers may be overcome, as PM sensors enable the detection of potential defects or maloperation of containment systems during production processes. Furthermore, potential dust emissions originating from a leakage might be localized based on the detection of the spatiotemporal dust distribution.

4. Conclusion

The present study deals with the application of low-cost particulate matter sensors for detection of pharmaceutical dusts in a novel chamber setup for investigation of the spatiotemporal dust distribution. In contrast to traditional filter-based methods, such as IOM samplers used in previous studies, the sensors offer the advantage of not only being able to detect the spatial, but also the spatiotemporal distribution of dust in real-time. The results of this study revealed, that the sensors should be suitable for real-time detection of dust in production environments and may be used for monitoring ambient air as well as for leakage localization of containment systems. The only limitation of the sensors is their maximum detectable particle size of 2.5 µm. Therefore, future investigations of the spatial dust distribution will deal with multi-channel sensors, able to detect a wider particle size range and size-specific airborne particle concentrations, which will enable the chamber setup to simultaneously monitor specific fractions of inhalable airborne dust. Moreover, the ability of different sensor technologies for substance-specific aerosol detection will be investigated. The results of these investigations might give valuable insights into the size- and substance-dependent spatiotemporal distribution and sedimentation of dusts and may allow the implementation of optical sensors as part of real-time feedback containment systems. Thereby, the outcome of these studies may significantly improve safety in the contained manufacture of pharmaceuticals.

Funding Statement

This research received no external funding.

CRediT authorship contribution statement

Hendrik Küllmar: Writing – review & editing, Writing – original draft, Visualization, Validation, Software, Methodology, Investigation, Formal analysis, Data curation, Conceptualization. **Martin Schöler:** Writing – review & editing, Validation, Conceptualization. **Kai U. Braunschweig:** Writing – review & editing, Validation, Software. **Claudia S. Leopold:** Writing – review & editing, Validation, Supervision, Formal analysis.

Declaration of Competing Interest

The authors declare that they have no known competing financial interests or personal relationships that could have appeared to influence the work reported in this paper.

Acknowledgments

The authors would like to express their gratitude to Petra Borbe for her technical and analytical assistance and to the Electron Microscopy Service Unit of the University of Hamburg, especially to Dr. Charlotte Ruhmlieb, for the SEM data.

Data availability

Data will be made available on request.

References

[1] C.A. Challener, Conjugation chemistry with highly potent compounds, Pharm. Technol. 40 (2016) 34–37.
[2] E. Dunny, I. O'Connor, J. Bones, Containment challenges in HPAPI manufacture for ADC generation, Drug Discov. Today 22 (2017) 947–951, https://doi.org/10.1016/j.drudis.2017.02.003.
[3] J.R. Broach, J. Thorner, High-throughput screening for drug discovery, Nature 384 (1996) 14–16.
[4] G. Mari, A. Moccaldi, G. Ludovisi, Handling of high potency drugs: Process and containment, Trans, Ecol. Environ. 85 (1999) 257–265, https://doi.org/10.2495/EEH050281.
[5] D. Paul, G. Sanap, S. Shenoy, D. Kalyane, K. Kalia, R.K. Tekade, Artificial intelligence in drug discovery and development, Drug Discov. Today 26 (2021) 80–93, https://doi.org/10.1016/j.drudis.2020.10.010.
[6] D. Vemula, P. Jayasurya, V. Sushmitha, Y.N. Kumar, V. Bhandari, CADD, AI and ML in drug discovery: a comprehensive review, Eur. J. Pharm. Sci. 181 (2023) 106324, https://doi.org/10.1016/j.ejps.2022.106324.
[7] S. Wollowitz, Managing high-potency active pharmaceutical ingredients - a drug sponsor's guide, Drug Dev. Res. 71 (2010) 420–428, https://doi.org/10.1002/ddr.20385.
[8] R.H. Ku, An overview of setting occupational exposure limits (OELs) for pharmaceuticals, Chem. Heal. Saf. 9098 (2000) 34–37, https://doi.org/10.1016/S1074-9098(99)00070-2.
[9] B.D. Naumann, E.V. Sargent, B.S. Starkman, W.J. Fraser, G.T. Becker, G.D. Kirk, Performance-based exposure control limits for pharmaceutical active ingredients, Am. Ind. Hyg. Assoc. J. 57 (1996) 33–42, https://doi.org/10.1080/15428119691015197.
[10] R.J.L. Heron, F.C. Pickering, Health effects of exposure to active pharmaceutical ingredients (APIs), Occup. Med. 53 (2003) 357–362, https://doi.org/10.1093/occmed/kqg115.
[11] International Society for Pharmaceutical Engineering, Good Practice Guide: Assessing the Particulate Containment Performance of Pharmaceutical Equipment, G. Petroka, J.P. Wood (Eds.), ISPE, North Bethesda, 2012.
[12] I. Grayson, J. Becker, T. Pohlmann, K. Blumbach, K. McCleary, M. Van Hoosier, Development and implementation of a large-scale HPAPI manufacturing process, Chim. Oggi-Chemistry Today 35 (2019) 20–24.
[13] P. Tiwari, S.R. Chowdhury, Sustainable production of highly active pharmaceutical ingredients (HAPIs), Int. J. Sci. Res. Publ. 4 (2014) 2250–3153.

[14] International Society for Pharmaceutical Engineering, Containment Manual, Working Group Containment (Ed.), ISPE, North Bethesda, 2017.
[15] J. Stein, T. Fuchs, C. Mattern, Advanced milling and containment technologies for superfine active pharmaceutical ingredients, Chem. Eng. Technol. 33 (2010) 1464–1470, https://doi.org/10.1002/ceat.200900590.
[16] N.J. Adams, D.L. Johnson, R.A. Lynch, The effect of pressure differential and care provider movement on airborne infectious isolation room containment effectiveness, Am. J. Infect. Control 39 (2011) 91–97, https://doi.org/10.1016/j.ajic.2010.05.025.
[17] International Society for Pharmaceutical Engineering, Good Practice Guide SMEPAC, R. Nicolai, G.S. Petroka, K. Whitaker (Eds.), 3rd ed., ISPE, North Bethesda, 2024.
[18] D. Mark, J.H. Vincent, A new personal sampler for airborne total dust in workplaces, Ann. Occup. Hyg. 30 (1986) 89–102, https://doi.org/10.1093/annhyg/30.1.89.
[19] D. Mark, J.H. Vincent, H. Gibson, G. Lynch, A new static sampler for airborne total dust in workplaces, Am. Ind. Hyg. Assoc. J. 46 (1985) 127–133, https://doi.org/10.1080/15298668591394536.
[20] O. Butler, J. Forder, J. Saunders, Analytical protocol for the sensitive determination of mannitol, sorbitol and glucose containing powders in pharmaceutical workplaces by ion chromatography using a pulsed amperometric detector, J. Pharm. Biomed. Anal. 106 (2015) 204–209, https://doi.org/10.1016/j.jpba.2014.10.006.
[21] G. Lidén, Dustiness testing of materials handled at workplaces, Ann. Occup. Hyg. 50 (2006) 437–439, https://doi.org/10.1093/annhyg/mel042.
[22] World Health Organization, Hazard Prevention and Control in the Work Environment: Airborne Dust, WHO, Geneva, Switzerland, 1999. https://iris.who.int/handle/10665/66147 (accessed 27 October 2024).
[23] N. Shandilya, E. Kuijpers, I. Tuinman, W. Fransman, Powder intrinsic properties as dustiness predictor for an efficient exposure assessment? Ann. Work Expo. Heal. 63 (2019) 1029–1045, https://doi.org/10.1093/annweh/wxz065.
[24] M.A.E. Plinke, R. Maus, D. Leith, Experimental examination of factors that affect dust generation by using Heubach and MRI testers, Am. Ind. Hyg. Assoc. J. 53 (1992) 325–330, https://doi.org/10.1080/15298669291359726.
[25] P.T. O'Shaughnessy, M. Kang, D. Ellickson, A novel device for measuring respirable dustiness using low-mass powder samples, J. Occup. Environ. Hyg. 9 (2012) 129–139, https://doi.org/10.1080/15459624.2011.652061.
[26] S. Bach, U. Eickmann, E. Schmidt, Comparison of established systems for measuring the dustiness of powders with the UNC dustiness tester developed especially for pharmaceutical substances, Ann. Occup. Hyg. 57 (2013) 1078–1086, https://doi.org/10.1093/annhyg/met022.
[27] K.M. Davies, C.M. Hammond, R.W. Higman, A.B. Wells, Progress in dustiness estimation: British Occupational Hygiene Society Technology Committee Working Party on dustiness estimation, Ann. Occup. Hyg. 32 (1988) 535–544, https://doi.org/10.1093/annhyg/32.4.535.
[28] W.A. Heitbrink, W.F. Tood, T.C. Cooper, D.M. O'Brien, The application of dustiness tests to the prediction of worker dust exposure, Am. Ind. Hyg. Assoc. J. 51 (1990) 217–223, https://doi.org/10.1080/15298669091369565.
[29] W.A. Heitbrink, P.A. Baron, K. Willeke, An investigation of dust generation by free falling powders, Am. Ind. Hyg. Assoc. J. 53 (1992) 617–624, https://doi.org/10.1080/15298669291360256.
[30] B. Cawley, D. Leith, Bench-top apparatus to examine factors that affect dust generation, Appl. Occup. Environ. Hyg. 8 (1993) 624–631, https://doi.org/10.1080/1047322X.1993.10388170.
[31] M.A.E. Plinke, D. Leith, M.G. Boundy, F. Löffler, Dust generation from handling powders in industry, Am. Ind. Hyg. Assoc. J. 56 (1995) 251–257, https://doi.org/10.1080/15428119591017088.
[32] F. Hamelmann, E. Schmidt, Methods of estimating the dustiness of industrial powders – a review, Kona Powder Part. J. 21 (2003) 7–18, https://doi.org/10.14356/kona.2003006.
[33] F. Hamelmann, E. Schmidt, Methods for characterizing the dustiness estimation of powders, Chem. Eng. Technol. 27 (2004) 844–847, https://doi.org/10.1002/ceat.200403210.
[34] S. Bach, E. Schmidt, Determining the dustiness of powders - a comparison of three measuring devices, Ann. Occup. Hyg. 52 (2008) 717–725, https://doi.org/10.1093/annhyg/men062.
[35] M. Boundy, D. Leith, T. Polton, Method to evaluate the dustiness of pharmaceutical powders, Ann. Occup. Hyg. 50 (2006) 453–458, https://doi.org/10.1093/annhyg/mel004.
[36] T. Ohta, H. Maeda, R. Kubota, A. Koga, K. Terada, Establishment of powder dustiness evaluation method by dustmeter with small amount of pharmaceutical ingredients, Int. J. Pharm. 472 (2014) 251–256, https://doi.org/10.1016/j.ijpharm.2014.05.067.
[37] S. Wirth, M. Schöler, J. Brügmann, C.S. Leopold, A novel Two-Chamber Setup for containment investigations with special focus on the dustiness of pharmaceutical powders depending on the airflow, Pharmaceutics 14 (2022) 2387, https://doi.org/10.3390/pharmaceutics14112387.
[38] K.H. Kim, E. Kabir, S. Kabir, A review on the human health impact of airborne particulate matter, Environ. Int. 74 (2015) 136–143, https://doi.org/10.1016/j.envint.2014.10.005.
[39] A. Mukherjee, M. Agrawal, World air particulate matter: sources, distribution and health effects, Environ. Chem. Lett. 15 (2017) 283–309, https://doi.org/10.1007/s10311-017-0611-9.
[40] W.E. Wilson, J.C. Chow, C. Claiborn, W. Fusheng, J. Engelbrecht, J.G. Watson, Monitoring of particulate matter outdoors, Chemosphere 49 (2002) 1009–1043, https://doi.org/10.1016/S0045-6535(02)00270-9.
[41] S.S. Amaral, J.A. de Carvalho, M.A.M. Costa, C. Pinheiro, An overview of particulate matter measurement instruments, Atmos. 6 (2015) 1327–1345, https://doi.org/10.3390/atmos6091327.
[42] A.L. Northcross, R.J. Edwards, M.A. Johnson, Z.M. Wang, K. Zhu, T. Allen, K. R. Smith, A low-cost particle counter as a realtime fine-particle mass monitor, Environ. Sci. Process. Impacts 15 (2013) 433–439, https://doi.org/10.1039/c2em30568b.
[43] S. Sousan, S. Regmi, Y.M. Park, Laboratory evaluation of low-cost optical particle counters for environmental and occupational exposures, Sensors 21 (2021) 4146, https://doi.org/10.3390/s21124146.
[44] Sensirion, Datasheet SPS30: Particulate matter sensor for air quality monitoring and control, Version 2.0 (2023) 1–26. https://sensirion.com/media/documents/8600FF88/64A3B8D6/Sensirion_PM_Sensors_Datasheet_SPS30.pdf (accessed 02 February 2025).
[45] B. Alfano, L. Barretta, A. Del Giudice, S. De Vito, G. Di Francia, E. Esposito, F. Formisano, E. Massera, M.L. Miglietta, T. Polichetti, A Review of low-cost particulate matter sensors from the developers' perspectives, Sensors 20 (2020) 6819, https://doi.org/10.3390/s20236819.
[46] S. Trilles, A.B. Vicente, P. Juan, F. Ramos, S. Meseguer, L. Serra, Reliability validation of a low-cost particulate matter IoT sensor in indoor and outdoor environments using a reference sampler, Sustainability 11 (2019) 7220, https://doi.org/10.3390/su11247220.
[47] H. Küllmar, M. Schöler, C.S. Leopold, Optimization of a newly developed chamber setup for spatial dust measurements in the context of containment, Pharmaceutics 17 (2025) 565, https://doi.org/10.3390/pharmaceutics17050565.
[48] H. Küllmar, M. Schöler, J. Brügmann, C.S. Leopold, Investigations on the spatial dust distribution for emission site localization in containment, AAPS PharmSciTech 26 (2025) 239, https://doi.org/10.1208/s12249-025-03236-y.
[49] D.E. Evans, L.A. Turkevich, C.T. Roettgers, G.J. Deye, P.A. Baron, Dustiness of fine and nanoscale powders, Ann. Occup. Hyg. 57 (2013) 261–277, https://doi.org/10.1093/annhyg/mes060.
[50] European Directorate for the Quality of Medicines & Health Care, 2.9.34. Bulk density of powders, in: Eur. Pharmacopoeia 11.5, EDQM, Strasbourg, 2024, pp. 5830–5833.
[51] C.P. Pujara, D.O. Kildsig, Effect of individual particle characteristics on airborne emissions, in: J.P. Wood (Ed.), Containment in the Pharmaceutical Industry, Marcel Dekker Inc., New York, 2001, pp. 29–53, https://doi.org/10.1201/9780429074943-4.
[52] European Directorate for the Quality of Medicines & HealthCare, 2.9.36. Powder flow, in: Eur. Pharmacopoeia 11.5, EDQM, Strasbourg, 2024, pp. 5834–5836.
[53] H. Küllmar, M. Schöler, C.S. Leopold, Real time spatial dust distribution of pharmaceutical powders with low-cost particulate matter sensors for containment detection in continuous manufacturing, in: Proceedings of the 5th APV Continuous Manufacturing Conference, 2024, Mölndal, Sweden.
[54] S. Wirth, M. Schöler, C.S. Leopold, Investigations on the dustiness of binary acetaminophen - lactose monohydrate powder blends, Powder Technol. 448 (2024) 120317, https://doi.org/10.1016/j.powtec.2024.120317.
[55] A. Jarray, H. Shi, B.J. Scheper, M. Habibi, S. Luding, Cohesion-driven mixing and segregation of dry granular media, Sci. Rep. 9 (2019) 1–12, https://doi.org/10.1038/s41598-019-49451-z.
[56] F. Podczeck, The relationship between particulate properties of carrier materials and the adhesion force of drug particles in interactive powder mixtures, J. Adhes. Sci. Technol. 11 (1997) 1089–1104, https://doi.org/10.1163/156856197X00859.
[57] H. Adi, I. Larson, H. Chiou, P. Young, D. Traini, P. Stewart, Agglomerate strength and dispersion of salmeterol xinafoate from powder mixtures for inhalation, Pharm. Res. 23 (2006) 2556–2565, https://doi.org/10.1007/s11095-006-9082-6.
[58] F. Podczeck, Adhesion forces in interactive powder mixtures of a micronized drug and carrier particles of various particle size distributions, J. Adhes. Sci. Technol. 12 (1998) 1323–1339, https://doi.org/10.1163/156856198X00461.
[59] S. Chakravarty, O. Le Bihan, M. Fischer, M. Morgeneyer, Dust generation in powders: effect of particle size distribution, EPJ Web Conf. 140 (2017) 1–4, https://doi.org/10.1051/epjconf/201714013018.
[60] E.M. Lifshitz, M. Hamermesh, The theory of molecular attractive forces between solids, in: Perspect. Theor. Phys., Elsevier, 1992: pp. 329–349. Doi: 10.1016/B978-0-08-036364-6.50031-4.

Discussion

The newly developed chamber setup for the investigation of spatial dust distributions presented in this work is described in three publications. Prior to these studies, the conceptualization, the construction of the chamber setup, and preliminary tests were performed over a time period of more than 2 years. During conceptualization, fundamental aspects had to be specified, such as the type of powder atomization, dust detection, and the shape and size of the chamber setup, to allow an investigation of the spatial dust distribution. In addition, it had to be tested how to mechanically stabilize the setup to ensure its tightness even under overpressure caused by the atomization process. All these aspects had to be decided on while keeping the planned modularity of the system in mind. In the preliminary tests, the intended functionality of all pneumatic components and of the switching sequence, controlled by the programmable logic controller (PLC), was confirmed.

In a first investigation, the necessary evacuation time of the detection chamber was determined with the fume of sulfuric acid. To gather 99 % of the fume through IOM samplers, 278 min were required, corresponding to a fivefold air exchange. Therefore, the detection time in the PLC was set accordingly for each experiment of the first two studies. However, the filter-based aerosol detection represents a cumulative method and cannot reflect time-resolved spatial dust distributions. Therefore, the chamber setup was equipped with low-cost particulate matter sensors which allowed a spatiotemporal detection of airborne dust in the third study. The results revealed that the spatial distribution of airborne dust in the detection chamber occurred in the first few minutes. Approximately 4-5 minutes after atomization, the airborne dust concentration balanced out as a result of diffusive mass transport. Consequently, a significant reduction in the runtime of each experiment was possible with these sensors.

In the first study, experiments with the surrogate ACAM were initially carried out with the opposite arrangement of the chamber setup. It was assumed that with this arrangement, higher amounts of airborne dust would be detected, as the airflow after atomization is directed towards the measurement spots. Therefore, the opposite arrangement was expected to be best suited for a first stage in the proof of concept. This assumption was confirmed by the obtained results: With the opposite arrangement, the measured dustiness was higher than with the orthogonal arrangement. With both arrangements, a linear relationship between sample mass and settled amount of ACAM was evident. A detailed examination of the atomization parameters in the second study further confirmed this observation. However, a maximum of the measured dustiness was reached at a sample mass of about 400 mg. This maximum is presumably caused by the ball-valve geometry, which limits the cross-sectional area of the sample exposed to pressurized air during atomization. However, this limitation does not represent a disadvantage for measurements with the chamber setup, as the sample quantities to be examined in a pharmaceutical context should be as small as possible because of high costs and sometimes limited availability. In the experiments of the first study, the percentage of sample mass captured by the samplers was less than 0.05 % of the total sample mass applied. Therefore, the measurement procedure was optimized in the second study to increase this percentage. With a change to a friction-free cleaning method, electrostatic charges on the chamber panels were diminished, leading to a tenfold increase of captured airborne dust. This cleaning method is particularly recommended if powders with a high tendency to become electrostatically charged, such as ACAM, are measured. In addition, the influence of the surrogate particle characteristics on dust generation was investigated. It became evident that ACAM powder consisting of small, granular, almost spherically shaped particles led to higher dust emissions than ACAM powder with elongated, needle-

like particles. This observation not only allowed a further increase in the percentage of captured dust but also gave valuable insights into a potential reduction of the dust emissions in an industrial production environment.

The main focus of the chamber setup was the determination of spatial dust distributions. With the opposite arrangement, the highest amount of ACAM settled on the filter within the IOM sampler positioned in the middle of the detection site and directly opposite to the emission chamber. In most of the surrounding IOM samplers significantly less airborne dust was detected. With the orthogonal arrangement, the highest amount of ACAM was detected with IOM samplers positioned on the right-hand side of the detection chamber and thus most distant to the emission chamber. The settled amount of ACAM was lower on the filters within the IOM samplers positioned in the center column than on those positioned on the right-hand side. The lowest settled amount was detected with the samplers on the left-hand side, closest to the emission chamber. The combined results of both arrangements confirmed the ability of the chamber setup to detect the spatial distribution of airborne dust and allow a three-dimensional emission site localization. Nevertheless, these results were unexpected, as the highest concentration of airborne dust was expected to be close to the emission site with decreasing values at more distantly positioned measurement spots. The spatial dust distribution was assumed to be caused by a strong convective mass transport of the dust particles resulting from the airflow directed through the connecting orifice of the emission chamber to the opposite panel of the detection chamber and subsequent lateral distribution. To confirm this assumption, CFD simulations were performed to simulate the airflow caused by the atomization of the samples with pressurized air for both arrangements of the chamber setup. The simulations demonstrated that both airflow patterns caused by the atomization

process were similar to the observed spatial dust distributions, emphasizing a strong convective mass transport of the airborne dust particles.

To investigate the influence of the individual atomization parameters on the dust emissions and their spatial distribution in more detail, a DoE approach was applied in the second study. As mentioned above, there was a linear relationship between the sample mass and the totally settled amount of ACAM. Interestingly, a linear relationship was also found between the sample mass and the vertical dust distribution. Between the two other atomization parameters, in particular the atomization duration and the atomization volume flow rate, a two-factor interaction was evident not only with regard to the amount of dust generated but also to its spatial distribution. It became apparent that the combination of these two parameters not only determines the amount of energy input into the sample but also the convective transport of airborne particles.

In the third study, the modularity of the chamber setup proved to be beneficial, as preliminary studies showed that by repositioning the emission chamber closer to the orthogonally arranged panel equipped with the optical sensors, a spatiotemporal detection of airborne dust was achieved. Furthermore, the influence of the atomization duration on the airborne dust concentration and the spatial dust distribution was confirmed. An extension of the atomization duration from 1 to 2 s led to a significantly increased dust concentration in the detection chamber. In contrast, with a further extension from 2 to 3 s, no significantly higher dust concentrations were observed. Apparently, an atomization duration of 2 s was sufficient for complete atomization of the powder samples and for the convective particle transport from the emission to the detection chamber. Furthermore, an incremental increase in the gauge pressure of the compressed air used for atomization led to higher airborne dust concentrations detected with the PM sensors.

Similar to the first two studies, the highest ACAM concentration was detected with the sensor positioned on the right-hand side of the center row of measurement spots, being most distant to the emission site. From this sensor position the ACAM concentration decreased in a circular pattern, as observed in the first two studies based on IOM samplers. The processing of plain substances only plays a minor role in the manufacture of oral solid dosage forms, as the API is usually processed in blends during manufacturing. Therefore, a binary blend of coarse LAC as excipient and fine particulate ACAM as a surrogate API was investigated. The results showed a decreased, yet higher than expected dust emission of the binary blend compared to plain ACAM, indicating particle interactions of both components which may affect the propensity of the blend to generate airborne dust.

In contrast to the filter-based detection with IOM samplers, the optical sensors allow a real-time and size-specific detection of airborne dust. However, to date, the fraction of a single component in the total dust of an atomized powder blend can only be determined by filter-based sampling with subsequent chemical analysis. Therefore, the detection method should be selected based on the subject matter to be investigated in the context of containment. An optimum sensor should offer real-time monitoring and simultaneous analysis of the particle size as well as differentiation between individual substances contained in the airborne dust.

In summary, the successful development of a chamber setup for the investigation of the spatial dust distribution of pharmaceutical powders is presented in this work. With this setup, valuable insights into physicochemical powder properties as well as atomization and detection parameters affecting dust emissions and the spatial dust distribution were achieved. Hereby, the safety in the contained manufacture of pharmaceuticals may be improved by the spatial detection and localization of leakages in containment systems

based on stationary exposure data. Thus, the newly developed chamber setup represents a valuable tool for the investigation of dust emissions as well as spatial dust distributions. Because of its modularity, it may be adapted to specific technical requirements and even allows the implementation of new optical sensor technologies.

References

[1] D. Bormett, High-potency APIs: Containment and handling issues, Pharm. Technol. 32 Suppl. 1 (2008) S12–S16.

[2] E.T. Michalson, High potency active pharmaceutical ingredients: An overview of safety and manufacturing concerns, Chim. Oggi-Chem. Today 25 (2007) 18–20.

[3] A.W. Ader, J.P. Farris, R.H. Ku, Occupational health categorization and compound handling practice systems - roots, application and future, Chem. Heal. Saf. 12 (2005) 20–26, https://doi.org/10.1016/j.chs.2005.01.016.

[4] V. Ahuja, M. Krishnappa, Approaches for setting occupational exposure limits in the pharmaceutical industry, J. Appl. Toxicol. 42 (2022) 154–167, https://doi.org/10.1002/jat.4218.

[5] J.R. Broach, J. Thorner, High-throughput screening for drug discovery, Nature 384 Suppl. 1 (1996) S14–S16.

[6] G. Mari, A. Moccaldi, G. Ludovisi, Handling of high potency drugs: Process and containment, Trans, Ecol. Environ. 85 (1999) 257–265, https://doi.org/10.2495/EEH050281.

[7] D. Paul, G. Sanap, S. Shenoy, D. Kalyane, K. Kalia, R.K. Tekade, Artificial intelligence in drug discovery and development, Drug Discov. Today 26 (2021) 80–93, https://doi.org/10.1016/j.drudis.2020.10.010.

[8] D. Vemula, P. Jayasurya, V. Sushmitha, Y.N. Kumar, V. Bhandari, CADD, AI and ML in drug discovery: a comprehensive review, Eur. J. Pharm. Sci. 181 (2023) 106324, https://doi.org/10.1016/j.ejps.2022.106324.

[9] Y. Yang, F. Cheng, Artificial intelligence streamlines scientific discovery of drug–target interactions, Br. J. Pharmacol. (2025) 1–18, https://doi.org/10.1111/bph.17427.

[10] C.A. Challener, Challenges to formulation development for highly potent APIs, Pharm. Technol. 46 (2022) 24–27.

[11] E. Dunny, I. O'Connor, J. Bones, Containment challenges in HPAPI manufacture for ADC generation, Drug Discov. Today 22 (2017) 947–951, https://doi.org/10.1016/j.drudis.2017.02.003.

[12] C.A. Challener, Conjugation chemistry with highly potent compounds, Pharm. Technol. 40 (2016) 34–37.

[13] J.P. Wood, Containment in the pharmaceutical industry, CRC Press, New York, 2000, https://doi.org/10.1201/9780429074943.

[14] P. Tiwari, S.R. Chowdhury, Sustainable production of highly active pharmaceutical ingredients (HAPIs), Int. J. Sci. Res. Publ. 4 (2014) 2250–3153.

[15] R.J.L. Heron, F.C. Pickering, Health effects of exposure to active pharmaceutical ingredients (APIs), Occup. Med. 53 (2003) 357–362, https://doi.org/10.1093/occmed/kqg115.

[16] N.F.J. Van Nimmen, K.L.C. Poels, H.A.F. Veulemans, Identification of exposure pathways for opioid narcotic analgesics in pharmaceutical production workers, Ann. Occup. Hyg. 50 (2006) 665–677, https://doi.org/10.1093/annhyg/mel028.

[17] International Society for Pharmaceutical Engineering, Containment Manual, Working Group Containment (Ed.), ISPE, North Bethesda, 2017.

[18] J.O. Eniola, R. Kumar, M.A. Barakat, J. Rashid, A review on conventional and advanced hybrid technologies for pharmaceutical wastewater treatment, J. Clean. Prod. 356 (2022) 131826, https://doi.org/10.1016/j.jclepro.2022.131826.

[19] W. Xu, R. Zou, B. Jin, G. Zhang, Y. Su, Y. Zhang, The ins and outs of pharmaceutical wastewater treatment by microbial electrochemical technologies, Sustain. Horizons 1 (2022) 100003, https://doi.org/10.1016/j.horiz.2021.100003.

[20] B.L. Phoon, C.C. Ong, M.S. Mohamed Saheed, P.L. Show, J.S. Chang, T.C. Ling, S.S. Lam, J.C. Juan, Conventional and emerging technologies for removal of antibiotics from wastewater, J. Hazard. Mater. 400 (2020) 122961, https://doi.org/10.1016/j.jhazmat.2020.122961.

[21] M. Levin, I.K. Koponen, K.A. Jensen, Exposure assessment of four pharmaceutical powders based on dustiness and evaluation of damaged HEPA filters, J. Occup. Environ. Hyg. 11 (2014) 165–177, https://doi.org/10.1080/15459624.2013.848038.

[22] C.S.J. Tsai, M.E. Echevarría-Vega, G.A. Sotiriou, C. Santeufemio, D. Schmidt, P. Demokritou, M. Ellenbecker, Evaluation of environmental filtration control of engineered nanoparticles using the Harvard Versatile Engineered Nanomaterial Generation System (VENGES), J. Nanoparticle Res. 14 (2012), https://doi.org/10.1007/s11051-012-0812-x.

[23] European Medicines Agency (EMA), Guideline on setting health based exposure limits for use in risk identification in the manufacture of different medicinal products in shared facilities (EMA/CHMP/CVMP/SWP/169430/2012), Eur. Com. J. 44 (2014) 1–9.

[24] International Society for Pharmaceutical Engineering, Good Practice Guide: Assessing the Particulate Containment Performance of Pharmaceutical Equipment, G. Petroka, J.P. Wood (Eds.), ISPE, North Bethesda, 2012.

[25] S. Wollowitz, Managing high-potency active pharmaceutical ingredients - a drug sponsor’s guide, Drug Dev. Res. 71 (2010) 420–428, https://doi.org/10.1002/ddr.20385.

[26] J. Becker, T. Pohlmann, Development and implementation of a large-scale HPAPI manufacturing process, Chim. Oggi-Chem. Today 35 (2017) 20–24.

[27] R.H. Ku, An overview of setting occupational exposure limits (OELs) for pharmaceuticals, Chem. Heal. Saf. 9098 (2000) 34–37, https://doi.org/10.1016/S1074-9098(99)00070-2.

[28] B.D. Naumann, E.V. Sargent, B.S. Starkman, W.J. Fraser, G.T. Becker, G.D. Kirk, Performance-based exposure control limits for pharmaceutical active ingredients, Am. Ind. Hyg. Assoc. J. 57 (1996) 33–42, https://doi.org/10.1080/15428119691015197.

[29] International Society for Pharmaceutical Engineering, Good Practice Guide SMEPAC, R. Nicolai, G.S. Petroka, K. Whitaker (Eds.), 3rd ed., ISPE, North Bethesda, 2024.

[30] G. Franco, Ramazzini and workers' health, Lancet 354 (1999) 858–861, https://doi.org/10.1016/S0140-6736(99)80042-7.

[31] J.P. Bercu, E.J. Morinello, C. Sehner, B.K. Shipp, P.A. Weideman, Point of departure (PoD) selection for the derivation of acceptable daily exposures (ADEs) for active pharmaceutical ingredients (APIs), Regul. Toxicol. Pharmacol. 79 Suppl. 1 (2016) S48–S56, https://doi.org/10.1016/j.yrtph.2016.05.028.

[32] R.G. Sussman, B.D. Naumann, T. Pfister, C. Sehner, C. Seaman, P.A. Weideman, A harmonization effort for acceptable daily exposure derivation – Considerations for application of adjustment factors, Regul. Toxicol. Pharmacol. 79 Suppl. 1 (2016) S57–S66, https://doi.org/10.1016/j.yrtph.2016.05.023.

[33] J.F. Reichard, M.A. Maier, B.D. Naumann, A.M. Pecquet, T. Pfister, R. Sandhu, E. V. Sargent, A.J. Streeter, P.A. Weideman, Toxicokinetic and toxicodynamic considerations when deriving health-based exposure limits for pharmaceuticals, Regul. Toxicol. Pharmacol. 79 Suppl. 1 (2016) S67–S78, https://doi.org/10.1016/j.yrtph.2016.05.027.

[34] L. Schenk, S.O. Hansson, C. Rudén, M. Gilek, Occupational exposure limits: A comparative study, Regul. Toxicol. Pharmacol. 50 (2008) 261–270, https://doi.org/10.1016/j.yrtph.2007.12.004.

[35] E. V. Sargent, E. Faria, T. Pfister, R.G. Sussman, Guidance on the establishment of acceptable daily exposure limits (ADE) to support risk-based manufacture of pharmaceutical products, Regul. Toxicol. Pharmacol. 65 (2013) 242–250, https://doi.org/10.1016/j.yrtph.2012.12.007.

[36] S.P. Binks, Occupational toxicology and the control of exposure to pharmaceutical agents at work, Occup. Med. 53 (2003) 363–370, https://doi.org/10.1093/occmed/kqg116.

[37] B.D. Naumann, P.A. Weideman, R. Sarangapani, S.C. Hu, R. Dixit, E. V. Sargent, Investigations of the use of bioavailability data to adjust occupational exposure limits for active pharmaceutical ingredients, Toxicol. Sci. 112 (2009) 196–210, https://doi.org/10.1093/toxsci/kfp195.

[38] G.D. Nielsen, S. Øvrebø, Background, approaches and recent trends for setting health-based occupational exposure limits: A minireview, Regul. Toxicol. Pharmacol. 51 (2008) 253–269, https://doi.org/10.1016/j.yrtph.2008.04.002.

[39] E.L. Barle, G.C. Winkler, S. Glowienke, A. Elhajouji, J. Nunic, H.J. Martus, Setting occupational exposure limits for genotoxic substances in the pharmaceutical industry, Toxicol. Sci. 151 (2016) 2–9, https://doi.org/10.1093/toxsci/kfw028.

[40] J.C. Graham, J. Hillegass, G. Schulze, Considerations for setting occupational exposure limits for novel pharmaceutical modalities, Regul. Toxicol. Pharmacol. 118 (2020) 104813, https://doi.org/10.1016/j.yrtph.2020.104813.

[41] M. Deveau, C.P. Chen, G. Johanson, D. Krewski, A. Maier, K.J. Niven, S. Ripple, P.A. Schulte, J. Silk, J.H. Urbanus, D.M. Zalk, R.W. Niemeier, The global landscape of occupational exposure limits-Implementation of harmonization principles to guide limit selection, J. Occup. Environ. Hyg. 12 Suppl. 1 (2015) S127–S144, https://doi.org/10.1080/15459624.2015.1060327.

[42] S. Karthikeyan, J.A. Inbaraj, P. Thangavel, D. Deepa, N. Saravanan, R. Karthikeyan, Selection of containment system for handling cytotoxic drugs in pharmaceutical industry, Educ. Adm. Theory Pract. 30 (2024) 6806–6811, https://doi.org/10.53555/kuey.v30i4.2101.

[43] Volkmann GmbH, Relationship between ADE, OEL and OEB, (2020). https://volkmann.info/news/containment-oeb-5-handling-von-kritischen-und-toxischen-stoffen (accessed 26 June 2025).

[44] T. Calkins, D. Bormett, Effective containment the key to safe HPAPI manufacture, Chim. Oggi-Chem. Today 30 (2012) 40–42.

[45] J. Stein, T. Fuchs, C. Mattern, Advanced milling and containment technologies for superfine active pharmaceutical ingredients, Chem. Eng. Technol. 33 (2010) 1464–1470, https://doi.org/10.1002/ceat.200900590.

[46] N.J. Adams, D.L. Johnson, R.A. Lynch, The effect of pressure differential and care provider movement on airborne infectious isolation room containment effectiveness, Am. J. Infect. Control 39 (2011) 91–97, https://doi.org/10.1016/j.ajic.2010.05.025.

[47] V. Kanjiyangat, M. Hareendran, Engineering intervention to reduce API dust exposure during milling operation, J. Chem. Heal. Saf. 25 (2018) 36–39, https://doi.org/10.1016/j.jchas.2017.07.002.

[48] E. Ales, Directive 89/391/EEC on the introduction of measures to encourage improvements in the safety and health of workers at work, in: E. Ales, M. Bell, O. Deinert, S. Robin-Olivier (Eds.), International and European Labour Law: Article-by-Article Commentary, Nomos, Baden-Baden, 2018, pp. 1210–1242, https://doi.org/10.5771/9783845266190.

[49] U.S. Congress, Occupational Safety and Health Act of 1970, GovInfo, 2019. https://www.govinfo.gov/app/details/COMPS-1523 (accessed 27 June 2025).

[50] International Labour Organization (ILO), Guidelines on occupational safety and health management systems: ILO-OSH 2001, ILO, Geneva, 2001.

[51] International Council for Harmonisation (ICH), Harmonised Tripartite Guideline: Good Manufacturing Practice Guide for Active Pharmaceutical Ingredients Q7, 2000.

[52] U.S. Food and Drug Administration (FDA), Guidance for Industry - Non-Penicillin Beta-Lactam Drugs: A CGMP Framework for Preventing Cross-Contamination, Silver Spring, MD, 2013, pp. 1–7.

[53] E. V. Sargent, A. Flueckiger, E.L. Barle, W. Luo, L.R. Molnar, R. Sandhu, P.A. Weideman, The regulatory framework for preventing cross-contamination of pharmaceutical products: History and considerations for the future, Regul. Toxicol. Pharmacol. 79 Suppl. 1 (2016) S3–S10, https://doi.org/10.1016/j.yrtph.2016.05.029.

[54] M. Pathodiya, Cross-contamination risk assessment using FMEA tool, J. Drug Deliv. Ther. 14 (2024) 164–167, https://doi.org/10.22270/jddt.v14i9.6765.

[55] R. Lynch, D. Barabani, K. Bellorado, P. Canisius, D. Heathcote, A. Johnson, N. Wyman, D.W. Parry, Guidelines for risk-based changeover of biopharma multi-product facilities, PDA J. Pharm. Sci. Technol. 72 (2018) 91–103, https://doi.org/10.5731/pdajpst.2016.007419.

[56] T. Sandle, M.R. Saghee, Some considerations for the implementation of disposable technology and single-use systems in biopharmaceuticals, J. Commer. Biotechnol. 17 (2011) 319–329, https://doi.org/10.1057/jcb.2011.21.

[57] D. Eibl, R. Eibl, Single-use equipment in biopharmaceutical manufacture, in: D. Eibl, R. Eibl (Eds.), Single-Use Technology in Biopharmaceutical Manufacture, Wiley, Hoboken, NJ, 2019, pp. 1–11, https://doi.org/10.1002/9781119477891.ch1.

[58] A.A. Shukla, U. Gottschalk, Single-use disposable technologies for biopharmaceutical manufacturing, Trends Biotechnol. 31 (2013) 147–154, https://doi.org/10.1016/j.tibtech.2012.10.004.

[59] W.G. Whitford, M.A. Petrich, W.P. Flanagan, Environmental impacts of single-use systems, in: D. Eibl, R. Eibl (Eds.), Single-Use Technology in Biopharmaceutical Manufacture, Wiley, Hoboken, NJ, 2019, pp. 169–179, https://doi.org/10.1002/9781119477891.ch13.

[60] Bundesministerium der Justiz (BMJ), Verordnung über die Anwendung der Guten Herstellungspraxis bei der Herstellung von Arzneimitteln und Wirkstoffen und über die Anwendung der Guten fachlichen Praxis bei der Herstellung von Produkten menschlicher Herkunft (Arzneimittel- und Wirkstoffherstellungsverordnung - AMWHV), 2006. Gesetze im Internet, https://www.gesetze-im-internet.de/amwhv/BJNR252310006.html (accessed 30 June 2025).

[61] N. Hirst, M. Brocklebank, M. Ryder, Containment systems: a design guide, IChemE, Rugby, UK, 2002.

[62] H. Stahl, How to make tablets from potent APIs, PROCESS Worldwide, 2011. https://www.process-worldwide.com/how-to-make-tablets-from-potent-apis-a-342457 (accessed 27 May 2020).

[63] F.C. Simeone, M. Blosi, S. Ortelli, A.L. Costa, Assessing occupational risk in designs of production processes of nano-materials, NanoImpact 14 (2019) 100149, https://doi.org/10.1016/j.impact.2019.100149.

[64] European Commission, EudraLex Volume 4 - EU Guidelines for Good Manufacturing Practice for Medicinal Products for Human and Veterinary Use, Part I, Chapter 3: Premises and Equipment, Brussels, 2014.

[65] European Commission, EudraLex Volume 4 - EU Guidelines for Good Manufacturing Practice for Medicinal Products for Human and Veterinary Use, Part I, Chapter 5: Production, Brussels, 2014.

[66] David Barr, M. Montalvo, API Facilities, in: A.A. Signore, T. Jacobs (Eds.), Good Design Practices for GMP Pharmaceutical Facilities, Taylor & Francis, Boca Raton, FL, 2005, pp. 313–356.

[67] C. Zanini, F. Severina, G. Lando, C. Fanizza, E. Cesana, D. Desidera, M. Bonifacio, Good design practices for an integrated containment and production system for advanced therapies, Biotechnol. Bioeng. 117 (2020) 2319–2330, https://doi.org/10.1002/bit.27376.

[68] O. Butler, J. Forder, J. Saunders, Analytical protocol for the sensitive determination of mannitol, sorbitol and glucose containing powders in pharmaceutical workplaces by ion chromatography using a pulsed amperometric detector, J. Pharm. Biomed. Anal. 106 (2015) 204–209, https://doi.org/10.1016/j.jpba.2014.10.006.

[69] D. Mark, J.H. Vincent, H. Gibson, G. Lynch, A new static sampler for airborne total dust in workplaces, Am. Ind. Hyg. Assoc. J. 46 (1985) 127–133, https://doi.org/10.1080/15298668591394536.

[70] D. Mark, J.H. Vincent, A new personal sampler for airborne total dust in workplaces, Ann. Occup. Hyg. 30 (1986) 89–102, https://doi.org/10.1093/annhyg/30.1.89.

[71] J.H. Vincent, Aerosol sampling: Science, Standards, Instrumentation and Applications, John Wiley & Sons, Chichester, UK, 2007.

[72] Health and Safety Executive (HSE), General methods for sampling and gravimetric analysis of respirable, thoracic and inhalable aerosols MDHS14/4, HSE Books, Bootle, UK, 2019, pp. 1–13.

[73] K.D. Dial, S. Hiemstra, J.E. Thompson, Simultaneous measurement of optical scattering and extinction on dispersed aerosol samples, Anal. Chem. 82 (2010) 7885–7896, https://doi.org/10.1021/ac100617j.

[74] R. Xu, Optical Particle Counting, in: B. Scarlett (Ed.), Particle Characterization: Light Scattering Methods, Particle Technology Series, vol. 13, Springer, Dordrecht, 2002, pp. 182–222, https://doi.org/10.1007/0-306-47124-8_4.

[75] M. Kuhli, M. Weiss, H. Steckel, A new approach to characterise pharmaceutical aerosols: Measurement of aerosol from a single dose aqueous inhaler with an optical particle counter, Eur. J. Pharm. Sci. 39 (2010) 45–52, https://doi.org/10.1016/j.ejps.2009.10.009.

[76] M. Boundy, D. Leith, T. Polton, Method to evaluate the dustiness of pharmaceutical powders, Ann. Occup. Hyg. 50 (2006) 453–458, https://doi.org/10.1093/annhyg/mel004.

[77] T. Ohta, H. Maeda, R. Kubota, A. Koga, K. Terada, Establishment of powder dustiness evaluation method by dustmeter with small amount of pharmaceutical ingredients, Int. J. Pharm. 472 (2014) 251–256, https://doi.org/10.1016/j.ijpharm.2014.05.067.

[78] F.J. Murray, A.D. Monnot, D. Jacobson-Kram, S.M. Cohen, J.F. Hardisty, S.B. Bandara, M. Kovochich, M. Deore, S.K. Pitchaiyan, C.K. Gelotte, J.C.K. Lai, E. Atillasoy, A. Hermanowski-Vosatka, E. Kuffner, K.M. Unice, K. Yang, Y. Gebremichael, B.A. Howell, G. Eichenbaum, A critical review of the acetaminophen preclinical carcinogenicity and tumor promotion data and their implications for its carcinogenic hazard potential, Regul. Toxicol. Pharmacol. 118 (2020) 104801, https://doi.org/10.1016/j.yrtph.2020.104801.

[79] E.P. Krenzelok, The FDA acetaminophen advisory committee meeting – what is the future of acetaminophen in the United States? The perspective of a committee member, Clin. Toxicol. 47 (2009) 784–789, https://doi.org/10.1080/15563650903232345.

[80] S. Wirth, M. Schöler, J. Brügmann, C.S. Leopold, An investigation on the relationship between dust emission and air flow as well as particle size with a novel containment two-chamber setup, Pharmaceutics 16 (2024), https://doi.org/10.3390/pharmaceutics16081088.

[81] S. Wirth, M. Schöler, J. Brügmann, C.S. Leopold, A novel two-chamber setup for containment investigations with special focus on the dustiness of pharmaceutical powders depending on the airflow, Pharmaceutics 14 (2022) 2387, https://doi.org/10.3390/pharmaceutics14112387.

[82] E. Rahimpour, E. Mazaher Haji Agha, F. Martinez, M. Barzegar-Jalali, A. Jouyban, Solubility study of acetaminophen in the mixtures of acetonitrile and water at different temperatures, J. Mol. Liq. 324 (2021) 114708, https://doi.org/10.1016/j.molliq.2020.114708.

[83] T. Nagai, S. Prakongpan, Solubility of acetaminophen in cosolvents, Chem. Pharm. Bull. 32 (1984) 340–343, https://doi.org/10.1248/cpb.32.340.

[84] L.J. Jallo, R.N. Dave, Explaining electrostatic charging and flow of surface-modified acetaminophen powders as a function of relative humidity through surface energetics, J. Pharm. Sci. 104 (2015) 2225–2232, https://doi.org/10.1002/jps.24479.

[85] H. Küllmar, M. Schöler, C.S. Leopold, Optimization of a newly developed chamber setup for spatial dust measurements in the context of containment, Pharmaceutics 17 (2025) 565, https://doi.org/10.3390/pharmaceutics17050565.

[86] L. Kenny, Scientific principles and pragmatic solutions for the measurement of exposure to inhalable dust, Ann. Occup. Hyg. 47 (2003) 437–440, https://doi.org/10.1093/annhyg/meg049.

[87] N.P. Vaughan, C.P. Chalmers, R.A. Botham, Field comparison of personal samplers for inhalable dust, Ann. Occup. Hyg. 34 (1990) 553–573, https://doi.org/10.1093/annhyg/34.6.553.

[88] T.L. Ogden, J.L. Birkett, The human head as a dust sampler, in: Inhaled Particles IV, Pergamon Press, Oxford, 1977, pp. 93–105.

[89] M.R. Flynn, D.K. George, Aerodynamics and exposure variability, Appl. Occup. Environ. Hyg. 6 (1991) 36–39, https://doi.org/10.1080/1047322X.1991.10387823.

[90] M.R. Flynn, B.L. Gatano, J.L. McKernan, K.H. Dunn, B.A. Blazicko, G.N. Carlton, Modeling breathing-zone concentrations of airborne contaminants generated during compressed air spray painting, Ann. Occup. Hyg. 43 (1999) 67–76, https://doi.org/10.1016/S0003-4878(98)00078-7.

[91] G. Lidén, L.C. Kenny, Errors in inhalable dust sampling for particles exceeding 100 µm, Ann. Occup. Hyg. 38 (1994) 373–384, https://doi.org/10.1093/annhyg/38.4.373.

[92] L. Armbruster, H. Breuer, Investigations into defining inhalable dust, Ann. Occup. Hyg. 26 (1982) 21–32, https://doi.org/10.1093/annhyg/26.1.21.

[93] J.H. Vincent, L. Armbruster, On the quantitative definition of the inhalability of airborne dust, Ann. Occup. Hyg. 24 (1981) 245–248, https://doi.org/10.1093/annhyg/24.2.245.

[94] C. Cowhere, M.A. Grelinger, K.F. Wong, Dust inhalation exposures from the handling of small volumes of powders, Am. Ind. Hyg. Assoc. J. 50 (1989) 131–138, https://doi.org/10.1080/15298668991374417.

[95] International Organization for Standardization, ISO 7708: Air quality – Particle size fraction definitions for health-related sampling, 1995.

[96] American Conference of Governmental Industrial Hygienists (ACGIH), Threshold Limit Values for Chemical Substances and Physical Agents and Biological Exposure Indices, 1992–1993, ACGIH, Cincinnati, OH, 1992, pp. 81–83.

[97] European Committee for Standardization (CEN), EN 481: Workplace atmospheres – Size fraction definitions for measurement of airborne particles, Brussels, 1993.

[98] G. Lidén, M. Harper, Analytical performance criteria the need for an international sampling convention for inhalable dust in calm air, J. Occup. Environ. Hyg. 3 (2006) D94–D101, https://doi.org/10.1080/15459620600920580.

[99] F. Hamelmann, E. Schmidt, Methods for characterizing the dustiness estimation of powders, Chem. Eng. Technol. 27 (2004) 844–847, https://doi.org/10.1002/ceat.200403210.

[100] F. Hamelmann, E. Schmidt, Methods of estimating the dustiness of industrial powders – A review, Kona Powder Part. J. 21 (2003) 7–18, https://doi.org/10.14356/kona.2003006.

[101] World Health Organization, Hazard Prevention and Control in the Work Environment: Airborne Dust, WHO, Geneva, Switzerland, 1999. https://iris.who.int/handle/10665/66147 (accessed 27 October 2024).

[102] International Organization for Standardization, ISO 4225: Air quality – General aspects – Vocabulary, 1994.

[103] K. Saleh, M.T. Moufarej Abou Jaoude, M. Morgeneyer, E. Lefrancois, O. Le Bihan, J. Bouillard, Dust generation from powders: A characterization test based on stirred fluidization, Powder Technol. 255 (2014) 141–148, https://doi.org/10.1016/j.powtec.2013.10.051.

[104] K.H. Kim, E. Kabir, S. Kabir, A review on the human health impact of airborne particulate matter, Environ. Int. 74 (2015) 136–143, https://doi.org/10.1016/j.envint.2014.10.005.

[105] Q. Deng, L. Deng, Y. Miao, X. Guo, Y. Li, Particle deposition in the human lung: Health implications of particulate matter from different sources, Environ. Res. 169 (2019) 237–245, https://doi.org/10.1016/j.envres.2018.11.014.

[106] C. Ou, J. Hang, Q. Deng, Particle deposition in human lung airways: Effects of airflow, particle size, and mechanisms, Aerosol Air Qual. Res. 20 (2020) 2846–2858, https://doi.org/10.4209/aaqr.2020.02.0067.

[107] C. Darquenne, Aerosol deposition in health and disease, J. Aerosol Med. Pulm. Drug Deliv. 25 (2012) 140–147, https://doi.org/10.1089/jamp.2011.0916.

[108] F.J. Miller, D.E. Gardner, J.A. Graham, R.E. Lee, W.E. Wilson, J.D. Bachmann, Size considerations for establishing a standard for inhalable particles, J. Air Pollut. Control Assoc. 29 (1979) 610–615, https://doi.org/10.1080/00022470.1979.10470831.

[109] A. Mukherjee, M. Agrawal, World air particulate matter: sources, distribution and health effects, Environ. Chem. Lett. 15 (2017) 283–309, https://doi.org/10.1007/s10311-017-0611-9.

[110] G. Boulanger, P. Andujar, J.C. Pairon, M.A. Billon-Galland, C. Dion, P. Dumortier, P. Brochard, A. Sobaszek, P. Bartsch, C. Paris, M.C. Jaurand, Quantification of short and long asbestos fibers to assess asbestos exposure: A review of fiber size toxicity, Environ. Heal. 13 (2014) 1–18, https://doi.org/10.1186/1476-069X-13-59.

[111] O.Y.O. Osinubi, M. Gochfeld, H.M. Kipen, Health effects of asbestos and nonasbestos fibers, Environ. Health Perspect. 108 (2000) 665–674, https://doi.org/10.1289/ehp.00108s4665.

[112] G. Lidén, Dustiness testing of materials handled at workplaces, Ann. Occup. Hyg. 50 (2006) 437–439, https://doi.org/10.1093/annhyg/mel042.

[113] C.P. Pujara, Determination of factors that affect the generation of airborne particles from bulk pharmaceutical powders, Ph.D. thesis, Purdue University, West Lafayette, IN, 1997.

[114] N. Shandilya, E. Kuijpers, I. Tuinman, W. Fransman, Powder intrinsic properties as dustiness predictor for an efficient exposure assessment? Ann. Work Expo. Heal. 63 (2019) 1029–1045, https://doi.org/10.1093/annweh/wxz065.

[115] K.H. Carlson, D.R. Herman, T.F. Markey, R.K. Wolff, M.A. Dorato, A comparison of two dustiness evaluation methods, Am. Ind. Hyg. Assoc. J. 53 (1992) 448–454, https://doi.org/10.1080/15298669291359933.

[116] N.O. Breum, The rotating drum dustiness tester: Variability in dustiness in relation to sample mass, testing time, and surface adhesion, Ann. Occup. Hyg. 43 (1999) 557–566, https://doi.org/10.1016/S0003-4878(99)00049-6.

[117] E. Petavratzi, S.W. Kingman, I.S. Lowndes, Assessment of the dustiness and the dust liberation mechanisms of limestone quarry operations, Chem. Eng. Process. Process Intensif. 46 (2007) 1412–1423, https://doi.org/10.1016/j.cep.2006.11.005.

[118] K.M. Davies, C.M. Hammond, R.W. Higman, A.B. Wells, Progress in dustiness estimation: British Occupational Hygiene Society Technology Committee Working Party on dustiness estimation, Ann. Occup. Hyg. 32 (1988) 535–544, https://doi.org/10.1093/annhyg/32.4.535.

[119] K. Hjemsted, T. Schneider, Documentation of a dustiness drum test, Ann. Occup. Hyg. 40 (1996) 627–643, https://doi.org/10.1016/S0003-4878(96)00024-5.

[120] S. Bach, E. Schmidt, Determining the dustiness of powders - a comparison of three measuring devices, Ann. Occup. Hyg. 52 (2008) 717–725, https://doi.org/10.1093/annhyg/men062.

[121] S.A. Sethi, T. Schneider, A gas fluidization dustiness tester, J. Aerosol Sci. 27 Suppl. 1 (1996) S305–S306, https://doi.org/10.1016/0021-8502(96)00225-X.

[122] P.T. O'Shaughnessy, M. Kang, D. Ellickson, A novel device for measuring respirable dustiness using low-mass powder samples, J. Occup. Environ. Hyg. 9 (2012) 129–139, https://doi.org/10.1080/15459624.2011.652061.

[123] S. Bach, U. Eickmann, E. Schmidt, Comparison of established systems for measuring the dustiness of powders with the UNC dustiness tester developed especially for pharmaceutical substances, Ann. Occup. Hyg. 57 (2013) 1078–1086, https://doi.org/10.1093/annhyg/met022.

[124] B. Cawley, D. Leith, Bench-top apparatus to examine factors that affect dust generation, Appl. Occup. Environ. Hyg. 8 (1993) 624–631, https://doi.org/10.1080/1047322X.1993.10388170.

[125] W.A. Heitbrink, P.A. Baron, K. Willeke, An investigation of dust generation by free falling powders, Am. Ind. Hyg. Assoc. J. 53 (1992) 617–624, https://doi.org/10.1080/15298669291360256.

[126] P. Dubey, U. Ghia, L.A. Turkevich, Computational fluid dynamics analysis of the venturi dustiness tester, Powder Technol. 312 (2017) 310–320, https://doi.org/10.1016/j.powtec.2017.02.030.

[127] M.A.E. Plinke, R. Maus, D. Leith, Experimental examination of factors that affect dust generation by using Heubach and MRI testers, Am. Ind. Hyg. Assoc. J. 53 (1992) 325–330, https://doi.org/10.1080/15298669291359726.

[128] J.R. van Ommen, J.M. Valverde, R. Pfeffer, Fluidization of nanopowders: A review, J. Nanoparticle Res. 14 (2012) 737, https://doi.org/10.1007/s11051-012-0737-4.

[129] C.P. Pujara, D.O. Kildsig, Effect of individual particle characteristics on airborne emissions, in: J.P. Wood (Ed.), Containment in the Pharmaceutical Industry, Marcel Dekker Inc., New York, 2001, pp. 29–53, https://doi.org/10.1201/9780429074943-4.

[130] F. Podczeck, Adhesion forces in interactive powder mixtures of a micronized drug and carrier particles of various particle size distributions, J. Adhes. Sci. Technol. 12 (1998) 1323–1339, https://doi.org/10.1163/156856198X00461.

[131] R.F. Phalen, W.C. Hinds, L. Angeles, W. John, I. Researcher, P.J. Lioy, Particle size-selective sampling in the workplace : Rationale and recommended techniques, Ann. Occup. Hyg. 32 (1988) 403–411, https://doi.org/10.1093/annhyg/32.inhaled.

[132] S. Chakravarty, O. Le Bihan, M. Fischer, M. Morgeneyer, Dust generation in powders: Effect of particle size distribution, EPJ Web Conf. 140 (2017) 1–4, https://doi.org/10.1051/epjconf/201714013018.

[133] T. Deng, K.A. Paul, M.S.A. Bradley, L. Immins, C. Preston, J.F. Scott, E.H. Welfare, Investigations on air induced segregation of pharmaceutical powders and effect of material flow functions, Powder Technol. 203 (2010) 354–358, https://doi.org/10.1016/j.powtec.2010.05.028.

[134] K. Hjemsted, T. Schneider, Dustiness from powder materials, J. Aerosol Sci. 27 Suppl. 1 (1996) S485–S486, https://doi.org/10.1016/0021-8502(96)00315-1.

[135] J.W. Cherrie, A.T. Gillies, A. Sleeuwenhoek, M. Van Tongeren, P. McDonnell, M. Coggins, S.R. Bailey, Modelling exposure to pharmaceutical agents, J. Phys. Conf. Ser. 151 (2009), https://doi.org/10.1088/1742-6596/151/1/012063.

[136] H. Hurychová, M. Kuentz, Z. Šklubalová, Fractal aspects of static and dynamic flow properties of pharmaceutical excipients, J. Pharm. Innov. 13 (2018) 15–26, https://doi.org/10.1007/s12247-017-9302-0.

[137] K.A. Jensen, I.K. Koponen, P.A. Clausen, T. Schneider, Dustiness behaviour of loose and compacted bentonite and organoclay powders: What is the difference in exposure risk?, J. Nanoparticle Res. 11 (2009) 133–146, https://doi.org/10.1007/s11051-008-9420-1.

[138] G.G. Stokes, On the theories of the internal friction of fluids in motion, and of the equilibrium and motion of elastic solids, Trans. Camb. Philos. Soc. 8 (1845) 287–319.

[139] R. Mukherjee, V. Gupta, S. Naik, S. Sarkar, V. Sharma, P. Peri, B. Chaudhuri, Effects of particle size on the triboelectrification phenomenon in pharmaceutical excipients: Experiments and multi-scale modeling, Asian J. Pharm. Sci. 11 (2016) 603–617, https://doi.org/10.1016/j.ajps.2016.04.006.

[140] W. Kaialy, A review of factors affecting electrostatic charging of pharmaceuticals and adhesive mixtures for inhalation, Int. J. Pharm. 503 (2016) 262–276, https://doi.org/10.1016/j.ijpharm.2016.01.076.

[141] T. Nomura, T. Satoh, H. Masuda, The environment humidity effect on the tribo-charge of powder, Powder Technol. 135–136 (2003) 43–49, https://doi.org/10.1016/S0032-5910(03)00157-8.

[142] C. Ribalta, M. Viana, A. López-Lilao, S. Estupiñá, M.C. Minguillón, J. Mendoza, J. Díaz, D. Dahmann, E. Monfort, On the relationship between exposure to particles and dustiness during handling of powders in industrial settings, Ann. Work Expo. Heal. 63 (2019) 107–123, https://doi.org/10.1093/annweh/wxy092.

[143] U. Bröckel, M. Wahl, R. Kirsch, H.J. Feise, Formation and growth of crystal bridges in bulk solids, Chem. Eng. Technol. 29 (2006) 691–695, https://doi.org/10.1002/ceat.200600066.

[144] N.P. Kruyt, O. Millet, An analytical theory for the capillary bridge force between spheres, J. Fluid Mech. 812 (2017) 129–151, https://doi.org/10.1017/jfm.2016.790.

[145] Y.I. Rabinovich, M.S. Esayanur, B.M. Moudgil, Capillary forces between two spheres with a fixed volume liquid bridge: Theory and experiment, Langmuir 21 (2005) 10992–10997, https://doi.org/10.1021/la0517639.

[146] M. Levin, E. Rojas, E. Vanhala, M. Vippola, B. Liguori, K.I. Kling, I.K. Koponen, K. Mølhave, T. Tuomi, D. Gregurec, S. Moya, K.A. Jensen, Influence of relative humidity and physical load during storage on dustiness of inorganic nanomaterials : Implications for testing and risk assessment, J. Nanoparticle Res. 17 (2015) 1–13, https://doi.org/10.1007/s11051-015-3139-6.

[147] P. Görner, R. Wrobel, V. Mička, V. Škoda, J. Denis, J.F. Fabriès, Study of fifteen respirable aerosol samplers used in occupational hygiene, Ann. Occup. Hyg. 45 (2001) 43–54, https://doi.org/10.1016/S0003-4878(00)00014-4.

[148] S. Wirth, M. Schöler, C.S. Leopold, Investigations on the dustiness of binary acetaminophen - lactose monohydrate powder blends, Powder Technol. 448 (2024) 120317, https://doi.org/10.1016/j.powtec.2024.120317.

[149] A. Jarray, H. Shi, B.J. Scheper, M. Habibi, S. Luding, Cohesion-driven mixing and segregation of dry granular media, Sci. Rep. 9 (2019) 1–12, https://doi.org/10.1038/s41598-019-49451-z.

[150] F. Podczeck, The relationship between particulate properties of carrier materials and the adhesion force of drug particles in interactive powder mixtures, J. Adhes. Sci. Technol. 11 (1997) 1089–1104, https://doi.org/10.1163/156856197X00859.

[151] H. Adi, I. Larson, H. Chiou, P. Young, D. Traini, P. Stewart, Agglomerate strength and dispersion of salmeterol xinafoate from powder mixtures for inhalation, Pharm. Res. 23 (2006) 2556–2565, https://doi.org/10.1007/s11095-006-9082-6.

[152] D.E. Evans, L.A. Turkevich, C.T. Roettgers, G.J. Deye, P.A. Baron, Dustiness of fine and nanoscale powders, Ann. Occup. Hyg. 57 (2013) 261–277, https://doi.org/10.1093/annhyg/mes060.

[153] T. Likitwattanasade, S.A. Barringer, The influence of particle size on separation and dustiness in powder mixtures during nonelectrostatic and electrostatic coating, J. Electrostat. 77 (2015) 44–50, https://doi.org/10.1016/j.elstat.2015.07.001.

[154] H. Rumpf, Die Wissenschaft des Agglomerierens, Chemie Ing. Tech. 46 (1974) 1–11, https://doi.org/10.1002/cite.330460102.

[155] E.M. Lifshitz, M. Hamermesh, The theory of molecular attractive forces between solids, in: L.P. Pitaevskii (Ed.), Perspectives in Theoretical Physics, Elsevier, Amsterdam, 1992, pp. 329–349, https://doi.org/10.1016/B978-0-08-036364-6.50031-4.

[156] W.A. Heitbrink, W.F. Todd, T.J. Fischbach, Correlation of tests for material dustiness with worker exposure from the bagging of powders, Appl. Ind. Hyg. 4 (1989) 12–16, https://doi.org/10.1080/08828032.1989.10389884.

[157] W.A. Heitbrink, W.F. Tood, T.C. Cooper, D.M. O'Brien, The application of dustiness tests to the prediction of worker dust exposure, Am. Ind. Hyg. Assoc. J. 51 (1990) 217–223, https://doi.org/10.1080/15298669091369565.

[158] M.A.E. Plinke, D. Leith, M.G. Boundy, F. Löffler, Dust generation from handling powders in industry, Am. Ind. Hyg. Assoc. J. 56 (1995) 251–257, https://doi.org/10.1080/15428119591017088.

[159] S. Chakravarty, M. Fischer, O. Le Bihan, M. Morgeneyer, Towards a theoretical understanding of dustiness, Granul. Matter 21 (2019) 1–22, https://doi.org/10.1007/s10035-019-0929-z.

[160] C. Cowherd, M.A. Grelinger, P.J. Englehart, R.F. Kent, K.F. Wong, An apparatus and methodology for predicting the dustiness of materials, Am. Ind. Hyg. Assoc. J. 50 (1989) 123–130, https://doi.org/10.1080/15298668991374408.

[161] T. Schneider, K.A. Jensen, Combined single-drop and rotating drum dustiness test of fine to nanosize powders using a small drum, Ann. Occup. Hyg. 52 (2008) 23–34, https://doi.org/10.1093/annhyg/mem059.

[162] J.H. Vincent, D. Mark, The basis of dust sampling in occupational hygiene: A critical review, Ann. Occup. Hyg. 24 (1981) 375–390, https://doi.org/10.1093/annhyg/24.4.375.

[163] R.F. Phalen, W.C. Hinds, W. John, P.J. Lioy, M. Lippmann, M.A. McCawley, O.G. Raabe, S.C. Soderholm, B.O. Stuart, Particle size-selective sampling in the workplace: Rationale and recommended techniques, in: J. Dodgson, R.I. McCallum, M.R. Bailey, D.R. Fisher (Eds.), Inhaled Particles VI, Pergamon Press, Oxford, 1988, pp. 403–411, https://doi.org/10.1016/B978-0-08-034185-9.50046-2.

[164] T.L. Ogden, J.L. Birkett, An inhalable-dust sampler, for measuring the hazard from total airborne particulate, Ann. Occup. Hyg. 21 (1978) 41–50, https://doi.org/10.1093/annhyg/21.1.41.

[165] R. Hameed, P.H. McMurry, K.T. Whitby, A new rotating coarse particle sampler, Aerosol Sci. Technol. 2 (1983) 69–78, https://doi.org/10.1080/02786828308958614.

[166] J.H. Vincent, P.C. Emmett, D. Mark, The effects of turbulence on the entry of airborne particles into a blunt dust sampler, Aerosol Sci. Technol. 4 (1985) 17–29, https://doi.org/10.1080/02786828508959036.

[167] R.M. Buchan, S.C. Soderholm, M.I. Tillery, Aerosol sampling efficiency of 37 mm filter cassettes, Am. Ind. Hyg. Assoc. J. 47 (1986) 825–831, https://doi.org/10.1080/15298668691390728.

[168] V. Aizenberg, S.A. Grinshpun, K. Willeke, J. Smith, P.A. Baron, Performance characteristics of the button personal inhalable aerosol sampler, Am. Ind. Hyg. Assoc. J. 61 (2000) 398–404, https://doi.org/10.1080/15298660008984550.

[169] K.Y.K. Chung, T.L. Ogden, N.P. Vaughan, Wind effects on personal dust samplers, J. Aerosol Sci. 18 (1987) 159–174, https://doi.org/10.1016/0021-8502(87)90053-X.

[170] G. Lidén, L.C. Kenny, The performance of respirable dust samplers: Sampler bias, precision and inaccuracy, Ann. Occup. Hyg. 36 (1992) 1–22, https://doi.org/10.1093/annhyg/36.1.1.

[171] S.J. Dunnett, X. Wen, A numerical study of the sampling efficiency of a tube sampler operating in calm air facing both vertically upwards and downwards, J. Aerosol Sci. 33 (2002) 1653–1665, https://doi.org/10.1016/S0021-8502(02)00118-0.

[172] Y. Zhou, Y.S. Cheng, Evaluation of IOM personal sampler at different flow rates, J. Occup. Environ. Hyg. 7 (2009) 88–93, https://doi.org/10.1080/15459620903418746.

[173] I. Guest, D. Newton, Industrial hygiene in the pharmaceutical industry, Occup. Med. 12 (1997) 81–94.

[174] W.A. Heitbrink, Factors affecting the Heubach and MRI dustiness tests, Am. Ind. Hyg. Assoc. J. 51 (1990) 210–216, https://doi.org/10.1080/15298669091369556.

[175] A. Klippel, M. Schmidt, U. Krause, Dustiness in workplace safety and explosion protection - Review and outlook, J. Loss Prev. Process Ind. 34 (2015) 22–29, https://doi.org/10.1016/j.jlp.2015.01.011.

[176] H. Chen, M.A. Jog, L.A. Turkevich, Computational fluid dynamics simulations of aerosol behavior in a high-speed (Heubach) rotating drum dustiness tester, Particuology 72 (2023) 68–80, https://doi.org/10.1016/j.partic.2022.02.010.

[177] Deutsches Institut für Normung (DIN), DIN EN 15051-1: Exposition am Arbeitsplatz - Messung des Staubungsverhaltens von Schüttgütern - Teil 1: Anforderungen und Auswahl der Prüfverfahren, Beuth Verlag, Berlin, 2014.

[178] J. Volckens, T.M. Peters, Counting and particle transmission efficiency of the aerodynamic particle sizer, J. Aerosol Sci. 36 (2005) 1400–1408, https://doi.org/10.1016/j.jaerosci.2005.03.009.

[179] S. Wirth, A novel two-chamber setup for containment investigations with special focus on powder dustiness, Ph.D. thesis, University of Hamburg, 2025.

[180] R. Zhang, H. Zhao, Small-angle particle counting coupled photometry for real-time detection of respirable particle size segmentation mass concentration, Sensors 21 (2021), https://doi.org/10.3390/s21175977.

[181] A.L. Northcross, R.J. Edwards, M.A. Johnson, Z.M. Wang, K. Zhu, T. Allen, K. R. Smith, A low-cost particle counter as a realtime fine-particle mass monitor, Environ. Sci. Process. Impacts 15 (2013) 433–439, https://doi.org/10.1039/c2em30568b.

[182] S. Mico, M. Alushllari, A. Deda, P. Dhoqina, E. Tsaousi, The variability of aerosol particle number concentrations using optical particle counter and scanning electron microscope, AIP Conf. Proc. 2075 (2019) 160037, https://doi.org/10.1063/1.5091364.

[183] J.P. Mitchell, M. Nagel, Particle size analysis of aerosols from medicinal inhalers, KONA Powder Part. J. 22 (2004) 32–65, https://doi.org/10.14356/kona.2004010.

[184] S.S. Amaral, J.A. de Carvalho, M.A.M. Costa, C. Pinheiro, An overview of particulate matter measurement instruments, Atmos. 6 (2015) 1327–1345, https://doi.org/10.3390/atmos6091327.

[185] B. Dahneke, Aerosol beam spectrometry, Nat. Phys. Sci. 244 (1973) 54–55, https://doi.org/10.1038/physci244054a0.

[186] J.P. Mitchell, M.W. Nagel, Time-of-flight aerodynamic particle size analyzers: Their use and limitations for the evaluation of medical aerosols, J. Aerosol Med. 12 (1999) 217–240, https://doi.org/10.1089/jam.1999.12.217.

[187] Y.S. Cheng, E.B. Barr, I.A. Marshall, J.P. Mitchell, Calibration and performance of an API aerosizer, J. Aerosol Sci. 24 (1993) 501–514, https://doi.org/10.1016/0021-8502(93)90034-7.

[188] P.A. Baron, M.K. Mazumder, Y.S. Cheng, Direct-reading techniques using optical particle detection, in: P.A. Baron, K. Willeke (Eds.), Aerosol Measurement: Principles, Techniques, and Applications, 2nd ed., Wiley-Interscience, New York, 2001, pp. 403–408.

[189] H. Maleki, A. Sorooshian, G. Goudarzi, A. Nikfal, M.M. Baneshi, Temporal profile of PM10 and associated health effects in one of the most polluted cities of the world (Ahvaz, Iran) between 2009 and 2014, Aeolian Res. 22 (2016) 135–140, https://doi.org/10.1016/j.aeolia.2016.08.006.

[190] A. Tornevi, H. Olstrup, B. Forsberg, Short-term associations between PM10 and respiratory health effects in Visby, Sweden, Toxics 10 (2022), https://doi.org/10.3390/toxics10060333.

[191] S. Sousan, S. Regmi, Y.M. Park, Laboratory evaluation of low-cost optical particle counters for environmental and occupational exposures, Sensors 21 (2021) 4146, https://doi.org/10.3390/s21124146.

[192] W.E. Wilson, J.C. Chow, C. Claiborn, W. Fusheng, J. Engelbrecht, J.G. Watson, Monitoring of particulate matter outdoors, Chemosphere 49 (2002) 1009–1043, https://doi.org/10.1016/S0045-6535(02)00270-9.

[193] Sensirion, Datasheet SPS30: Particulate matter sensor for air quality monitoring and control, Version 2.0 (2023) 1–26, https://sensirion.com/media/documents/8600FF88/64A3B8D6/Sensirion_PM_Sensors_Datasheet_SPS30.pdf (accessed 02 February 2025).

[194] B. Alfano, L. Barretta, A. Del Giudice, S. De Vito, G. Di Francia, E. Esposito, F. Formisano, E. Massera, M.L. Miglietta, T. Polichetti, A Review of low-cost particulate matter sensors from the developers' perspectives, Sensors 20 (2020) 6819, https://doi.org/10.3390/s20236819.

[195] S. Trilles, A.B. Vicente, P. Juan, F. Ramos, S. Meseguer, L. Serra, Reliability validation of a low-cost particulate matter IoT sensor in indoor and outdoor environments using a reference sampler, Sustainability 11 (2019) 7220, https://doi.org/10.3390/su11247220.

[196] I. Agranovski (Ed.), Aerosols: Science and Technology, Wiley-VCH, Weinheim, 2011.

[197] P.J. Dacunto, N.E. Klepeis, K.C. Cheng, V. Acevedo-Bolton, R.T. Jiang, J.L. Repace, W.R. Ott, L.M. Hildemann, Determining PM2.5 calibration curves for a low-cost particle monitor: Common indoor residential aerosols, Environ. Sci. Process. Impacts 17 (2015) 1959–1966, https://doi.org/10.1039/c5em00365b.

[198] R. Franken, T. Maggos, A. Stamatelopoulou, M. Loh, E. Kuijpers, J. Bartzis, S. Steinle, J.W. Cherrie, A. Pronk, Comparison of methods for converting Dylos particle number concentrations to PM2.5 mass concentrations, Indoor Air 29 (2019) 450–459, https://doi.org/10.1111/ina.12546.

[199] A.S. Francis, F.P. Chee, J.H.W. Chang, J. Sentian, J. Dayou, C.M. Payus, Parametric model for estimation of mass concentration based on particle count distribution for ambient air monitoring, J. Phys. Conf. Ser. 1358 (2019) 012042, https://doi.org/10.1088/1742-6596/1358/1/012042.

[200] R. Paolucci, M. Rotilio, S. Ricci, A. Pelliccione, G. Ferri, A sensor-based system for dust containment in the construction site, Energies 15 (2022) 7272, https://doi.org/10.3390/en15197272.

[201] S. Mahajan, P. Kumar, Evaluation of low-cost sensors for quantitative personal exposure monitoring, Sustain. Cities Soc. 57 (2020) 102076, https://doi.org/10.1016/j.scs.2020.102076.

[202] Y. Qian, G.H. Deng, Y. Rao, In situ spectroscopic probing of polarity and molecular configuration at aerosol particle surfaces, J. Phys. Chem. Lett. 11 (2020) 6763–6771, https://doi.org/10.1021/acs.jpclett.0c02013.

[203] J.E. Krechmer, M. Groessl, X. Zhang, H. Junninen, P. Massoli, A.T. Lambe, J.R. Kimmel, M.J. Cubison, S. Graf, Y.H. Lin, S.H. Budisulistiorini, H. Zhang, J.D. Surratt, R. Knochenmuss, J.T. Jayne, D.R. Worsnop, J.L. Jimenez, M.R. Canagaratna, Ion mobility spectrometry-mass spectrometry (IMS-MS) for on- and offline analysis of atmospheric gas and aerosol species, Atmos. Meas. Tech. 9 (2016) 3245–3262, https://doi.org/10.5194/amt-9-3245-2016.

[204] K.J. Gillig, C.-H. Chen, Increasing the performance of portable ion mobility analyzers: Development of the periodic focusing differential mobility analyzer (PFDMA), Mass Spectrom. 3 Suppl. 1 (2014) S0032, https://doi.org/10.5702/massspectrometry.s0032.

[205] B. Hettinger, V. Hohreiter, M. Swingle, D.W. Hahn, Laser-induced breakdown spectroscopy for ambient air particulate monitoring: Correlation of total and speciated aerosol particle counts, Appl. Spectrosc. 60 (2006) 237–245, https://doi.org/10.1366/000370206776342544.

[206] P.A. Babushkin, G.G. Matvienko, V.K. Oshlakov, Determination of the elemental composition of aerosol by femtosecond laser-induced breakdown spectroscopy, Atmos. Ocean. Opt. 35 (2022) 19–26, https://doi.org/10.1134/S102485602201002X.

[207] D.A. Lack, E.R. Lovejoy, T. Baynard, A. Pettersson, A.R. Ravishankara, Aerosol absorption measurement using photoacoustic spectroscopy: Sensitivity, calibration, and uncertainty developments, Aerosol Sci. Technol. 40 (2006) 697–708, https://doi.org/10.1080/02786820600803917.

[208] T. Ajtai, S. Hodovány, M. Schnaiter, G. Szabó, Z. Bozóki, Absorption based size characterisation of aerosol by using photoacoustic spectroscopy, Atmos. Environ. 304 (2023) 2–6, https://doi.org/10.1016/j.atmosenv.2023.119772.

[209] D. Al Fischer, G.D. Smith, A portable, four-wavelength, single-cell photoacoustic spectrometer for ambient aerosol absorption, Aerosol Sci. Technol. 52 (2018) 393–406, https://doi.org/10.1080/02786826.2017.1413231.

[210] H. Kobayashi, M. Hayashi, K. Shiraishi, Y. Nakura, T. Enomoto, K. Miura, H. Takahashi, Y. Igarashi, H. Naoe, N. Kaneyasu, T. Nishizawa, N. Sugimoto, Development of a polarization optical particle counter capable of aerosol type classification, Atmos. Environ. 97 (2014) 486–492, https://doi.org/10.1016/j.atmosenv.2014.05.006.

[211] Q. Xu, N. Zeng, W. Guo, J. Guo, Y. He, H. Ma, Real time and online aerosol identification based on deep learning of multi-angle synchronous polarization scattering indexes, Opt. Express 29 (2021) 18540, https://doi.org/10.1364/oe.426501.

[212] N. Lavanya, S. Bhattacharyya, Computational fluid dynamics-the futuristic innovation in pharmaceutical industry, Indian J. Pharm. Educ. Res. 55 (2021) 930–938, https://doi.org/10.5530/ijper.55.4.193.

[213] M.H. Zawawi, A. Saleha, A. Salwa, N.H. Hassan, N.M. Zahari, M.Z. Ramli, Z.C. Muda, A review: Fundamentals of computational fluid dynamics (CFD), AIP Conf. Proc. 2030 (2018) 020252, https://doi.org/10.1063/1.5066893.

[214] J. Milenkovic, A.H. Alexopoulos, C. Kiparissides, Deposition and fine particle production during dynamic flow in a dry powder inhaler: A CFD approach, Int. J. Pharm. 461 (2014) 129–136, https://doi.org/10.1016/j.ijpharm.2013.11.047.

[215] M.A. El-Emam, L. Zhou, W. Shi, C. Han, L. Bai, R. Agarwal, Theories and applications of CFD–DEM coupling approach for granular flow: A review, Arch. Computat. Methods Eng. 28 (2021) 4979–5020, https://doi.org/10.1007/s11831-021-09568-9.

[216] H. Ma, L. Zhou, Z. Liu, M. Chen, X. Xia, Y. Zhao, A review of recent development for the CFD-DEM investigations of non-spherical particles, Powder Technol. 412 (2022) 117972, https://doi.org/10.1016/j.powtec.2022.117972.

[217] Z.B. Tong, B. Zheng, R.Y. Yang, A.B. Yu, H.K. Chan, CFD-DEM investigation of the dispersion mechanisms in commercial dry powder inhalers, Powder Technol. 240 (2013) 19–24, https://doi.org/10.1016/j.powtec.2012.07.012.

[218] Z. Zhao, L. Zhou, L. Bai, B. Wang, R. Agarwal, Recent advances and perspectives of CFD–DEM simulation in fluidized bed, Arch. Computat. Methods Eng. 31 (2024) 871–918, https://doi.org/10.1007/s11831-023-10001-6.

[219] S. Wangchai, D. Hastie, P. Wypych, DEM-CFD Modelling of particle flow mechanisms in dustiness testers, in: 12th International Conference on Bulk Materials Storage, Handling and Transportation (ICBMH 2016), Engineers Australia, Barton, ACT, 2016, pp. 540–549.

[220] F. Huang, Q. Zhu, X. Zhou, D. Gou, J. Yu, R. Li, Z. Tong, R. Yang, Role of CFD based in silico modelling in establishing an in vitro-in vivo correlation of aerosol deposition in the respiratory tract, Adv. Drug Deliv. Rev. 170 (2021) 369–385, https://doi.org/10.1016/j.addr.2020.09.007.

[221] H. Küllmar, M. Schöler, J. Brügmann, C.S. Leopold, Investigations on the spatial dust distribution for emission site localization in containment, AAPS PharmSciTech 26 (2025) 239, https://doi.org/10.1208/s12249-025-03236-y.

[222] H. Küllmar, M. Schöler, K.U. Braunschweig, C.S. Leopold, Low-cost particulate matter sensors for real-time spatiotemporal detection of pharmaceutical dust in containment, Eur. J. Pharm. Biopharm. 223 (2026), https://doi.org/10.1016/j.ejpb.2026.115069.

Appendix

Hazardous materials

Substance	Supplier	Danger symbol	Hazard statements	Precautionary statements
Acetaminophen	Caelo, Germany Fagron, Germany		H373	P260, P314, P501
Acetonitrile	VWR, USA		H225, H302, H312, H332	P210, P280, P301+P312, P304+P340, P403+P233
Lactose Monohydrate	Meggle, Germany		None	P261, P280
Methanol	VWR, USA		H225, H301, H311, H331, H370	P210, P233, P260, P280, P303+P361+P353, P304+P340, P310
Sulfuric Acid	Dräger, Germany		H290, H314	P260, P280, P303+P361+P353, P305+P351+P338, P310, P405

List of figures

Figure 1: Relationship between ADE, OEL, and OEB. 6
Figure 2: Classification of airborne aerosols according to occupational health criteria. 15
Figure 3: Model of the dust generation and quantification processes. 17
Figure 4: The original IOM sampler in its assembled (a) and disassembled (b) state. 22
Figure 5: Schematic illustration of the UNC dustiness tester. 25
Figure 6: Simplified scheme of the Heubach dustmeter. 26
Figure 7: Schematic illustration of the continuous drop test apparatus. 27
Figure 8: Schematic diagram of the MRI dustiness tester. 28
Figure 9: Simplified illustration of the Palas dustview. 29
Figure 10: Diagram of the low-mass dustiness tester. 30
Figure 11: Simplified illustration of the Two-chamber setup. 31
Figure 12: Schematic diagram of a time-of-flight aerodynamic particle sizer. 34
Figure 13: Simplified diagram of an OPC. 35
Figure 14: Visual summary of the study methodology and key results. 41
Figure 15: Visual description of the main findings and results of the study. 60
Figure 16: Overview of the methodology and the main results of the study. 78

List of tables

Table 1: Example of an OEB classification system. 5
Table 2: Selection criteria for pharmaceutical surrogate substances. 11
Table 3: Overview of commonly used pharmaceutical surrogate substances, their properties, and typical applications. 12
Table 4: Atomization forces for different dustiness testing devices. 23

Curriculum vitae

Name:	Küllmar, Hendrik	Date of birth:	Dec 28th, 1988
Marital status:	unmarried	Place of birth:	Frankfurt am Main

Education	since 12/2019	Doctoral candidate, Division of Pharmaceutical Technology, University of Hamburg, Supervisor: Prof. Dr. Dr. h.c. C.S. Leopold
	08/2019	License as pharmacist (Approbation)
	04/2014 – 10/2018	Study of Pharmacy, Philipps-University Marburg
	10/2009 – 08/2013	Study of Biotechnology/Biopharmaceutical Technology, University of Applied Sciences Mittelhessen, (B. Sc., Engineer)
	06/2008	‘Abitur‘, Elly-Heuss-Schule, Wiesbaden
Specialization	since 2020	‘Fachapotheker für Pharmazeutische Analytik und Technologie‘
Work experience and internships	since 04/2026	Project Manager (Development Projects), Rottendorf Pharma GmbH, Ennigerloh
	06/2024 – 03/2025	Development Engineer (Future Technologies), Fette Compacting GmbH, Schwarzenbek
	11/2018 – 04/2019	Intern, Hof-Apotheke, Bad Homburg v.d.H.
	08/2017 – 09/2017	Intern, Tongji Medical College of the Huazhong University of Science and Technology, Wuhan (China)
	10/2012 – 08/2013	Practical semester and Bachelor thesis, B. Braun Melsungen AG, Melsungen
	10/2011 – 03/2012	Student assistant, Institute of Bioprocess Engineering and Pharmaceutical Technology (IBPT), Gießen
	07/2010 – 09/2010	Internship, Analyticon Biotechnologies AG, Lichtenfels

Acknowledgements

This dissertation was carried out at the University of Hamburg, in the Department of Chemistry, in the division of Pharmaceutical Technology. It was initiated and supervised by Professor Dr. Dr. h.c. Claudia S. Leopold. In this part of the thesis, I would like to express my gratitude to all those people who supported and contributed to this work.

First of all, I would like to thank Prof. Dr. Dr. h.c. Claudia S. Leopold for welcoming me to her research group and providing me with this fascinating research topic. Her guidance, while always providing me with enough freedom, and the inspiring scientific discussions contributed significantly to this thesis.

Moreover, I am grateful to Prof. Dr. Hans-Ulrich Moritz for evaluating this thesis. I also thank Prof. Dr. Peter Burger and Priv. Doz. Dr. Christoph Wutz for being members of the examination committee.

Furthermore, I want to express my gratitude to Dr.-Ing. Martin Schöler for the co-supervision. His expertise, especially from an industrial point of view on the research topic of containment, substantially enriched this thesis.

I also want to thank Dr. Albrecht Sakmann for introducing me to the field of teaching and supervising students, as well as his support with the organisation of student laboratory courses.

Moreover, I am grateful to Petra Borbe and Kai Braunschweig for their untiring assistance and technical expertise with regard to TGA and HPLC analysis.

I want to extend my thanks to Jonas Brügmann for introducing me to the methodology of CFD simulations and to Dr. Charlotte Ruhmlieb for providing me with SEM images, which allowed a deeper understanding of the results of this thesis.

A heartfelt thank you goes to my colleagues from the research group of Pharmaceutical Technology. It was a pleasure to spend countless hours in the laboratory and in engaging

discussions during coffee breaks with you. I am grateful to be able to call you not only colleagues but also friends.

An additional thanks goes to Cristian Kulcițki, Simon Schulte Herbrüggen, Daniel Lutz and Arda Erol for proofreading this thesis.

I dearly want to thank all of my friends and my family for their understanding, patience, and support during the last years. A special thanks goes to my parents for never letting me down, to our dogs Ella and Fine for countless walks to clear my mind, and of course to Sophia Henke for her trust in me, her everlasting support, and for enriching our lives with our wonderful daughter Josephine.

Declaration on oath / Eidesstattliche Versicherung

Hiermit versichere ich an Eides statt, die vorliegende Dissertationsschrift selbst verfasst und keine anderen als die angegebenen Quellen und Hilfsmittel benutzt zu haben. Sofern im Zuge der Erstellung der vorliegenden Dissertationsschrift generative Künstliche Intelligenz (gKI) basierte elektronische Hilfsmittel verwendet wurden, versichere ich, dass meine eigene Leistung im Vordergrund stand und dass eine vollständige Dokumentation aller verwendeten Hilfsmittel gemäß der Guten wissenschaftlichen Praxis vorliegt. Ich trage die Verantwortung für eventuell durch die gKI generierte fehlerhafte oder verzerrte Inhalte, fehlerhafte Referenzen, Verstöße gegen das Datenschutz- und Urheberrecht oder Plagiate.

_____

Datum, Unterschrift